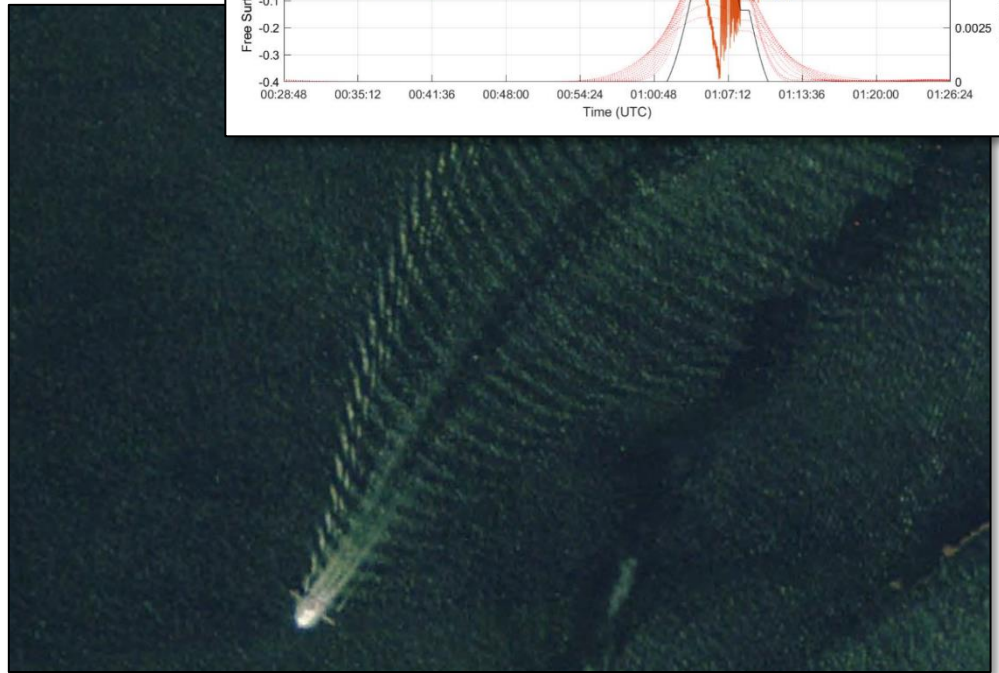
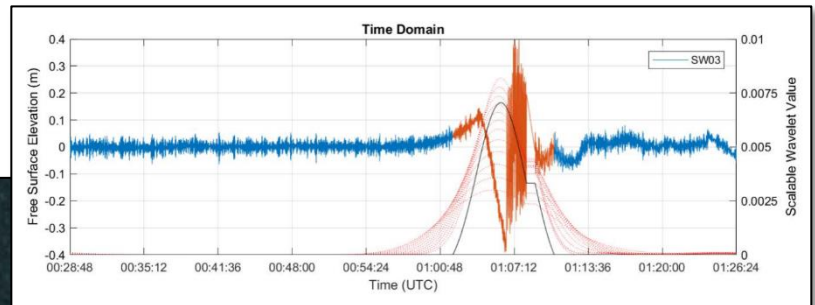


# Vessel Generated Wave Energy: Field Data Collection, Prediction, and Impacts Assessment

## Mobile Bay, Alabama

**Richard J. Allen**

U.S. Army Corps of Engineers, Mobile District  
109 Saint Joseph Street  
Mobile, AL 36602



**US Army Corps  
of Engineers**  
Mobile District

April 2018



## Abstract

---

The U.S. Army Corps of Engineers, Mobile District, is completing a General Re-Evaluation Report (GRR) for the Mobile Harbor Federal Navigation Channel. The GRR will determine if it is justifiable to deepen and widen the channel. As part of the analysis, potential for environmental impacts must be assessed. Vessel generated wave energy (VGWE) is a source of potential environmental impacts. A vessel generated wave energy (VGWE) assessment was conducted to quantify the relative changes in wave energy due to future vessels calling the port. The investigation included field data collection using a suite of 5 pressure sensors located north of Gaillard Island. A unique and efficient method of data processing was employed using a continuous wavelet transformation (CWT) to extract the vessel generated disturbances from a continuous time series by utilizing frequency modulation or “chirp” signal produced and shown to be valid within the context of large data sets where random errors can be averaged. VGWE was computed on the extracted time series using a fast Fourier transformation which is widely accepted and used for describing energy of a time series. The method proved successful for this study with the exception of cases with higher background energy or weak VGWE signals. VGWE computed using field data compared well with expected results based on theoretical values and dependencies. Overall, the field data collection collected for this study proved to be valid when used for general trending. VGWE was also estimated using the model described by Schoellhamer (1996) and compared to the collected data described in previous paragraph. The results were found to underestimate at all measured stations for Froude numbers greater than 0.5. For Froude numbers less than 0.5 the model tends to overestimate at the far field stations and underestimate for near measurement stations. The original field data and model were validated using a similar methodology to collect data between December 2018 and February 2019 in the southern bay. The southern bay validation indicated agreement with the Schoellhamer model but with less accuracy. As a result of this analysis, it is recommend the Schoellhamer (1996) should only be applied to Mobile Bay for low precision prediction of far field VGWE at Froude numbers greater than 0.5 with the understanding values could be slightly underestimated. Potential impacts of VGWE were evaluated at two locations in the Bay (i.e., the area where data was collected and another area in the southern part of the Bay where validation data was collected) by comparing the relative difference of with and without project conditions using forecasted vessel calls for years 2025 and 2035. Vessel speed was obtained from a statistical summary of 2016 Automatic Identification System (AIS) data categorized by vessel length. Cumulative VGWE was computed using the model published by Schoellhamer (1996). No increase in VGWE was determined as a result of the proposed project. The confidence of this finding was tested with respect to the assumption of vessel speed which determined for realistic potential increases in vessel speed as a result of the project the relative difference in VGWE does not become impactful. A cumulative impacts analysis of vessel generated wave energy (VGWE) effects on Mobile Bay shorelines was completed at three representative locations along the

western shore. One of these locations indicated a possible correlation between shoreline change rates and vessel calls from 1957 till approximately 1997, and no correlation at all sites between 1997 and present. Because there was no correlation found at any of the sites since 1997 and VGWE associated with the recommended plan is expected to be reduced, the present and foreseeable cumulative impacts of VGWE on Mobile Bay shorelines are considered not significant.

# Contents

---

## 1 Introduction

- Purpose
- Study Area
- Climatology
- Theoretical Background

## 2 Field Investigation

- Field Stations
- AIS Data
- Measured VGWE Processing Methodology
- Results
- Discussion and Data Quality
- Summary

## 3 Computing Vessel Generated Wave Energy

- Predictive Models
- Discussion
- Validation
- South Bay Validation
- Summary

## 4 Impact Assessment

- Vessel Traffic Frequency
- Vessel Speed
- Spatial Representation
- Computed Impact
- Sensitivity Analysis
- Summary

## 5 Cumulative Impacts Assessment

- Vessel Callings
- Shoreline Inventory
- Federal Navigation Channel Dimensions
- Shoreline Characterization and Change Analysis
- Comparison of Shoreline Change and Vessel Calls
- Summary

## 6 References

Appendix A – Vessel Generated Wave Energy Data by Transit

Appendix B – Detailed Inventory of Forecasted Fleet

# Figures and Tables

---

## Figures

Figure 1: Map of Mobile Bay, Alabama along with bathymetric contours obtained from NOAA (2010).

Figure 2: Wind Rose applicable to Mobile Bay obtained from WIS station 73154.

Figure 3: Percent occurrence of wind speed and direction at WIS station 73154.

Figure 4: Spatial distribution of significant wave heights in Mobile Bay as a result of southern wind field (reproduced from Chen et al, 2005).

Figure 5: Definition sketch of vessel disturbance in plan-form described by Havelock (1908).

Figure 6: Map of Station Locations

Figure 7: Typical Pressure Sensor Setup

Figure 8: Sensor Mounting System and Installation

Figure 9: RBR pressure sensor deployment parameters

Figure 10: Automatic Information System (AIS) System Schematic. (IMO, 2015)

Figure 11: Time-Frequency plane representing scenerios for time variance and frequency variance of the Heisenberg box used in the CWT computation. (Mallet, 2009)

Figure 12: Ideal case of CWT used for automatic identification of a vessel generated disturbance at Station SW04, Event ID: 259 for an inbound traveling vessel with dimensions of  $L = 229$  m,  $B = 32$  m,  $D = 13.7$  m. The orange highlighted area is the signal assumed to be generated by the vessel.

Figure 13: Comparison of measured background energy density measured at each station with the recorded wind speeds at NOAA station 8736897. The horizontal axis is indexed by vessel transit event ID.

Figure 14: Examples of possible inaccuracies using CWT method for extracting vessel disturbances from station time series; (upper) Event ID: 8, SW05, outbound,  $L = 176$ m,  $B = 35$ m,  $D = 5.8$ m; (lower) Event ID: 24, SW02, inbound,  $L = 228$ m,  $B = 42$ m,  $D = 12.2$ m.

Figure 15: Multiple vessel transits with small time intervals between events.

Figure 16: Vessel Generated Wave Energy (VGWE) partial identification error using the continuous wavelet transformation (CWT) method. Event ID: 203, SW01, outbound, L = 228m, B = 32m, D = 8.1m.

Figure 17: Vessel generated wave energy (VGWE) identification using a continuous wavelet transformation (CWT) (bottom) and frequency distribution using a fast Fourier transformation (FFT) for an ideal vessel transit event.

Figure 18: Vessel generated wave energy (VGWE) identification using a continuous wavelet transformation (CWT) (bottom) and frequency distribution using a fast Fourier transformation (FFT) for a case of high background wave energy with respect to VGWE.

Figure 19: Example of vessel generated disturbance transformation of the free surface elevation as a function of distance from the sailing line

Figure 20: Measured vessel generated wave energy (VGWE) verses distance from the sailing line with respect to individual events.

Figure 21: Observed breaking of vessel generated wake. Photos taken looking west from an outbound tanker on 09 November 2017. Vessel dimension: L = 244 m, B = 42m. Vessel draft on the date of picture was 8.5m. Left picture was 7 km and right picture 4km north of instrumentation stations.

Figure 22: Observed wave breaking of an inbound containership approximately 2 km north of Gaillard Island from aerial imagery collected 06 November 2013. Detailed vessel description is unavailable.

Figure 23: Vessel generated significant wave height computed using a wave train analysis verses distance from the sailing line with respect to individual events.

Figure 24: Measured vessel generated wave energy verses the depth based Froude number for all stations.

Figure 25: Measure vessel generated wave energy (VGWE) verse vessel draft (top) and vessel length (bottom).

Figure 26: One-to-One correlation plot of measured vessel generated wave energy (VGWE) and the equation from Schoellhamer (1996) for stations SW01 through SW04.

Figure 27: One-to-One correlation plot of measured vessel generated wave energy (VGWE) categorized by Froude number and the equation from Schoellhamer (1996) for stations SW01 through SW04. The regression line follows Froude numbers greater than 0.5.

Figure 28: One-to-One correlation plot of measured vessel generated wave energy (VGWE) and the equation from Schoellhamer (1996) for stations SW01 through SW04 categorized by direction of vessel transit. The regression line is color coded to match the respective transit direction.

Figure 29: Southern Bay Station Locations

Figure 30: One-to-One correlation plot of measured vessel generated wave energy (VGWE) at the south bay validation sites and the equation from Schoellhamer (1996) for stations SWS01 through SWS03 and SW05.

Figure 31: One-to-One correlation plot of measured vessel generated wave energy (VGWE) at the south bay validation sites categorized by Froude number and the equation from Schoellhamer (1996) for stations SWS01 through SWS03 and SW05. The regression line follows Froude numbers greater than 0.5.

Figure 32: One-to-One correlation plot of measured vessel generated wave energy (VGWE) at the south bay validation sites and the equation from Schoellhamer (1996) for stations SWS01 through SWS03 and SW05 categorized by direction of vessel transit. The regression line is color coded to match the respective

Figure 33: Location of sites used for spatial representation of Vessel Generated Wave Energy (VGWE) impact analysis within Mobile Bay, Alabama

Figure 34: Summary statistics of vessel speed using Shipborne Automated Identification System (AIS) data obtain for the 2016 calendar year for Mobile Bay, Alabama deep draft channel delineated by vessel length.

Figure 35: Variation of vessel speed for all classes and categories in Mobile Bay, Alabama with respect to three locations of interest.

Figure 36: Graphical sketch defining cross-sectional variables used in VGWE and vessel speed computations.

Figure 37: Summary of class 1 and 2 vessel calls obtained from WCUS annual reports (1956-2017) aggregated by draft plotted as a function of year.

Figure 38: All class 1 and 2 vessel calls obtained from WCUS annual reports (1956-2017) by year for all drafts greater than or equal to 19 feet.

Figure 39: Selected sites used to evaluate shoreline change.

Figure 40: Linear regression rate of shoreline change for SL1 for 1849/1850 through 2010/2011.

Figure 41: Linear regression rate of shoreline change for SL3 for 1849/1850 through 2010/2011.

Figure 42: Linear regression rate of shoreline change for SL6 for 1849/1850 through 2010/2011.

Figure 43: Temporal plot of channel modifications between 1913 and 1989. Channel dimensions are represented as a cross-sectional area in square feet of the navigable portion

Figure 44: Spatial and Temporal Distribution of shoreline armoring between 1955 and 1997 extracted from Douglass and Pickel (1999).

Figure 45: Temporal distribution of shoreline change rates at SL1 between 1917/18 and 2010/11 with linearly interpolated rate of rate of change.

Figure 46: Temporal distribution of shoreline change rates at SL3 between 1917/18 and 2010/11 with linearly interpolated rate of rate of change.

Figure 47: Temporal distribution of shoreline change rates at SL3 between 1917/18 and 2010/11 with linearly interpolated rate of rate of change.

Figure 48: Plot of vessel count for Mobile Harbor between 1956 and 2017 of all vessels having a draft greater than 19 feet compared to combined average shoreline change rates for sites SL1, SL3, and SL6. Channel dimension changes are identified using the plot background.

Figure 49: Plot of vessel count for Mobile Harbor between 1956 and 2017 of all vessels having a draft greater than 19 feet compared to average shoreline change rates computed for each site. Channel dimension changes are identified using the plot background color.

## Tables

Table 1: Station Details

Table 2: AIS Dataset Summary Statistics

Table 3: Average  $H_{mo}$  (VGWE) at each station categorized by vessel length

Table 4: Average  $H_{mo}$  (VGWE) at each station categorized by vessel draft

Table 5: Average  $H_{mo}$  (VGWE) at each station categorized by transit direction

Table 6: Average  $H_{mo}$  (VGWE) at each station categorized by speed

Table 7: Average  $H_{mo}$  (VGWE) at each station categorized by wind speed recorded at NOAA station 8736897

Table 8: Dependent variables used to evaluate Vessel Generated Wave Energy (VGWE) with respect to locations of interest.

Table 9: Forecast summary for the base year 2025 vessel calls delineated by vessel classes for with and without project conditions.

Table 10: Forecast summary for year 2035 vessel calls delineated by vessel classes for with and without project conditions.

Table 11: Computed Vessel Generated Wave Energy (VGWE) of with and without project scenarios using the forecasted base year 2025 at the upper bay site.

Table 12: Computed Vessel Generated Wave Energy (VGWE) of with and without project scenarios using the forecasted base year 2025 at the lower bay site.

Table 13: Computed Vessel Generated Wave Energy (VGWE) of with and without project scenarios using the forecasted year 2035 at the upper bay site.

Table 14: Computed Vessel Generated Wave Energy (VGWE) of with and without project scenarios using the forecasted year 2035 at the lower bay site.

Table 15: Results of three unique vessel speed sensitivity tests for the 2025 forecasted arrivals at the upper bay site.

Table 16: Inventory of shoreline position data, applicable locations, source, and selected data quality parameters.

Table 17: Summary of Channel Modifications between 1913 and 1989.



# 1 Introduction

---

## Purpose

The U.S. Army Corps of Engineers, Mobile District, is completing a General Re-Evaluation Report (GRR) for the Mobile Harbor Federal Navigation Channel. The GRR will determine if it is justifiable to deepen and widen the channel. As part of the analysis, potential for environmental impacts must be assessed. Vessel generated wave energy (VGWE) is a source of potential environmental impacts. This report describes the data collection of VGWE in Mobile Bay, Alabama and provides an assessment of relative change in VGWE as a result of deepening the Federal channel from 45 feet to 49 feet using a forecasted vessel fleet for the years 2025 and 2035 that may be used for assessment of impacts to various shoreline types and other environmental features identified by public comment, other government agencies, and local stakeholders.

## Study Area

Mobile Bay, Alabama can be described as a micro-tidal, drowned river valley located along the north central coastline of the Gulf of Mexico (Figure 1). Mobile Bay is approximately 50 km from the U.S. Highway 90 causeway in the north to Fort Morgan peninsula in the south. The width averages 17 km and is widest in the south (36 km). The Mobile Bay watershed is the sixth largest river basin in the United States and the fourth largest in terms of streamflow. It drains water from three-fourths of Alabama as well as portions of Georgia, Tennessee and Mississippi into Mobile Bay. Mobile bay has an average water depth of 3 meters and is transected by a 13 to 15 meter deep channel.

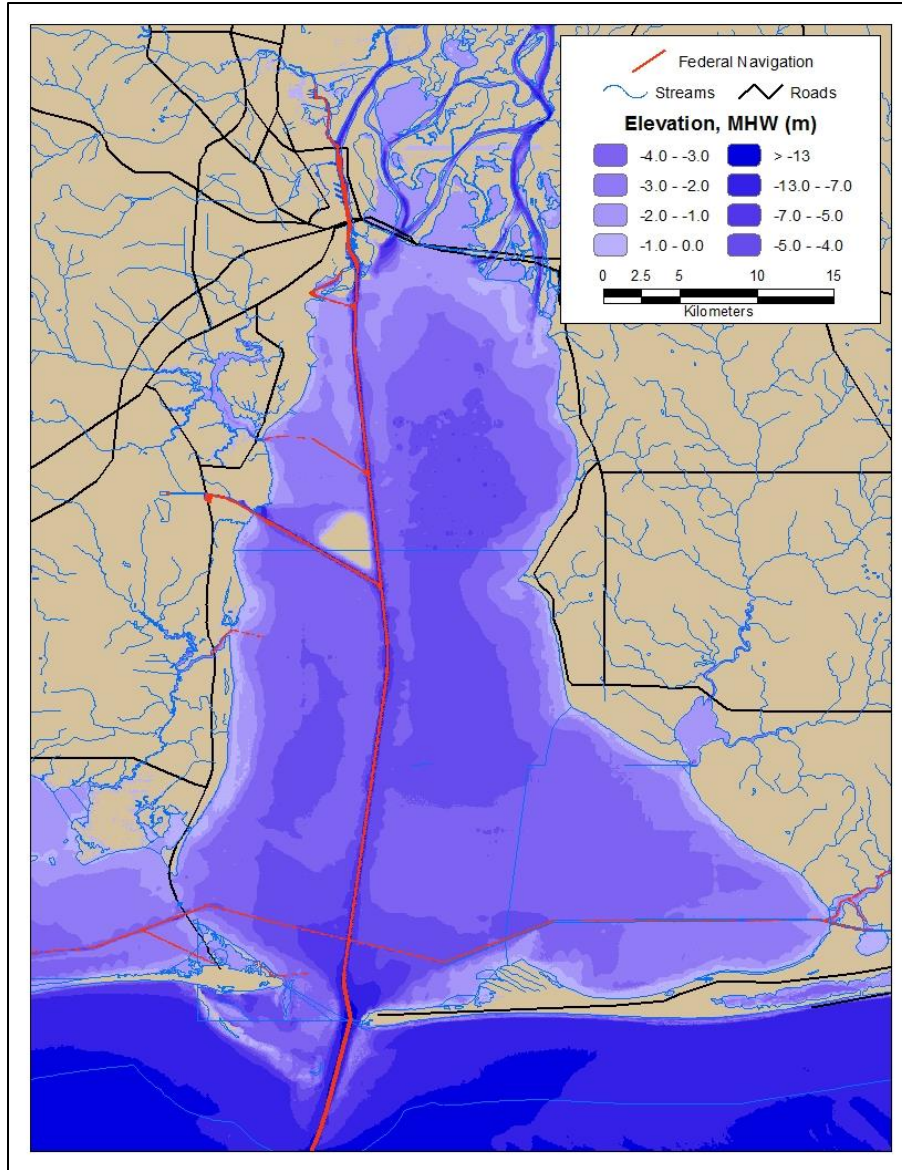


Figure 1: Map of Mobile Bay, Alabama along with bathymetric contours obtained from NOAA (2010).

## Climatology

Mobile Bay is located in a temperate climate with average temperatures of 30° C in the summer and 10° C in the winter. The wind climate is generally mild except for episodic events associated with tropical systems. A wind rose in Figure 2 and tabulated percent occurrence of wind speed and direction in Figure 3 obtained from WIS Station 73154 shows the dominate wind directions being between 90° and 135°. Seasonally, winds are northerly in the winter months, south easterly in the spring and early summer, then southwesterly in late summer to early fall.

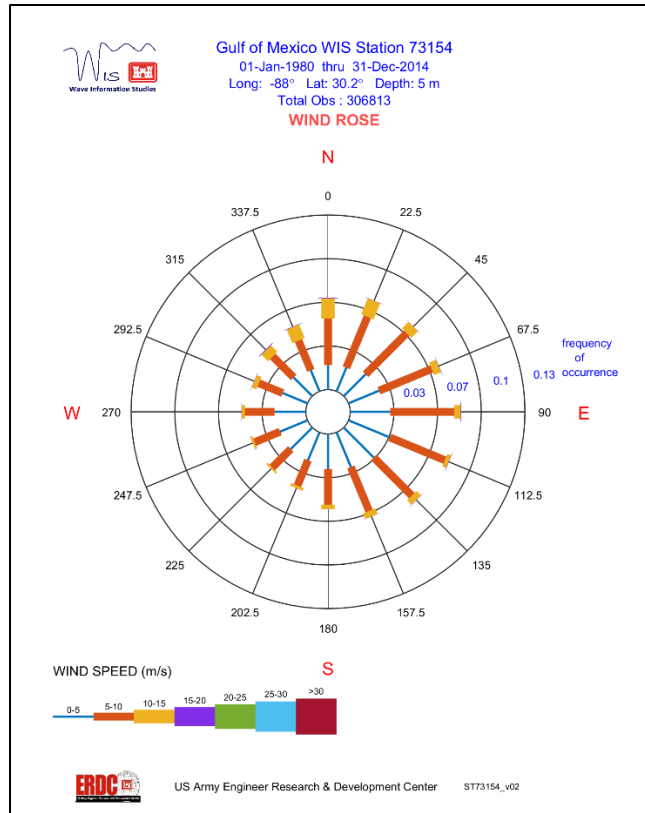


Figure 2: Wind Rose applicable to Mobile Bay obtained from WIS station 73154.

```

GULF OF MEXICO HINDCAST WAM4.5.1C : ST73154_v02
ALL MONTHS FOR YEARS PROCESSED : 1980 - 2014
STATION LOCATION : ( -88.00 W / 30.20 N )
DEPTH : 5.0 m

PERCENT OCCURRENCE (X1000) OF WIND SPEED AND DIRECTION
CENTRAL LOCAL ANGLE BANDS OF (+/- 11.25 DEG)

NO. CASES : 306812

WIND DIR      WIND SPEED (M/S)      TOTAL
DEG           <2.5  2.5-  5.0-  7.5- 10.0- 12.5- 15.0- 17.5- 20.0- 25.0-  GREATER
              4.9  7.4  9.9  12.4 14.9 17.4 19.9 24.9
0.0           43 1756 1715 1843 1190 404 57 2 0 0 0 7010
22.5          48 1829 2129 2071 1080 301 23 0 0 0 0 7481
45.0           42 2204 2638 1851 671 86 10 0 0 0 0 7502
67.5           40 2375 2736 1667 501 91 24 6 1 0 0 7441
90.0           54 2856 3299 1682 419 85 30 7 5 3 0 8440
112.5          60 3197 3318 1338 285 50 21 6 4 1 0 8280
135.0          66 3013 2959 1275 393 99 18 2 0 2 0 7827
157.5          58 2691 2516 1189 362 117 14 0 0 1 0 6948
180.0          67 2504 1933 861 278 70 6 0 4 1 0 5724
202.5          81 2131 1642 522 191 38 4 0 1 0 0 4610
225.0          71 2154 1633 438 136 27 1 1 0 0 0 4461
247.5          69 2097 1731 442 148 34 4 0 0 0 0 4525
270.0          73 2235 1801 517 191 75 14 0 2 0 0 4908
292.5          68 1887 1501 537 276 106 22 3 0 0 0 4400
315.0          61 1885 1471 817 527 210 50 4 2 0 0 5027
337.5          43 1620 1317 1157 876 287 38 0 0 0 0 5338
TOTAL         944 36434 34339 18207 7524 2080 336 31 19 8

MEAN WS (M/S) = 6.2    MAX WS (M/S) = 35.9    MEAN WIND DIR (DEG) = 211.0    FINITE

```

Figure 3: Percent occurrence of wind speed and direction at WIS station 73154.

Mobile Bay is a semi-enclosed estuary such that wave energy is mostly locally driven by the wind climate. Pandygraft and Gefenbaum (1994) collected wind and wave data at a site near Gaillard Island over a 2.5 year period. Data were segregated by seasons as well as wind directions in the report and found north winds generated a maximum significant wave height of 0.97 m, east winds generated a significant wave height of 1.00 m, and south winds generated a maximum measured significant wave height of 1.55 m. These findings tend to suggest a fetch limited wave condition in the northern part of the bay. Chen et al. (2005) used the data collected by Pandygraft and Gefenbaum (1994) to validate a numerical model for Mobile Bay confirming the fetch limited wind directions of north, east, and west. Comparatively, Chen et al. (2005) found a nearly fully developed wave field in the central part of the bay as shown in Figure 4 produced by south-southeast wind direction. The wave height decays in the northern part of the bay; this is likely a result of depth induced shoaling and wave breaking. Reduced wave heights are also observed north (leeward) of Gaillard Island and from this figure there appears to be no amplification or focusing of the wave height in the far leeward area north of the island.

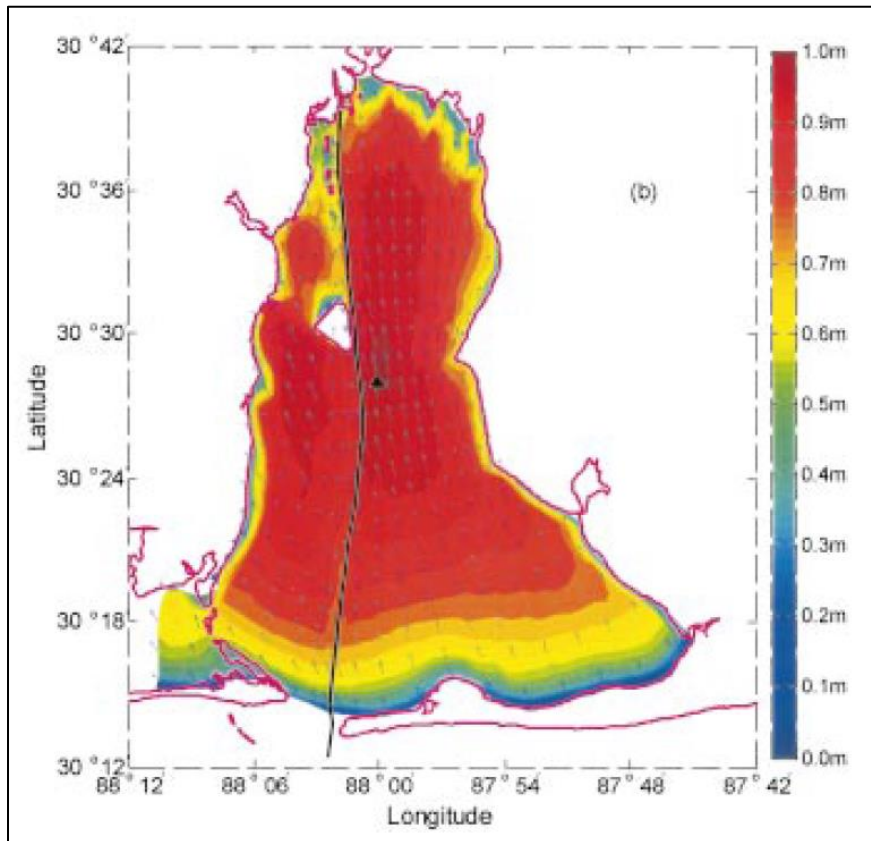


Figure 4: Spatial distribution of significant wave heights in Mobile Bay as a result of southern wind field (reproduced from Chen et al, 2005).

## Theoretical Background

Quantification or at least an understanding of vessel generated wave characteristics is of high importance to the practice of coastal engineering when designing in close proximity to frequently trafficked areas by small and large vessels or within quiescent coastal settings that include large deep-draft navigation channels, as is the case for nearly all major estuarine environments in the United States. Over the past century researchers and practitioners have produced a comprehensive collection of theories and methodologies for describing aspects of vessels wakes for a large range of applications. References identified for this report pertain to the theoretical components (Havelock, 1908), laboratory experiment derived models (Sorensen and Weggel, 1984; Weggel and Sorensen, 1986), field study derived models (Schoellhamer, 1996; Kriebel and Seelig, 2005; Maynard, 2011), and interaction with complex bathymetry and/or channel geometry (Rapaglia et al. 2011; de Jong et al 2013; Rodin et al 2015; Javanmardi et al. (2017)). A summation of these references and a general understanding of vessel disturbances along with dependencies is described in the follow paragraphs.

Water surface disturbances generated by a moving vessel create pressure gradients. As a vessel with forward motion displaces water a pressure gradient is formed at three locations, the bow, midship, and the stern. These pressure gradients are a function of relative change in water velocity induced by the vessel. The bow of the vessel causes water to abruptly change direction and speed creating a pressure gradient and will always be a function of vessel speed and hull geometry. A second gradient along the side of the vessel, also a function of vessel speed, is of lesser magnitude than the bow gradient but can be further exacerbated as a function of bathymetry or channel cross-section. As water passes the stern of the vessel a second positive pressure gradient is formed as the water changes direction and speed once more to return the free surface to equilibrium. These gradients cause the free surface elevation to rise at the bow and to a lesser magnitude at the stern while creating a negative free surface elevation at midship. As a result, the change in free surface elevation creates two patterns of surface oscillations (diverging and transverse waves) which propagate out from the sailing line. (Havelock, 1908)

Magnitude of VGWE can be assimilated to the formation of pressure gradients such that it is proportional to relative vessel speed, inversely proportional to channel cross-section area, and a complex function of hull geometry typically described using vessel dimensions, displacement, and the blocking coefficient. The root of these dependents are shown in Equation 1. Other less significant contributions usually described through coefficients in regression equations or “noise” in field studies could be derived from vessel asymmetry in a confined channel, vessel heading vs. course over ground (yaw), direction of propeller rotation, and vessel asymmetry with respect to free surface elevation. For this study only the variables described in Equation 1 will be considered in addition to those as dictated by published methodologies used in this study.

$$VGWE = f(V, L, B, D, C_b, d_c, x) \quad (1)$$

Where:

$V$  = Vessel Speed,  $L$  = Vessel Length,  $B$  = Vessel Beam,  $D$  = Vessel Draft,  $C_b$  = Blocking Coefficient,  $d_c$  = Channel Depth,  $x$  = perpendicular distance from sailing line

Wave energy generated at the sailing line propagates laterally based on the Kelvin wave theory (Thompson 1887), shown in Figure 5. Notably and relevant, Havelock (1908) showed the magnitude of the diverging wave cusp line intercept points are inversely proportional to the cube root of distance from the bow, and the transverse wave magnitude is inversely proportional to the square root of the perpendicular distance from the sailing line. This decay, however, is only applicable for deep-water waves and does not include energy losses as a result of shoaling, breaking, and channel cross-section.

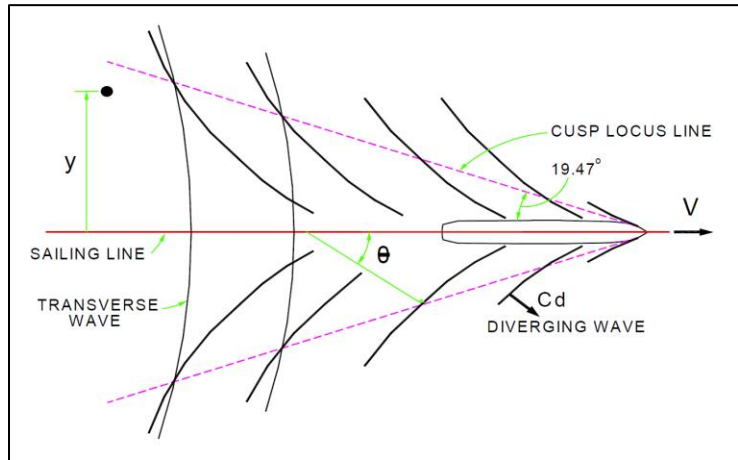


Figure 5: Definition sketch of vessel disturbance in plan-form described by Havelock (1908).

Using the depth-based Froude number,  $F_d$ , defined by Equation 2 effects on diverging waves would be evident at values greater than 0.56 and significantly affected for values greater than 0.70 (Sorensen, 1973). Transverse waves have a longer wave period and therefore will begin feeling the bottom sooner. As a result, the wave crest angle of the diverging wave will approach 90 degrees to the sailing line as the Froude number approaches unity due to the increased wave celerity using linear wave theory.

$$F_d = \frac{V}{\sqrt{gd_c}} \quad (2)$$

In general, wave energy generated by a vessel in a semi-confined channel, observed through measurement of the free surface, can be described as a large asymmetrical trough with little to no amplification above the still water surface or undulating pattern; as the disturbance propagates away from the sailing line, up the channel side slopes and into shallow water the free surface begins to respond. The small crest preceding the trough is traveling at a higher celerity and tends to decay as a function of distance from the sailing line. The trailing end of the larger trough begins to steepen as smaller, high frequency, oscillations moving at a higher celerity attempt to overtake the larger trough. Further from the channel the magnitude of the trough decays as the trailing oscillations slightly grow in magnitude and duration then begin to decay in magnitude but further increasing duration. The non-linear characteristics (asymmetric trough) of the initial vessel generated disturbance are of particular interest.

Linear wave theory is historically used for describing vessel generated disturbances (Havelock, 1908; Sorensen, 1973; Kriebel and Seelig, 2005). However, more recent investigations show the traditional kelvin wedge is often inadequate to describe vessel disturbances in detail for complex bathymetry, as the case for Mobile Bay. Several weak to fully non-linear approaches typically referred to as surge, rouge, and tsunami have been investigated such as the Boussinesq-type solutions (Bernoulli wake) (Jiang et al. 2002; David et al. 2017), modified Kadomtsev-Petviashvili (KP) equations for multi solitonic waves (Soomere, 2006), Riemann (simple) waves of depression (Rodin et al. 2015), and Korteweg-de Vries equations (Pelinvovsky et al, 2001). Each method or theory involves some form of application based on the Froude number relationship. Most define an inflection point between 0.5 and 0.7 for transcritical speeds. Where events having a Froude number less than 0.5, in certain instances, can weakly be associated with linear wave theory for initial generation and propagation from the sailing line. However, linear wave theory becomes less valid for Froude numbers in the transcritical speed regime ( $F > 0.5$ ).

An important note in the application of non-linear wave theories is rate of decay a lateral distance from the sailing line can be far less than assumed using linear wave theory (Soomere, 2006). Observations of vessel generated disturbances at large distances can be seen in Mobile Bay and have been documented in other sheltered estuaries and harbors with deep draft navigation such as Venice Lagoon, Italy (Parnell et al. 2015). A full understanding of the non-linear propagation is not considered in this study but could be considered in future work.

## 2 Field Investigation

### Field Stations

Data were collected at 5 stations between 18 November 2017 and 19 January 2018 (62 days). VGWE was measured identically at all stations using a pressure sensor. Stations, shown in Figure 6, were located in the upper reach of the bay at a latitude around 30.55°. Four stations were located north of Gaillard Island and west of the federal navigation channel and one east of the channel. Station locations were based on availability of existing infrastructure to affix instrumentation. Station details are provided in Table 1.

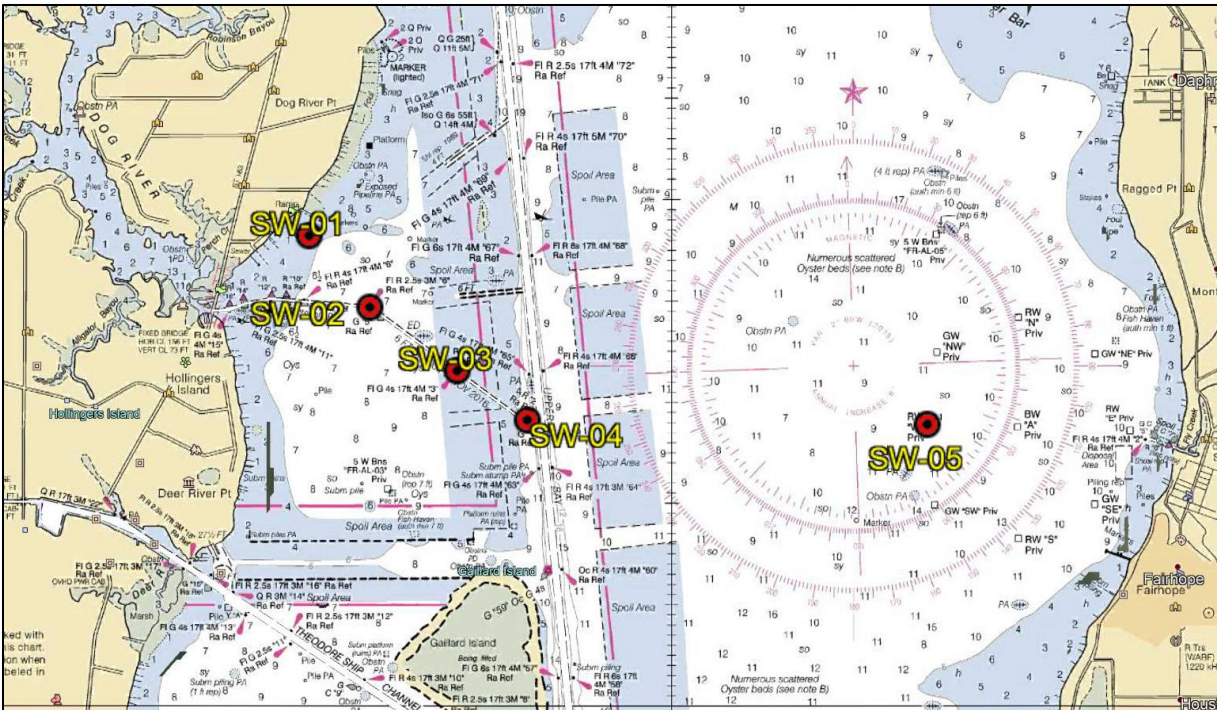


Figure 6: Map of Station Locations

Pressure sensors are manufactured by RBR Limited with a published pressure range of 20 meters, accuracy of  $\pm 0.05\%$  full scale, and resolution of  $<0.001\%$  (full scale) (RBR Limited, 2012). Sampling rate was set at 8 Hz and collected in bursts of 32,768 samples or 4,096 seconds followed by a rest period of 104 seconds to process and store data then repeated for the duration of the sampling campaign. A screen shot from the sensor software of the typical setup is shown in Figure 7. The sampling scheme produced a near continuous record for identifying the transient non-ergodic nature of VGWE. Raw data are stored as absolute pressure. Conversion to water surface elevation is completed internally based on pressure attenuation in the water column.

Table 1: Station Details

Station ID	Latitude	Longitude	Mean Water Depth, h (m)	Distance From Channel, x (m)	Sensor Serial Number
SW01	30.57770	-88.06896	2.13	3890	041460
SW02	30.56592	-88.05732	2.68	2890	041458
SW03	30.55550	-88.04062	2.6	1420	041456
SW04	30.54739	-88.02719	4.67	230	041459
SW05	30.54665	-87.97071	3.84	7080	041461

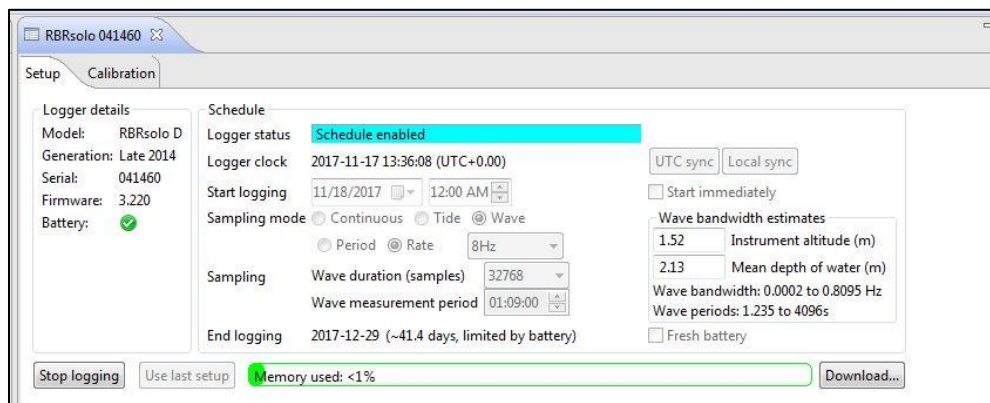


Figure 7: Typical Pressure Sensor Setup

Sensors were affixed to existing infrastructure (wooden piles) using a mount composed of rigid electrical conduit allowing the sensor to be mounted from above water and stand off the pile approximately 150 mm, see Figure 8. This mounting system provided rapid access for servicing and data downloads without requiring a diver, while maintaining a near static position.



Figure 8: Sensor Mounting System and Installation

Valid measurement frequency ranges of a pressure sensor are highly reliant on the vertical positioning in the water column. The goal is to mount the sensor as close to the surface without being exposed during extreme low tides or in this case large drawdown from a passing vessel. This phenomenon is based on the attenuation of orbital velocities and hence pressure with depth. High frequency waves, typically wind waves, attenuate more quickly than low frequency waves and can be unaccounted for in the time series if care is not taken to optimize the deployment. The sensor corrects for depth attenuation by way of the manufacture software based on the vertical location with respect to the seafloor, called altitude, and the mean depth of water. These parameters are shown graphically in Figure 9. The exact methods for attenuation used by the software are beyond the scope of this report but can be found in Gibbons et al. (2015).

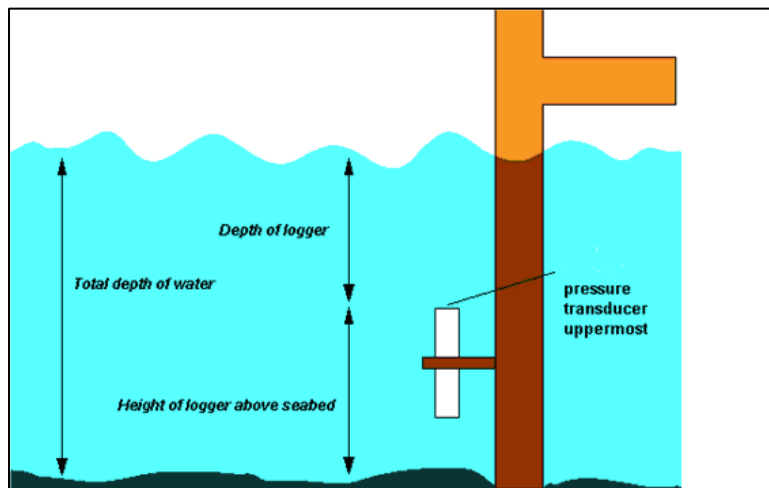


Figure 9: RBR pressure sensor deployment parameters

## AIS Data

Starting in 2002 the International Maritime Organization (IMO) began a phased implementation for certain merchant vessels to be fitted with shipborne Automatic Identification Systems (AIS) to enhance safety and efficiency in the maritime environment. The AIS system utilizes Very High Frequency (VHF) signals to transmit and receive vessel data via ship-to-ship and ship-to-shore. A network of shore-based stations are maintained by the U. S. Coast Guard (USCG). These stations receive and store AIS data which can be used in the future. A schematic of the AIS network is shown in Figure 10. Data transmission rates are dynamically based on speed over ground (SOG) and change in course over ground (COG). Average transmission rates for Class A vessels is 3 minutes but can be as fast as 2 seconds. AIS transmissions include three types of data (1) static information, (2) dynamic Information, and (3) voyage related information. (IMO, 2015)

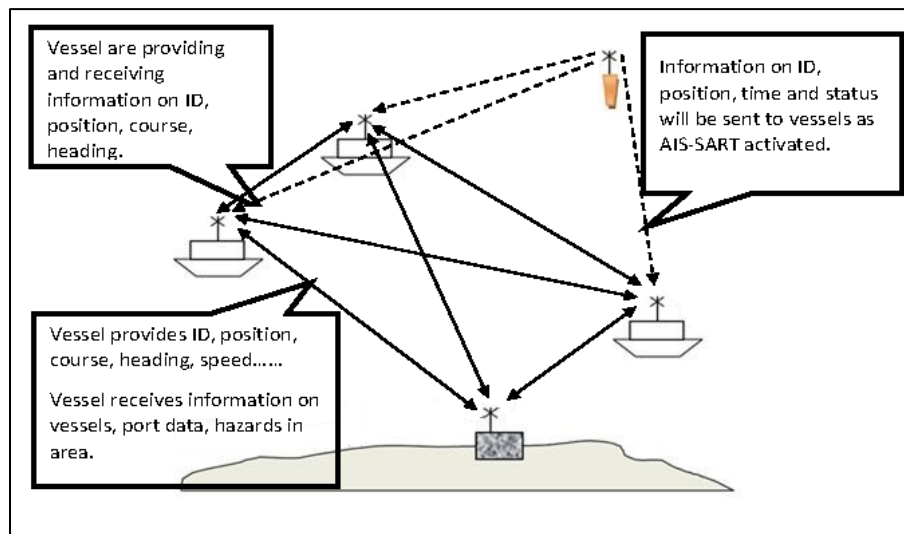


Figure 10: Automatic Information System (AIS) System Schematic. (IMO, 2015)

AIS data were used in this study to identify vessels transiting the channel in the vicinity of the field stations. For the duration of sensor deployment (18 November 2017 – 19 January 2018), AIS data were queried from the USCG via a USACE web portal which down-sampled the data to a constant rate of 5 minutes. Data were exported as vessel reports which includes some static and all dynamic data. Additionally, a single voyage record for each vessel was queried containing the remaining static and voyage data.

The static, dynamic, and voyage data records were coupled using a computer program based on the MMSI number. Continuing in the same program a data structure was created and the vessel length overall (LOA) and width (Beam) was computed based on the static location of the EPFS antenna information. The compiled AIS data were then parsed based on the needs of this study by position, length, and direction with a dependence of time. Transmissions with a position contained

in a bounding box having an upper left coordinate of 30.55919°, -88.02872° and a lower right coordinate of 30.53440°, -88.01940° were extracted. This box was defined based on the vicinity of the field stations and large enough to capture at least one record per transit for a given ship assuming an average speed of 10 knots and a sample rate of 5 minutes. Since AIS data transmission can come from all types and sizes of vessels it was found that a minimum vessel length would be needed to avoid tugs, tows, and non-commercial vessels. A minimum length of 120 m was chosen based on a review of the records and known vessel types to be avoided. Furthermore, vessels less than 120 m are not likely to generate a large enough wave energy signal to be impactful. The last filtering procedure queried within the parsed data to find records with all the same MMSI, direction, and date. If multiple records were found to have the same parameters all but one was parsed. An assumption was made that any one vessel would not transit the channel twice in the same day. This assumption proved accurate except for the Carnival Fantasy where records were manually corrected.

Vessel draft was identified at the beginning of this study to likely have a high dependence w.r.t. the VGWE. The AIS data query used unfortunately did not include the voyage file specific to the transit. Even if the voyage records were correctly attributed to a transit the data is manually entered and reliant on the crew of the vessel. Due to the reliance on vessel draft, this study requested vessel draft recorded by the Mobile Harbor Pilots for the duration of sampling which were compared and attributed to the transits.

The final AIS transit dataset for this study includes 327 records. Data quality checks were completed by randomly sampling and searching publically available data for the vessel record to verify the dimensions and class. All checks returned accurate vessel dimensions however the vessel class (type of ship) was incorrectly reported numerous times. Most incorrect entries were container ships being classified as cargo. In lieu of checking each record a length of 225 m was chosen as a break point between cargo and container vessel, where any vessel classed as cargo greater than 225 m was changed to container. The impact of this assumption could be inaccurately assigning hull geometry in the VGWE computations; however, the risk is warranted in the essence of time efficiency. Impacts to the analysis are assumed to be negligible since VGWE computations are not dependent on vessel class. Table 2 is a summary of the dataset as well as selected statistical values.

Table 2: AIS Dataset Summary Statistics

Vessel Type	Num. Transits	% Fleet	Average Speed (kts)	Average Length (m)	Average Width (m)	Average Draft (m)
<b>Overall</b>	<b>327</b>	<b>100</b>	<b>10.57</b>	<b>220.1</b>	<b>32.34</b>	<b>8.96</b>
Cargo	115	35.17	10.81	173.7	27.62	7.63
Container	117	35.78	10.44	264.4	34.85	10.57
Tanker	61	18.65	9.85	208.9	37.13	8.96
Passenger	28	8.56	11.96	260.9	32.71	8.16
Other	6	1.83	9.50	167.67	23.33	6.63

### Measured VGWE Processing Methodology

Continuous pressure data collected at a rate of 8 Hz from the 5 stations over an approximately 2 month duration equated to nearly 200 million data points. The data were imported as a water surface elevation time-series from the instrumentation software interface. From this dataset transient disturbances of short duration associated with vessel transits identified from the AIS record and thus vessel characteristics must be identified. A time dependent window is identified using the AIS data and an approximate celerity of the disturbance. The window size was chosen as 1 hour, which is much larger than the actual disturbance but served two purposes; ensure the complete vessel disturbance is captured and provide a long enough time series to estimate the measured background noise for filtering later in the data processing steps.

The standard, well established, understood, and simplistic method for completing this task is a manual delineation of the time series based on idealized water surface profiles and visual identification of maximum wave height. However this technique is subjective and not replicable for identifying the complete wave packet produced by the vessel; such that a more automated method based on a frequency spectrum would provide a more efficient and systematic approach. Spectrum analysis using a discrete Fourier transform results in a frequency domain while useful for ergodic (time-invariant) signals it is not applicable for identifying vessel generated disturbances (non-ergodic) within a larger time domain. To apply spectral analysis to a transient signal the Fourier transform can be computed in a time-frequency domain (i.e. compute Fourier transformation incrementally over the time domain). Alternatively, wavelet base transformations are similar to a Fourier base transform but defines transient and singularities using piecewise sparse representation of regular signals where coefficients are a function of the beginning and end points in small domains as well as sharp irregularities. Wavelet transformations are used widely in one-Dimensional signal processing for harmonics like audio and vibration data sets as well as two-Dimensional image processing but examples in literature for application to water waves is limited or non-existent (Chuang et al, 2013; Didenkulova et al, 2013; Sheremet, 2013).

Wavelet computations use various methodologies where a secondary but equal time dependent function,  $f(t)$ , is transformed over the time domain integral using dilation, time shift, or windowing; then summed over the time domain compared to the original  $f(t)$  in a time dependent integral over the frequency domain which creates larger coefficients across the time domain as a function of frequency modulation or a sparse representation. Wavelets for signal processing are described in more detail by Mallet (2009). A continuous wavelet transformation (CWT) variant (dilation) of the wavelet theory will be used in this study and is typically referenced in equations as  $\psi_{u,s}$ , where  $u$  is the time variable and  $s$  is the frequency variable. A CWT is well suited to 1 Dimensional, non-ergodic, datasets with sharp changes in frequency that occur in a relatively short time duration. The process can be described as a Fourier transform dilated by  $1/s$  in the nonzero positive frequency interval centered about a variable  $\eta$  creating a Heisenberg rectangle in the time-frequency plane with a range of  $(u, \eta/s)$  with time and frequency widths, respectively, proportional to  $s$  and  $1/s$  such that a variation of  $s$  will vary the cell size but not the area of the rectangle. This process is shown numerically in Equation 3 and graphically in Figure 11.

$$W f(u, s) = \langle f, \varphi_{u,s} \rangle = \int_{-\infty}^{+\infty} f(t) \frac{1}{\sqrt{s}} \varphi^* \left( \frac{t-u}{s} \right) dt \quad (3)$$

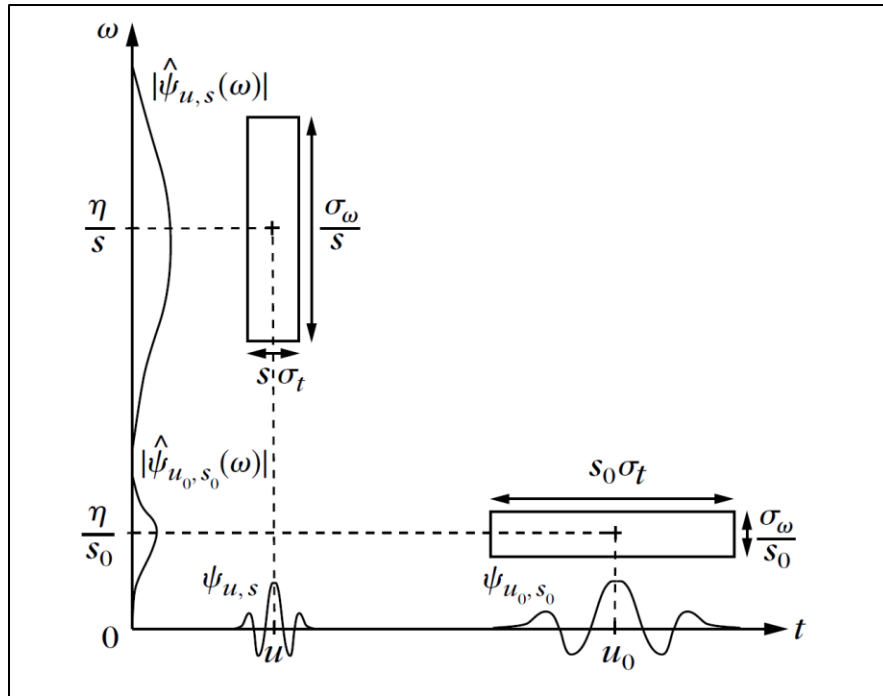


Figure 11: Time-Frequency plane representing scenarios for time variance and frequency variance of the Heisenberg box used in the CWT computation. (Mallet, 2009)

The CWT resultant is a time dependent frequency modulation (time-frequency amplitude) “spike”, related to the magnitude of frequency dissimilarity as a function of time, which is used as an identifier to parse the larger amplitude vessel disturbances from the complete time series at each station. Unfortunately, a numerical relationship between the vessel disturbance and the CWT magnitudes is not well understood or easily obtainable and was not used for directly extracting magnitudes of the vessel disturbance. The process for identification of the start and ending points begins by summing the magnitude of all frequency bins (resolution) with respect to the time domain and the resulting plot is demeaned to center about the x-axis of the time series. Demeaning the data is assumed to move lesser peaks of the resultant corresponding to noise below the x-axis. The process then identifies the maximum value and the corresponding location to either side of that maxima where it crosses the x-axis. The corresponding time of this crossing is used as the bounds and the inner data is assumed to contain the entire vessel generated disturbance. An ideal example of this process is shown in Figure 12.

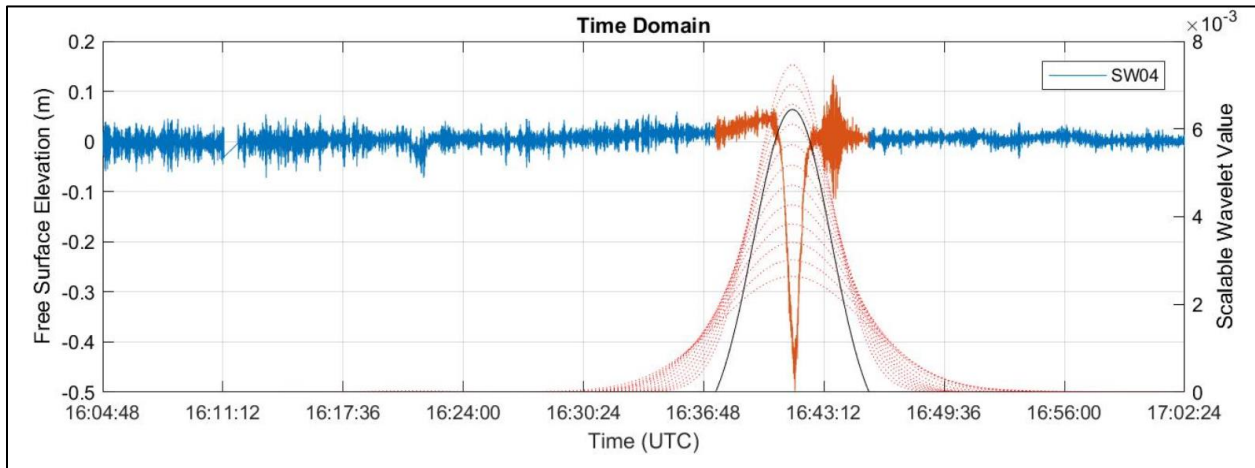


Figure 12: Ideal case of CWT used for automatic identification of a vessel generated disturbance at Station SW04, Event ID: 259 for an inbound traveling vessel with dimensions of  $L = 229$  m,  $B = 32$  m,  $D = 13.7$  m. The orange highlighted area is the signal assumed to be generated by the vessel.

Total energy density is rarely used to describe vessel disturbances. A majority of models compute the maximum vessel generated wave height, which is a good identifier and easily obtainable from a time series wave record, and some use a proxy for wave energy,  $E$ , based on the peak wave computed using Equation 4 which is based on linear wave theory and the resultant is a measure of Energy per unit crest width.

$$E = \frac{\gamma_w H^2 L}{8} \quad (4)$$

This study requires a quantifiable method to evaluate the total energy density imparted by the vessel to the water column and subsequent propagation from the sailing line to potentially impacted sites (i.e. shorelines) for adequately determining the totality of impacts investigated. The challenge for describing vessel disturbances as energy density as defined in linear wave theory is defining the length of record for an event in a repetitive method. It has been suggested to base the energy of each event on a percent of the waves within the record (Sorensen 1997) which is a good method if the record is processed using the simplistic wave train method. However, a more inclusive approach would use spectral analysis to describe the energy density in a repeatable manner.

Frequency spectrums for each event at each station were determined using a fast Fourier transform computed on the extracted time series obtained from the CWT analysis. This spectral analysis allows the energy density or in other words the spectrally significant wave height  $H_{mo}$ , to be computed by summing the area under the spectral energy curve. This method is widely used and accepted in the coastal engineering community and recommend by the Coastal Engineering Manual (2006) (CEM).  $H_{mo}$  is known as the equivalent deep water wave height. A transformation of this value to a shallow water wave height was found to create unnecessary error in the results due to multiple dependencies on origin, non-linearity, and environmental forcings. All other values describing the water surface profile in the study use the spectrally significant wave height as well which eliminates the bias within the dataset.

A summary of the data processing methodology is provided in the following logical steps.

#### I. Automated Vessel Identification (AIS)

1. Query and download data from USCG for the period of data collection (18Nov2017 - 19 Jan18).
2. Filter reports using an AOI box over the channel in close proximity to the instrumentation stations.
3. Parse filtered reported based on direction, date, and vessel so only one report will be kept for each unique vessel transit.
4. Associate vessel characteristics with the reports based on the MMSI number
5. Verify and correct drafts for each report using observed drafts obtained from the harbor pilots.
6. Filter events for vessels to return only those greater than 120 meter in length
7. Complete a quality check of data and format.

## II. Vessel Generated Wave Energy (VGWE)

1. Download continuous attenuation corrected WSE time series from instrumentation and format.
2. Define a 1 hour time window for each AIS event.
3. Identify the vessel disturbance using the CWT method.
4. Compute the frequency spectrum using a fast Fourier transformation.
5. Compute the statistically significant wave height,  $H_{mo}$ , for each event at each station by summing the area under the frequency spectrum curve.

### Results

Vessel generated wave energy (VGWE) was computed for 327 transits of vessels greater than 120 meters in length at 5 stations in Mobile Bay north of Gaillard Island. Average VGWE represented as the statistically significant wave height,  $H_{mo}$ , is provided in the following tables grouped by station and length (Table 3), draft (Table 4), transit direction (Table 5), and vessel speed (Table 6). These tables may be used to compare relative differences between measurement sites and are discussed later in this study for evaluating the relationship, holistically, with respect to vessel and transit characteristics. VGWE tabulated for each transit as well as selected AIS vessel attributes is provided in Appendix A. It should be noted, background energy density has not been filtered from any of the measured data reported unless otherwise specified.

Table 3: Average  $H_{mo}$  (VGWE) at each station categorized by vessel length

Station ID	All Vessels	Length, L (m)			
		L < 175 m	175 < L < 225	225 < L < 275	L > 275 m
SW01	0.0050	0.0026	0.0037	0.0063	0.0069
SW02	0.0084	0.0036	0.0058	0.0105	0.0132
SW03	0.0252	0.0102	0.0170	0.0276	0.0504
SW04	0.0442	0.0165	0.0278	0.0503	0.0887
SW05	0.0069	0.0055	0.0067	0.0078	0.0067

Table 4: Average  $H_{mo}$  (VGWE) at each station categorized by vessel draft

Station ID	All Vessels	Draft, D (m)			
		D < 5	5 < D < 8	8 < D < 11	D > 11
SW01	0.0050	0.0009	0.0056	0.0067	0.0041
SW02	0.0084	0.0011	0.0100	0.0117	0.0072
SW03	0.0252	0.0091	0.0316	0.0317	0.0299
SW04	0.0442	0.0106	0.0566	0.0529	0.0611
SW05	0.0069	0.0032	0.0073	0.0075	0.0071

Table 5: Average  $H_{mo}$  (VGWE) at each station categorized by transit direction

Station ID	All Vessels	Inbound	Outbound
SW01	0.0050	0.0064	0.0036
SW02	0.0084	0.0111	0.0058
SW03	0.0252	0.0269	0.0234
SW04	0.0442	0.0456	0.0428
SW05	0.0069	0.0077	0.0060

Table 6: Average  $H_{mo}$  (VGWE) at each station categorized by speed

Station ID	All Vessels	Speed, V (kts)			
		V < 8	8 < V < 10	10 < V < 12	V > 12
SW01	0.0050	0.0014	0.0027	0.0048	0.0099
SW02	0.0084	0.0017	0.0031	0.0086	0.0175
SW03	0.0252	0.0051	0.0135	0.0316	0.0277
SW04	0.0442	0.0173	0.0298	0.0546	0.0447
SW05	0.0069	0.0050	0.0073	0.0071	0.0069

Background wave energy was computed using a 1 hour time series bracketing the identified VGWE and associated with wind speed and direction data obtained from NOAA station 8736897 located approximately 10 km north of the field stations at U.S. Coast Guard Sector, Mobile, Alabama. A comparison of the measured background energy at each station with the wind speeds obtained from NOAA Station 8736897 is provided in Figure 13 where the horizontal axis is indexed by vessel transit event ID. Figure 7 is the average VGWE measured at each station categorized by recorded wind speed at NOAA station 8736897.

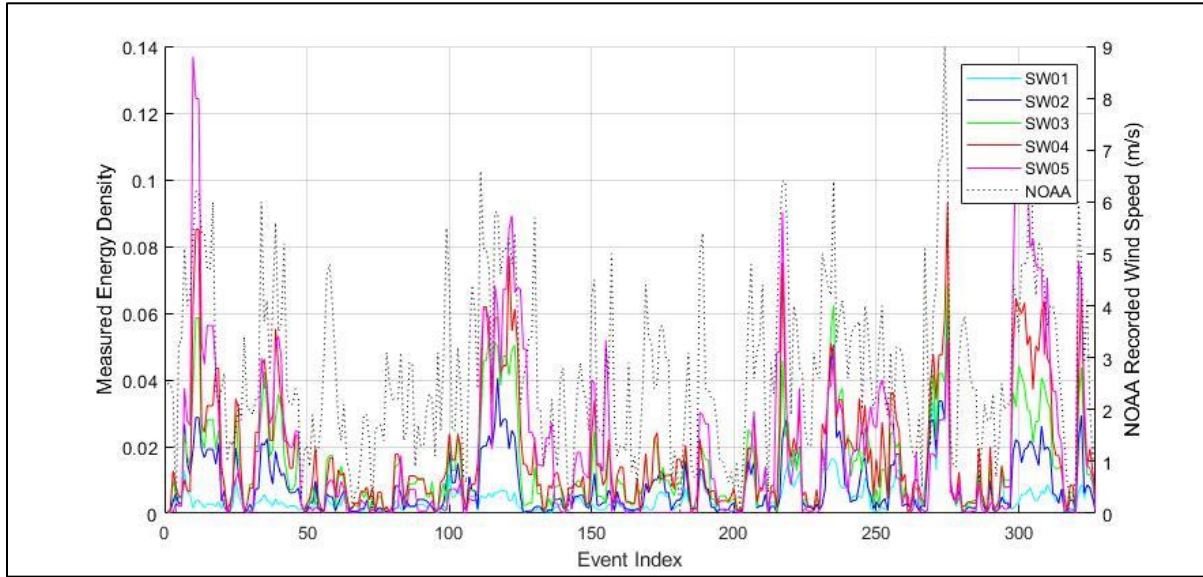


Figure 13: Comparison of measured background energy density measured at each station with the recorded wind speeds at NOAA station 8736897. The horizontal axis is indexed by vessel transit event ID.

Table 7: Average  $H_{mo}$  (VGWE) at each station categorized by wind speed recorded at NOAA station 8736897

Station ID	All Vessels	NOAA Recorded Wind Speed, $V_w$ (m/s)			
		$V_w < 1$	$1 < V_w < 3$	$3 < V_w < 5$	$V_w > 5$
SW01	0.0050	0.0047	0.0045	0.0052	0.0070
SW02	0.0084	0.0071	0.0082	0.0085	0.0108
SW03	0.0252	0.0220	0.0267	0.0215	0.0304
SW04	0.0442	0.0378	0.0446	0.0386	0.0618
SW05	0.0069	0.0017	0.0034	0.0102	0.0188

## Discussion and Data Quality

This study obtained measured VGWE for 327 vessel transits at 5 stations in Mobile Bay, Alabama based on standard, accepted, field data collection methods as well as a unique and novel post processing approach using a CWT method for VGWE demarcation. Field data are a valuable resource when properly used within bounds of the methods used to collect the data. As with any field data collection and processing, the quality and applicability should be examined. Field data are especially susceptible to poor quality and use in excess of the data collection methods. A thorough evaluation of data using expected theoretical results and comparison with any existing available data is good practice. The following paragraphs will discuss applicability of the methods,

examine data quality, and compare the field data collected in this study with expected results based on literature and theory.

The CWT method for automated identification of the vessel disturbance was efficient for this study since it involved a large number of vessel transits over long time series datasets. However, no quantitative analysis of the accuracy was completed, but observations tend to show the accuracy decreasing further from the channel. As vessel disturbances propagated SW03 and SW04 appeared more accurate than SW01 and SW02, while SW05 appears to contain the most inaccuracy. Sources of this error are a result of the numerical computation of the CWT as a function of the magnitude of background frequencies, the magnitude of the vessel disturbance, demarcation of the VGWE methods, and the width of the time window used to identify the vessel disturbance. The CWT method used in this study assumed the background frequencies and the vessel disturbance frequencies are dissimilar. If this assumption is violated the ability to identify the vessel disturbance decreases. Two examples of potential inaccurate identification are shown in Figure 14: Examples of possible inaccuracies using CWT method for extracting vessel disturbances from station time series; (upper) Event ID: 8, SW05, outbound,  $L = 176\text{m}$ ,  $B = 35\text{m}$ ,  $D = 5.8\text{m}$ ; (lower) Event ID: 24, SW02, inbound,  $L = 228\text{m}$ ,  $B = 42\text{m}$ ,  $D = 12.2\text{m}$

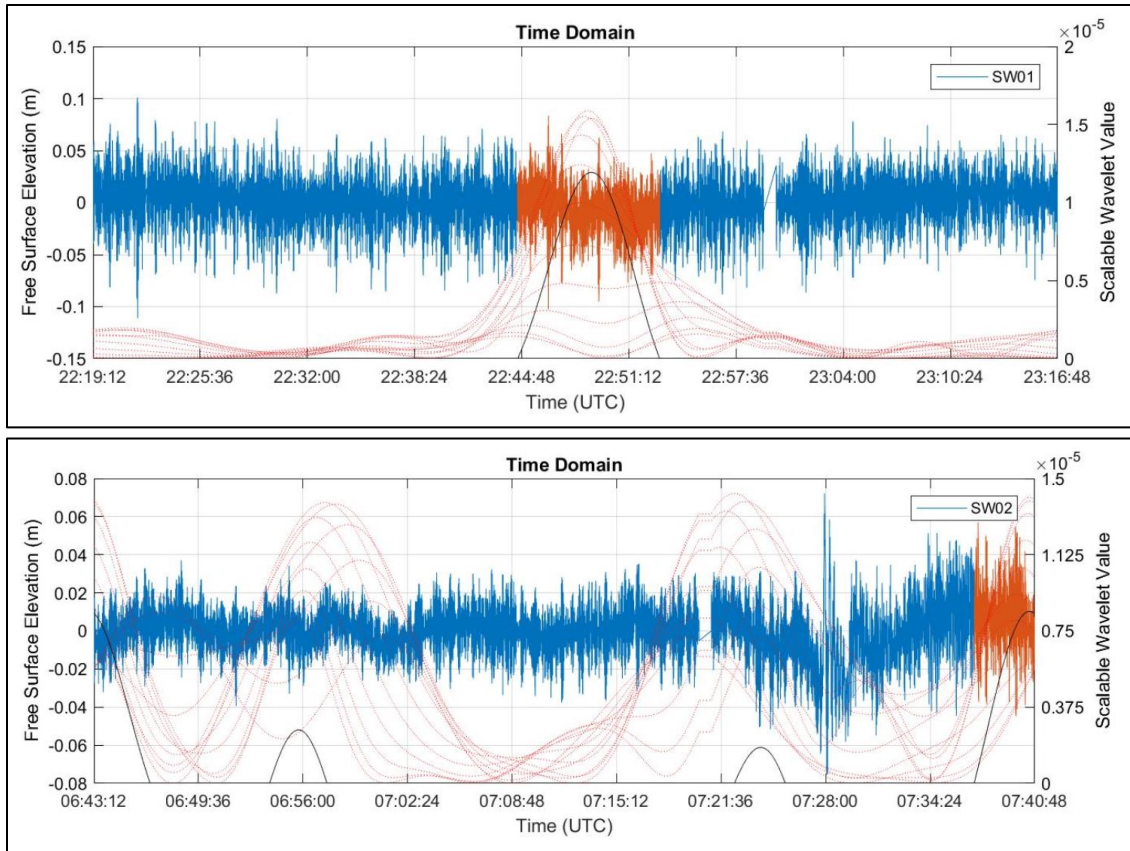


Figure 14: Examples of possible inaccuracies using CWT method for extracting vessel disturbances from station time series; (upper) Event ID: 8, SW05, outbound, L = 176m, B = 35m, D = 5.8m; (lower) Event ID: 24, SW02, inbound, L = 228m, B = 42m, D = 12.2m.

Multiple vessels transiting the channel in intervals less than 1 hour creates a second problem, when applying the CWT methods of identification. Pilots in Mobile Harbor are known to schedule multiple vessels traveling inbound or outbound within close proximity (Figure 15). And using the larger window can capture more than one vessel disturbance. The logical sequence in the automated CWT identification program does not account for this phenomenon. Since the program is only looking for the highest magnitudes of the frequency modulation (dotted red lines and black line in Figures 14-18), it can associate larger vessel disturbances with smaller vessels. While this is an inaccuracy the implications are conservative, therefore a solution is not considered for this study but could be addressed in future work.

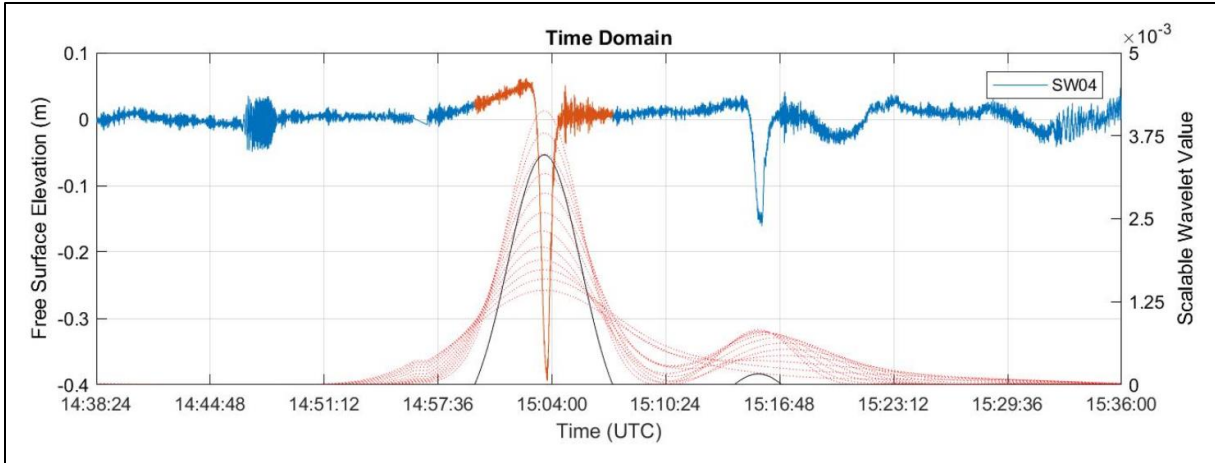


Figure 15: Multiple vessel transits with small time intervals between events.

A final observation to be noted from the CWT identification methodology is the potential for not capturing the entire VGWE signature. Again, no quantified investigation of this error was completed in the study but the error is observed more often for stations SW01, SW02, and SW05 which are farther from the sailing line. An example of this error is shown in Figure 16.

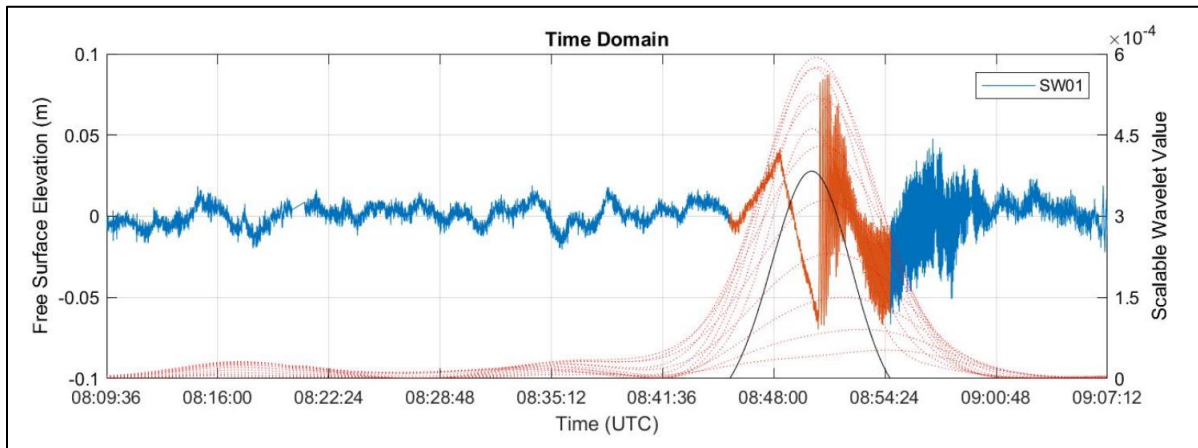


Figure 16: Vessel Generated Wave Energy (VGWE) partial identification error using the continuous wavelet transformation (CWT) method. Event ID: 203, SW01, outbound, L = 228m, B = 32m, D = 8.1m.

Quantifying the VGWE for each event at each station was completed using a fast Fourier transformation (FFT) which computed the frequency distribution, or sum of the sine waves, over the time series identified with the CWT method. The FFT provided a way to characterize the vessel disturbance by the energy density which enabled a similar and repeatable method for describing the total VGWE instead of subjective observations of the maximum wave height. Figure 17 is an example of the CWT identification method and resulting FFT for computing the frequency distribution.

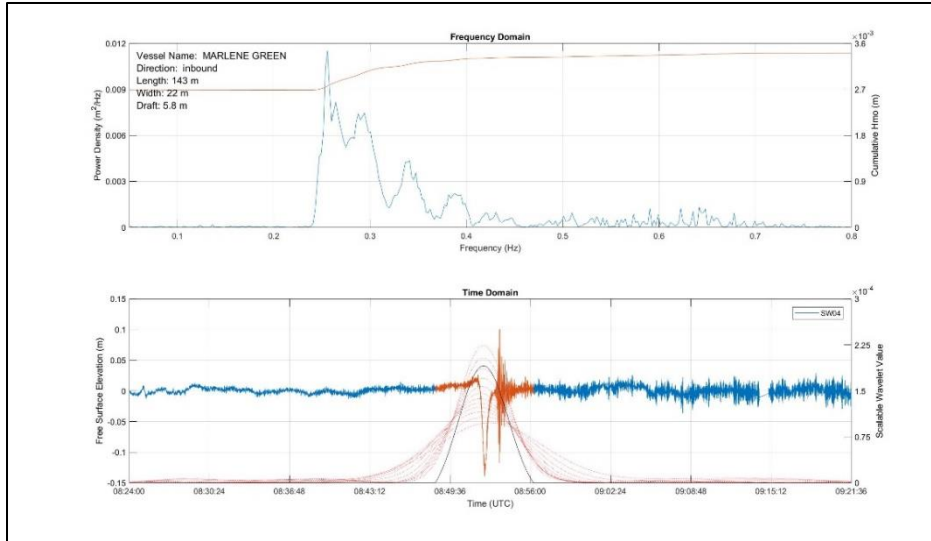


Figure 17: Vessel generated wave energy (VGWE) identification using a continuous wavelet transformation (CWT) (bottom) and frequency distribution using a fast Fourier transformation (FFT) for an ideal vessel transit event.

Figure 17 shows the distribution of frequencies in the range expected for a vessel disturbance with the peak frequencies greater than 0.05 but less than 0.4 Hz or wave periods of 2.5 to 20 seconds. The remaining higher frequencies are likely a result of the background wind-wave energy in the system or remnant disturbance of the vessel transit. However, Figure 17 is an ideal case of the CWT methodology and little background noise.

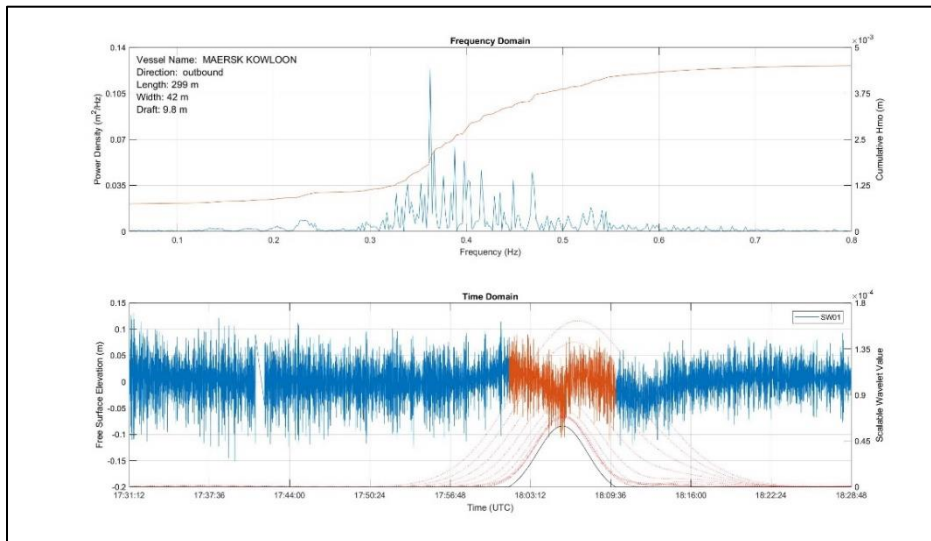


Figure 18: Vessel generated wave energy (VGWE) identification using a continuous wavelet transformation (CWT) (bottom) and frequency distribution using a fast Fourier transformation (FFT) for a case of high background wave energy with respect to VGWE.

Figure 18 represents a case of high background noise relative to the VGWE. While the CWT was able to accurately identify the VGWE signature the FFT does not appear to easily delineate the frequency distribution. The peak of distribution is located within the range of VGWE as well as a large percentage of the distribution being less than 0.4 Hz but without further investigation it would be difficult to definitively quantify the VGWE from the background energy. Due to the uncertainty caution should be used when utilizing VGWE values when the difference in magnitude of the background energy is relatively small.

VGWE propagating from the channel undergoes a transformation as a result of the interaction with bathymetry, background wind-wave energy magnitude and direction, and instabilities (non-linearity) of the signal. A detailed description of vessel generated wave transformation from a semi-confined channel is provided in the introductory theoretical background. Figure 19 is an example of that transformation across all sites.

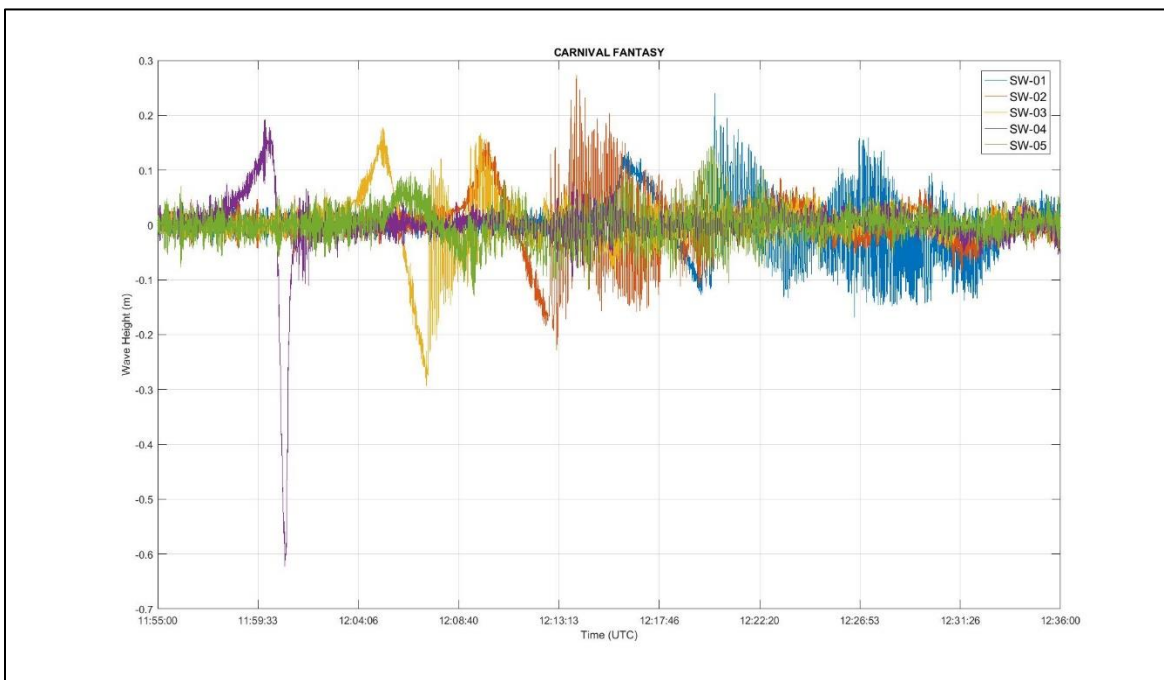


Figure 19: Example of vessel generated disturbance transformation of the free surface elevation as a function of distance from the sailing line

Several interesting, unique, and expected results are observed in Figure 19. At the station closest to the sailing line, SW04, a large asymmetric trough is observed with the leading positive surge, as the wave travels in time and spatially from the sailing line the magnitude of the trough decreases and a series of shorter period waves begin to trail the larger trough. At SW02 and further to SW01 the trough is further reduced and the trailing short period waves increase duration; however, the magnitude of trailing short period waves in SW01 is less than SW02. The leading trough in SW05 (furthest from the sailing line and opposite side of the channel) follows the same trending decay

and similarly the elongated duration of the trailing short period waves. Interestingly, the magnitude of the leading positive surge wave does not decay at the same rate as the primary trough. Surprisingly, the transformation shown in Figure 19 follows the expected theoretical decay of vessel generated disturbances. This finding confirms that regardless of the potential shortfalls in the data processing using the CWT and FFT method the time series data quality is sufficient and could be used independently for future analysis utilizing other data processing methods.

Individually, the data processing steps contain errors and in no way should those errors be discounted but as a whole the resulting VGWE should be evaluated by comparison with expected theoretical trends and dependencies. As previously mentioned this study is not intended to gain a complete and full understanding of the generation and propagation of VGWE, whereas this study intends to use data density as a way to minimize the effects of data error for the analysis. A means to determine if sufficient data density has been achieved the cumulative data measured will be compared with expected trends and more specifically the propagation of VGWE from the sailing line.

Already shown in Figure 19 the decay of VGWE as a function of distance from the sailing line is shown. However, this is a single idealized event and not necessarily representative of all transits. To better understand the cumulative data Figure 20 shows a relationship of VGWE measured over the four stations located to the west of the sailing line and the trend within each event by connecting the respective VGWE value at each station for a vessel transit.

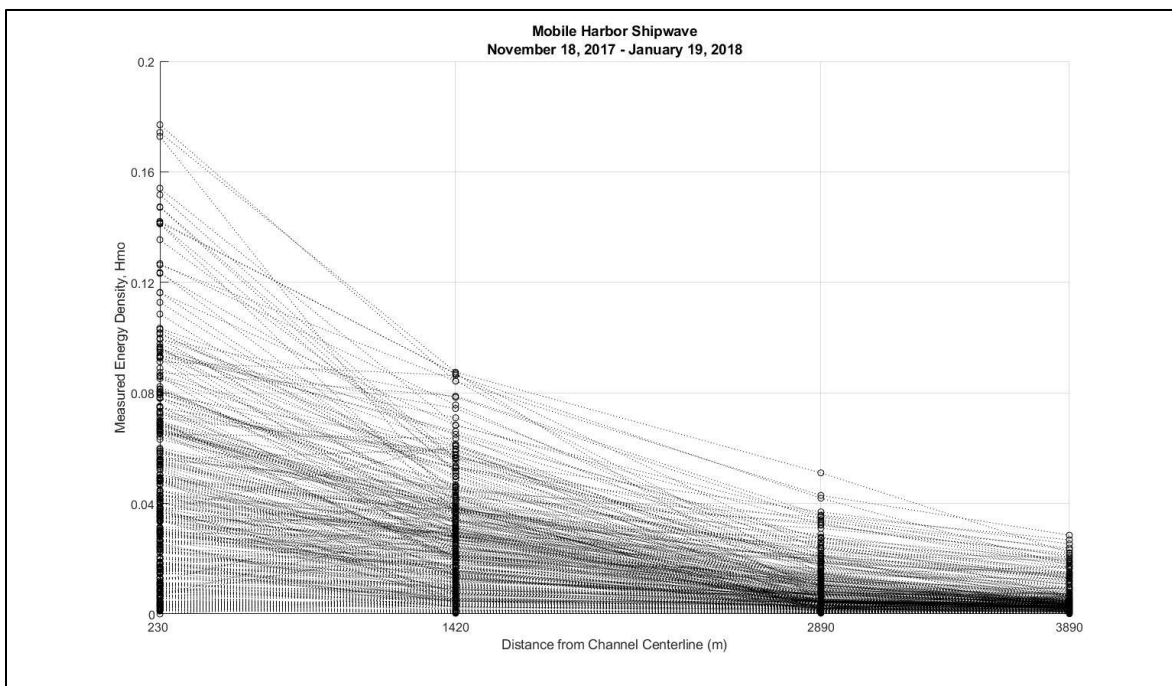


Figure 20: Measured vessel generated wave energy (VGWE) verses distance from the sailing line with respect to individual events.

The theoretical decay of VGWE as a function of distance from the sailing line in deep water is said to be,  $x^{-0.333}$ , where  $x$  is the distance from the sailing line (Havelock, 1908). However, Havelock (1908) did specify a separate exponent of -0.5 for transverse waves and Kriebel and Seelig (2005) measured ranges between -0.25 and -1.5 using field and laboratory data. Observation of Figure 20 appears to indicate the data measured in this study follow a similar trend of exponential decay with an exponent of -0.5 between stations but considerably more variation at SW01 and SW02. The variation could be a result of increased shoaling and potentially wave breaking due to water depths decreasing farther from the channel leading to a higher influence of bathymetry; all of which are not considered in the exponential decay model for VGWE.



Figure 21: Observed breaking of vessel generated wake. Photos taken looking west from an outbound tanker on 09 November 2017. Vessel dimension: L = 244 m, B = 42m. Vessel draft on the date of picture was 8.5m. Left picture was 7 km and right picture 4km north of instrumentation stations.



Figure 22: Observed wave breaking of an inbound containership approximately 2 km north of Gaillard Island from aerial imagery collected 06 November 2013. Detailed vessel description is unavailable.

Wave breaking has been observed during operations on transiting vessels and instrumentation servicing. Both pictures in Figure 21 are taken from a large outbound tanker on 09 November 2017 looking west-northwest. During this trip the observed wave breaking diminished and the breaking line moved farther from the vessel as it traveled south to a point where the breaking line was no longer visible just north of Gaillard Island. Figure 22 is aerial imagery captured on 06 November 2013 appearing to show sporadic breaking of the vessel wake produced by a large containership. Details of the vessel are not available. Figure 22 also confirms observations made while servicing instrumentation for this study and unrelated work in the vicinity north of Gaillard Island but south of the instrumentation stations. Observed wave breaking is not immediately discernable in Figure 20 for VGWE decay across the stations; however, measured data from this study were processed using a wave train analysis where vessel generated significant wave heights,  $H_s$ , (Figure 23) show a general increase in magnitude for a majority events at station SW03. This is indicative of wave

breaking and should be considered when describing VGWE propagation from the sailing line. Capturing the potential wave breaking phenomenon in the significant wave height is interesting. It also supports the use of the data processing methods described in this report in lieu of the more standard wave train approach. While future work may investigate the implication of wave breaking on VGWE to a further detail, for the study it is noted but not warranted.

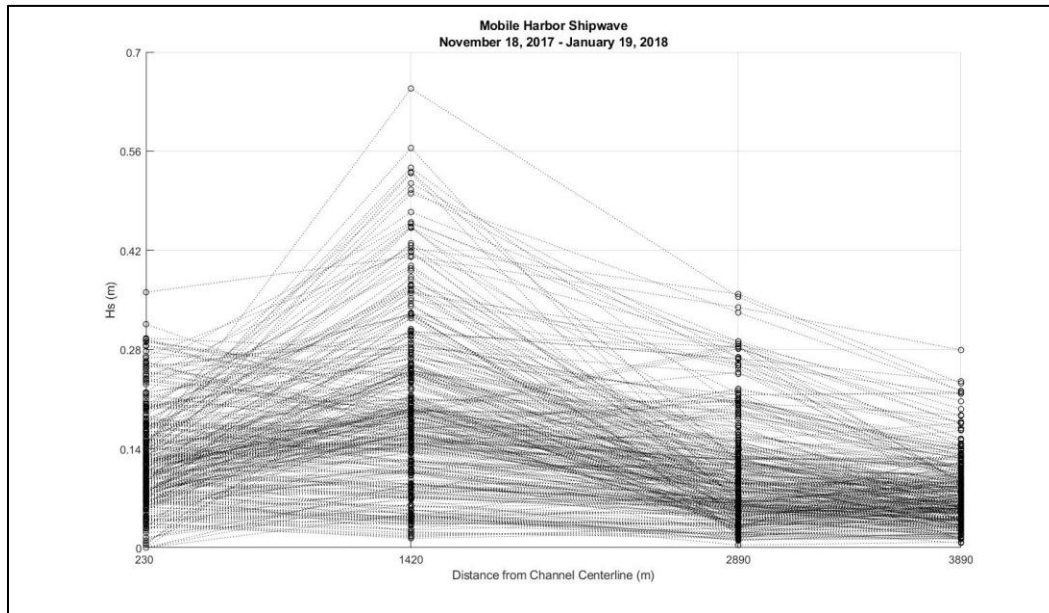


Figure 23: Vessel generated significant wave height computed using a wave train analysis verses distance from the sailing line with respect to individual events.

A secondary cause of increase of significant wave height from station SW04 to SW03 in Figure 23 is the data collection method and the manner in which the VGWE propagates over the initial distance from the sailing line. Observation while servicing instrumentation suggest the VGWE does not manifest as an undulating free surface prior to reaching SW04. This phenomenon is likely caused by the semi-confined geometry of the channel and the surge effect described in the theoretical background. The wave train method is based on a zero-crossing routine where a wave height is measured based on crossings of the horizontal axis. If undulations or crossings of the horizontal axis are not present it is impossible to quantify the energy within the vessel disturbance.

Most literature cites dependencies on vessel dimensions and speed, as described in Equation 1. Data collected in this study should follow similar dependency trends to be considered valid. VGWE relationship to vessel speed,  $V$ , is often the strongest dependency but varies significantly in literature with exponents from 0.587 (Bhowmik, 1975) to around 5.0 (Kriebel and Seelig, 2005) but most are near 2 (Gates and Herbich, 1977; U.S. Army Corps of Engineers, 1980; Blaauw et al. 1985). Vessel speed is typically non-dimensionalized and represented as the Froude Number,  $F_d$ , as presented in Equation 2. A relationship of measured VGWE and the Froude number is plotted in Figure 24 and shows a similar dependence as provided in literature. Of interest and importance

to be discussed later is the inflection, or peak, VGWE at a Froude number between 0.45 and 0.50 which is strikingly similar to a nodal point observed by Schoellhamer (1996). Sorensen and Weggel (1984) also identified a point within the Froude number range where the functional relationship changes but slightly higher. The relevance of this nodal point is the transition from subcritical to transcritical speed. It should be noted that vessel speed is reported as whole numbers. With the high dependency on vessel speed it would be advantageous to compute vessel speed from the AIS reports data to further resolve the inflection point observed in Figure 24 during future work with this data.

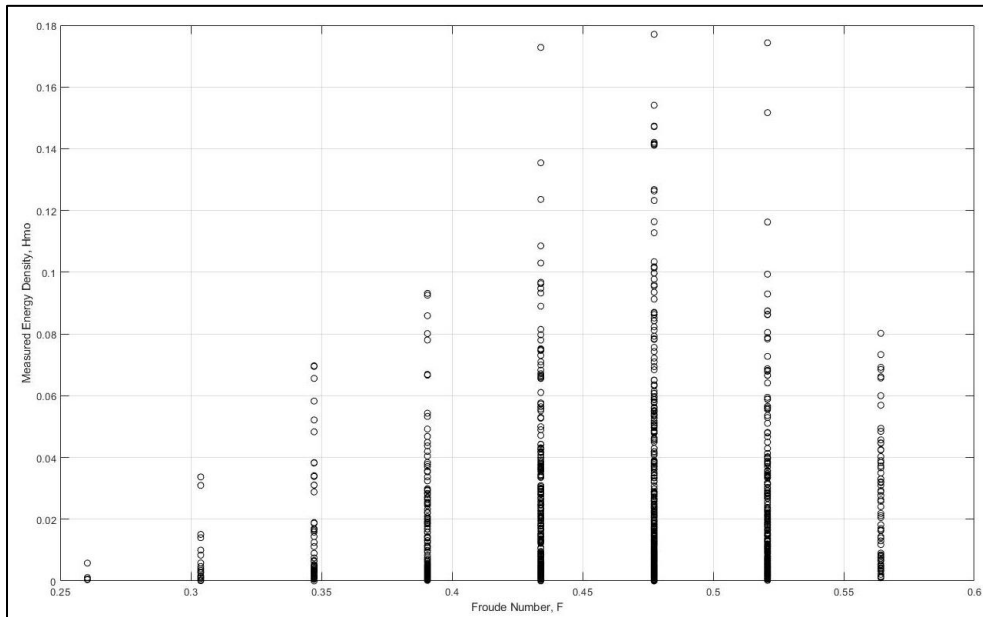


Figure 24: Measured vessel generated wave energy versus the depth based Froude number for all stations.

Vessel length is commonly referenced in published models as being a function of the VGWE to varying degrees (Sorensen, 1997). Most models in literature imbed the vessel dimension within a secondary parameter or function such as the blocking coefficient,  $S_c$ , (defined later in this study) or some other non-dimensional parameter. For simplicity the vessel length,  $L$ , and draft,  $D$ , were compared to the measured VGWE independently (Figure 25); vessel width is not shown as there was no distinctly observed relationship. While this simplistic method is difficult to compare directly with existing literature it will provide a relative understanding of the relationships to draw conclusions during the second part of this study.

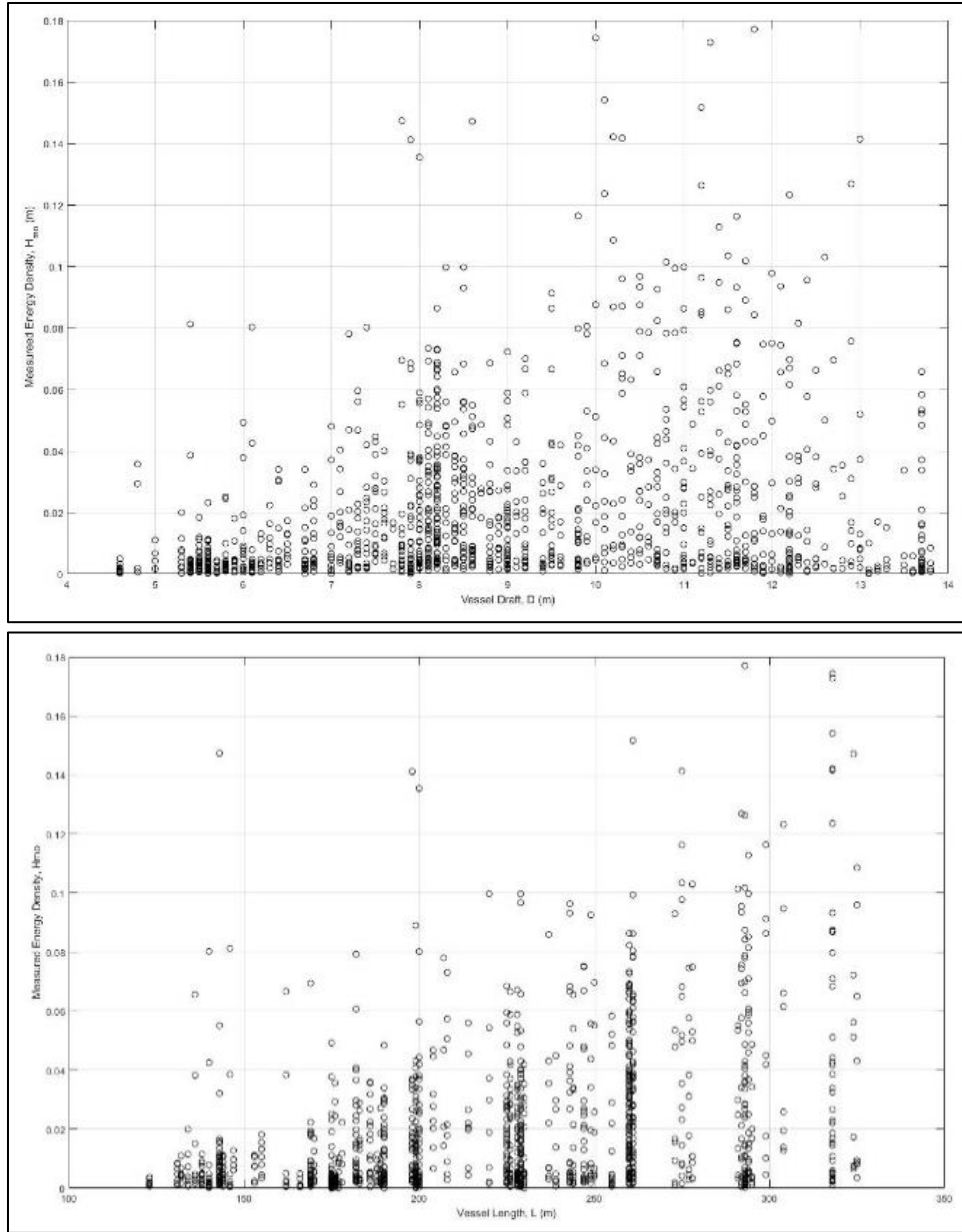


Figure 25: Measure vessel generated wave energy (VGWE) verse vessel draft (top) and vessel length (bottom).

Background energy density was computed using the same methods as for the VGWE except the window size of the data was chosen to be 1 hour. It is assumed all of the background energy computed is attributed to wind-wave energy and Figure 13 shows the measured background energy follows a similar trend as the recorded wind speed at NOAA station 8736897 supporting this assumption. A few exceptions to the trend are noted and appear to be lapses in either measured or NOAA data. The relationship between background wave energy and measured VGWE was investigated and found not to be related. It is well known wind-wave interaction and wave-wave interaction are realized; however, data quality errors are likely larger than influence of background

energy such that background energy cannot be extracted from the VGWE without potentially further inducing data errors in the VGWE.

## **Summary**

This field data study investigated vessel generated wave energy (VGWE) in Mobile Bay, Alabama using a suite of 5 pressure sensors located north of Gaillard Island. Data were collected continuously at a rate of 8 Hz between 18 November 2017 and 19 January 2018 (62 days). A unique and efficient method of data processing was employed using a continuous wavelet transformation (CWT) to extract the vessel generated disturbances from a continuous time series by utilizing frequency modulation or “chirp” signal produced. The CWT method is shown to be valid within the context of large data sets where random errors can be averaged. The VGWE was computed on the extracted time series using a fast Fourier transformation which is widely accepted and used for describing energy of a time series and the method proved successful for this study with the exception of cases with higher background energy or weak VGWE signals, specifically SW01, SW02, and SW05. VGWE at station SW05 was extremely weak and difficult to identify within the background energy, therefore it is recommended data from SW05 not be used for any further analysis. VGWE computed using field data in this study compared well with expected results based on theoretical values and dependencies. Overall, the field data collected in this study has proved to be valid when used for general trending. However, any subsampling of the dataset should be used with caution as random errors are realized.

Vessel characteristics were attributed to the computed VGWE using data from the Shipborne Automatic Identification System (AIS). AIS data was shown to be accurate for vessel dimensions but several errors in actual vessel draft were identified. Vessel speed is reported by the AIS data as whole numbers. While this is a practical definition for speed in the maritime industry, better understanding of the strong dependence between vessel speed and VGWE could be improved with higher precision computed using distance and time between AIS reports.

### 3 Computing Vessel Generated Wave Energy

---

Computing VGWE for semi-constricted channels is a complex task due to dependence on site specific variables. A large number of predictive models, using regression analysis, are published and careful consideration should be given to selecting an approach applicable to Mobile Bay. Mobile Bay is considered a semi-constricted channel and this study is focused on the VGWE a distance from the channel which implies channel geometry and distance from the sailing line should be included in the selected model in addition to variables identified previously for vessel characteristics such as speed and dimensions. A review of well-established and other recent and less known methods resulted in three models being identified for further evaluation along with several supporting references to better refine determinants. This chapter describes the three models identified as most applicable to the study area and validation using the measured data.

#### Predictive Models

*Sorensen and Weggel (1984):*

Sorensen and Weggel (1984) and Weggel and Sorenson (1986) is an often cited method for computing vessel generated maximum wave heights. Sorensen and Weggel (1984) is an interim report describing the initial model development and applicability based on an accumulation of data available in literature for laboratory and field studies. The initial regression analysis was based on field data provided in Sorensen (1966) which included vessels having a displacement between 0.00136 tonnes (3 tons) and 8.528 tonnes (18,800 tons), lengths from 7 m (23 ft) to 154 m (504 ft), and drafts of 0.52 m (1.7 feet) to 8.53 m (28 feet). The authors focused on the relationship of displacement,  $W$ , and through dimensional analysis developed the variables provided in the following equations for wave height, distance from sailing line, and depth as well as the Froude number,  $F_d$ , defined in Equation 2.

$$\frac{H}{W^{1/3}} = H^* \quad \text{dimensionless wave height}$$

$$\frac{x}{W^{1/3}} = x^* \quad \text{dimensionless distance from sailing line}$$

$$\frac{d}{W^{1/3}} = d^* \quad \text{dimensionless depth}$$

Explicit non-dimensional terms for vessel length, beam, and draft having a similar relationship to vessel displacement were considered as well but not included in the resulting regression analysis model publish. Since the vessel dimensions can be considered dependent variables of the

displacement it is logical these relationships were omitted since the dimensions would be captured in the vessel displacement. Using the non-dimensional variables described above Sorensen and Weggel (1984) presented the following empirical equation to predict maximum wave height generated by a passing vessel.

$$H^* = \alpha x^{*n} \quad (5)$$

The equation is based on the exponential relationship of distance from sailing line Havelock (1908) suggested and where Weggel and Sorensen (1984) showed the exponent,  $n$ , to be a function of the Froude number by the following relationship.

$$n = \beta d^{*\delta} \quad (6)$$

Both  $\beta$  and  $\delta$  are functions of the Froude number and defined by explicit ranges shown below

$$\begin{aligned} \beta &= -0.225 F_d^{-0.699} & \text{for } 0.2 \leq F_d \leq 0.55 \\ \beta &= -0.342 & \text{for } 0.55 \leq F_d \leq 0.88 \end{aligned}$$

and,

$$\begin{aligned} \delta &= -0.118 F_d^{-0.356} & \text{for } 0.2 \leq F_d \leq 0.55 \\ \delta &= -0.146 & \text{for } 0.55 \leq F_d \leq 0.88 \end{aligned}$$

The variable  $\alpha$  is also a function of the Froude number as well as the non-dimensional depth,  $d^*$ , as shown in the logarithmic second degree polynomial expression.

$$\log_{10} \alpha = a + b \log_{10}(d^*) + c \log_{10}^2(d^*) \quad (7)$$

where,

$$a = \frac{-0.6}{F_d} \quad b = 0.75 F_d^{-1.125} \quad c = 2.653 F_d - 1.95$$

The equations presented above by Sorensen and Weggel (1984) provide a method to compute vessel generated maximum wave heights within the bounds of data provided in Sorensen (1966). Weggel and Sorensen (1986) went on to provide a validation of the method using data from 11 data sources for 12 classes of vessels resulting in a modified version of Equation 5 using two additional coefficients  $A'$  and  $B'$  which are vessel class specific. The coefficients better define the vessel geometry, are vessel class specific, and range from 0.0 to 3.52.

$$H^* = A'H^*(\alpha x^{*n}) - B' \quad (8)$$

The modified method provided by Weggel and Sorensen (1986) in Equation 8 increased the applicability to additional vessel classes. However, it is noted by the authors the data were not consistent and sometimes not well defined leading to uncertainty. It is recommended the model only be used to compute the maximum vessel generated wave height,  $H_m$ , for low vessel draft to water depth ratios and limited ranges of the Froude number as defined in Weggel and Sorensen (1986).

*Kriebel and Seelig (2005):*

An empirical model for computing vessel generated wave heights was investigated by Kriebel and Seelig (2005). The model was based on 1,200 unique tests of laboratory data available in literature. The empirical relationship was then validated using field trials in a controlled setting within Chesapeake Bay, Maryland conducted by the authors using a small naval training vessel. The vessel was 31.1 m in length, 6.5 m beam, draft of 1.83 m, 154.7 m<sup>3</sup> displacement, block coefficient,  $C_b$ , of 0.41 and a  $Le/L$  ratio of 0.4. Tests were varied by vessel speed and ranged from 3.6 to 5.1 m/sec and data were collected at intervals of distance from the sailing line between 15 and 122 m.

Model development sought to more explicitly define the velocity head,  $V^2/2g$ , by normalizing in the form of  $gH/V^2$ . A second, and more significant, improvement over prior models was simplifying and normalizing model dependencies for wave attenuation as a ratio of distance from sailing line,  $x$ , to length of vessel,  $L$  given in Equation 9.

$$\left(\frac{x}{L}\right)^{-1/3} \quad (9)$$

The exponential decay of this relationship with respect to wave height was tested independently using all 1,200 unique tests which found the theoretical exponent given by Havelock (1908) of -0.3333 gave the best fit to the majority of data points and was used in the final model. However, it is noted the best fit for each set of test data ranged from -0.2 to -1.5 but no conclusive trend was apparent. The authors stated an exponent of -0.333 was most appropriate for higher speed tests but did not quantify the speed range or trend to side.

From the velocity head and distance attenuation dependencies the model was developed and incorporated sufficient function using a modified Froude number  $F^*$  given in Equation 10 which incorporated length and depth based Froude number relationships to function over deep and shallow water applications.

$$F^* = \frac{V}{\sqrt{gL}} \exp(\alpha D/d) \quad (10)$$

The modified Froude number was included in the empirical relationship and along with the velocity head and distance attenuation relationships, Equation 11 was produced for computing maximum vessel generated wave heights.

$$\frac{gH}{V^2} = \beta(F^* - 0.1)^2 \left(\frac{x}{L}\right)^{-1/3} \quad (11)$$

where,

$$\alpha = 2.35(1 - C_b) \quad \beta = 1 + 8 \tanh^3 \left( 0.45 \left( \frac{L}{L_e} - 2 \right) \right)$$

$$C_b = \frac{W}{L*B*D}$$

The entrance length,  $L_e$ , is typically a measured value representative of the bow geometry but can be estimated using Equation 12 provided in Gates and Herbich (1977) based on 16 tanker and bulk cargo ships.

$$\frac{L_e}{L} = 0.417 - 0.00235L \quad (12)$$

The model presented in Kriebel and Seelig (2005) was validated over a range of vessel speeds and distances but it is noted a range of 0.1 to 0.5 for the modified Froude number,  $F^*$ , computed using Equation 10 should be observed for applicability, and further limited to when the velocity head,  $gH/V_2$ , does not exceed 0.4.

*Schoellhamer (1996):*

A regression analysis using data collected for a site specific field study developed a relationship between amplitude of vessel generated long wave (normalized by water depth at measurement location), the depth-based Froude number,  $F_d$ , and the blocking coefficient,  $S_c$ . The blocking coefficient is a ratio of the vessel cross-section and the channel cross-section as defined in Equation 13.

$$S_c = \frac{B*D}{b*d} \quad (13)$$

The field study was completed in Hillsborough Bay, FL which has an average depth of 3.2 m and is transected by a semi-confined deep draft navigation channel approximately 11-13 m deep and 150 m wide with depths of 5 m immediately adjacent, according to current nautical charts. Three field sites were established, two within 1 km of the channel in water depths of approximately 5 meters and a third approximately 3 km from the channel with a water depth of approximately 1 meter. Instrumentation included near bottom velocity probes and a pressure transducer sampling at a rate of 2 Hz. Instrument deployment was sporadic and varied between sites but for the vessel long wave analysis 4 continuous days of sampling were used. During these 4 days a total of 28 large vessels (> 100 m) transiting the channel were identified. Using data from these vessels a regression analysis provided a simple model defined by Equation 14.

$$\frac{H}{h} = F_d^{2.4} S_c^{1.6} \quad (14)$$

The vessels used in this analysis were characterized by the Froude number ranging from 0.29 – 0.84 and the blocking coefficient ranging from 0.033 – 0.22. It is stated that only 57% of the vessels generated a long wave at the near channel sites and 29% of vessel transits observed long waves at the far site which the author correlated to ranges of Froude numbers such that long waves were not observed when the Froude number was less than 0.48 and always observed for Froude numbers greater than 0.54.

## Discussion

The first two models, Sorensen and Weggel (1984) and Kriebel and Seelig (2005) are well known and commonly cited for predicting vessel generated maximum wave heights. Both of these models have parts that may be applicable and provides a base of theory and approach when evaluating vessel wakes by emphasizing the criticality of dependence on the Froude number and vessel dimensions. However, neither model take into account channel geometry. It is known channel geometry will affect the vessel disturbance and as such each of these models as a whole should be discarded for use in Mobile Bay, less the knowledge gleaned from the magnitude of dependencies of those variables presented. Kriebel and Seelig (2005) went beyond the original Sorensen and Weggel (1984) work by better and more simplistically defining and validating the theoretical relationship of distance from the sailing line. A novel approach to normalize the inverse cube root distance function, described in the theoretical background, as a ratio to vessel length will be considered for applicability in the computation of VGWE for this study in Mobile Bay, Alabama as well as the variation of exponential decay as a function of vessel speed.

Schoellhamer (1996) is lesser known for contributions to the computation of vessel generated disturbances but was identified for this study based on the stark similarities between Mobile Bay and the field study site used in his analysis. The vessel ranges and speeds used are also surprisingly similar and will be helpful for comparison in this study. Finally, the simplistic and inclusive nature

of the predictive equation published by Schoellhamer (1996) is appealing. However, the field data collection chapter showed vessel length and distance from sailing line have some relationship with VGWE and neither are considered in the Schoellhamer (1996) model implying VGWE does not decay as a function of distance from the sailing line such that at a constant depth VGWE would continue infinitely. If assuming a Kelvin wake theory this assumption would be illogical but more recent work by Soomere (2006) using non-linear wave theories suggests VGWE does not decay at an exponential rate, potentially persists for long distances from the sailing line, and consistent with properties of non-linear wave theory discussed by others in Chapter 1.

Schoellhamer (1996) did not provide any discussion to omitting distance from the sailing line but considering the farthest station in his work was not validated in the model suggests a potential shortfall when applied to far lateral distances. In Equation 14, water depth at the point of measurement is used to non-dimensionalize the left hand side of the equation. However, depth at the measurement station cannot be directly related to VGWE theories for either linear or non-linear waves. Inclusion of depth at the measurement station is most likely to compensate or at least provide a proxy for distance from the sailing line such that the decay in Equation 14 is entirely dependent on shallow water dispersion relationships.

Predictive models for computed maximum vessel generated wave heights presented in Sorensen and Weggel (1984), Kriebel and Seelig (2005), and Schoellhamer (1996) were reviewed in the previous section and critically discussed above. The methodology and resulting equations were presented in detail as well as the stated applicability per the respective author. Each model was shown to have some constructive qualities and this study will attempt to leverage each of these model's strengths to produce a model that may be more applicable to Mobile Bay, Alabama.

## **Validation**

Vessel Generated Wave Energy (VGWE) was best estimated at stations SW01 through SW04 (SW05 omitted due to data quality) using the model from Schoellhamer (1996) as described in Equation 14. The computed values were compared using a one-to-one plot with the measured VGWE. Figure 26 shows all data points and a best fit linear regression curve (red line). The black line represents a perfect one-to-one relationship.

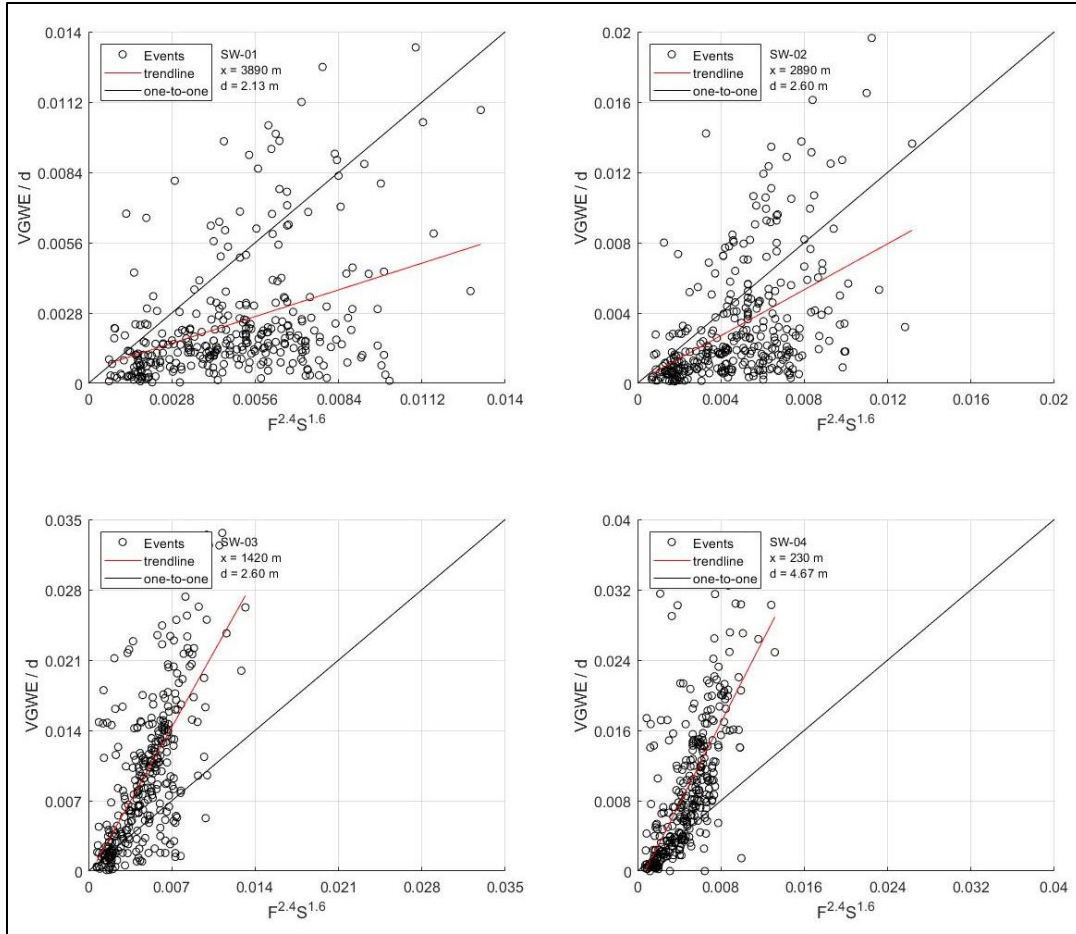


Figure 26: One-to-One correlation plot of measured vessel generated wave energy (VGWE) and the equation from Schoellhamer (1996) for stations SW01 through SW04.

It is evident from Figure 26, Equation 14 underestimates the VGWE at Stations SW03 and SW04 but appear to follow a related trend and are collapsed on the regression curve. SW01 and SW02 are over predicted for all but the higher values of measured VGWE which do not appear consistent with the majority grouping below the one-to-one line. Filtered points for the higher measured energy density for SW01 and SW02 have a strong correlation to the Froude number within a range of  $F > 0.5$ . This secondary correlation (Figure 27) shows the relationship for Froude numbers greater than 0.5 with the regression line following those values of the Froude number.

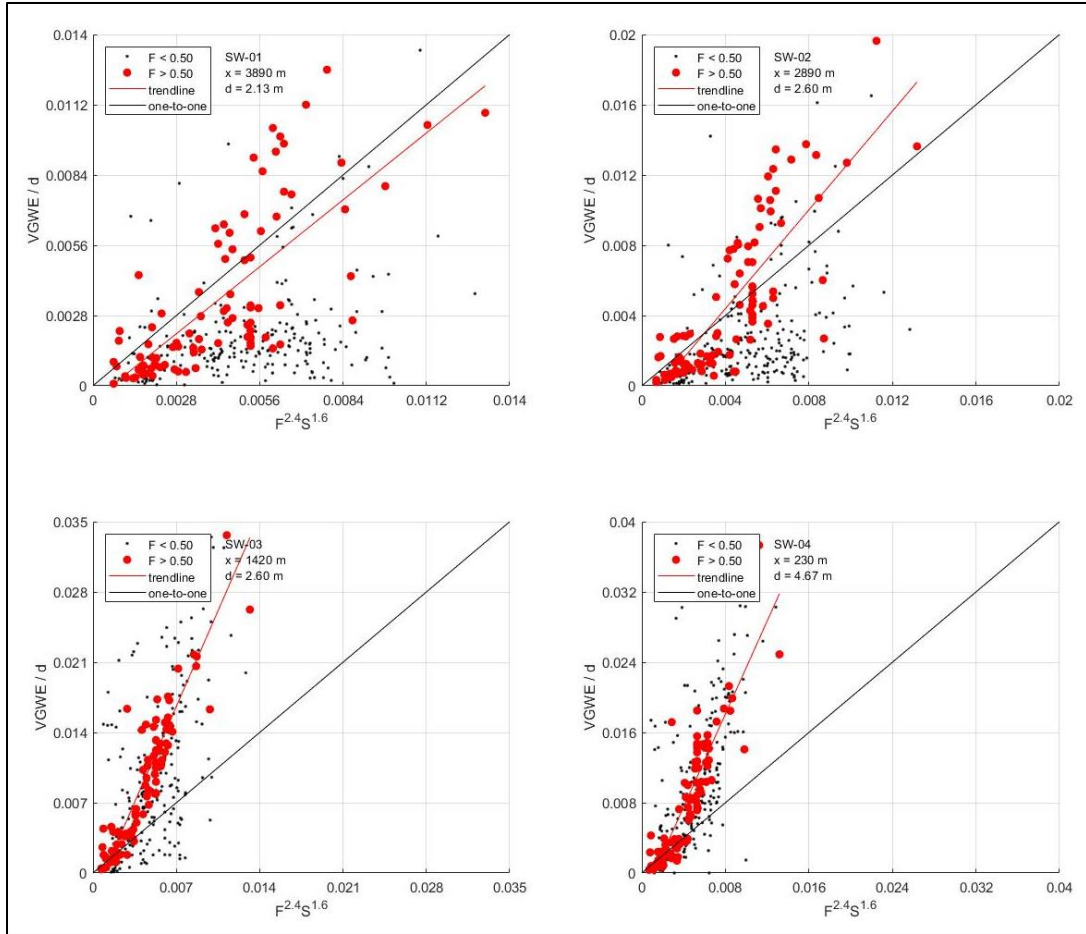


Figure 27: One-to-One correlation plot of measured vessel generated wave energy (VGWE) categorized by Froude number and the equation from Schoellhamer (1996) for stations SW01 through SW04. The regression line follows Froude numbers greater than 0.5.

Data points corresponding to  $F > 0.5$  collapse about the linear regression curve (red line) at all sites and to a higher degree for SW01 and SW02 but now data points corresponding to  $F > 0.5$  for SW01 and SW02 are above the one-to-one line leading to the Schoellhamer (1996) model now over predicting these stations as well. With the information presented in the theoretical background and field data collection chapter as it relates to the inflection point of the Froude number, it is interesting to note the Schoellhamer (1996) equation collapses data points more for larger Froude numbers in the transcritical range as opposed to the subcritical values which are better described using linear wave theory methods. Other data point filters based on known dependent relationships were tested and none produced as strong a relationship as the Froude number. However, one interesting find is the relationship to transit direction. Figure 28 is the same one-to-one plot relationship but the data are categorized by transit direction.

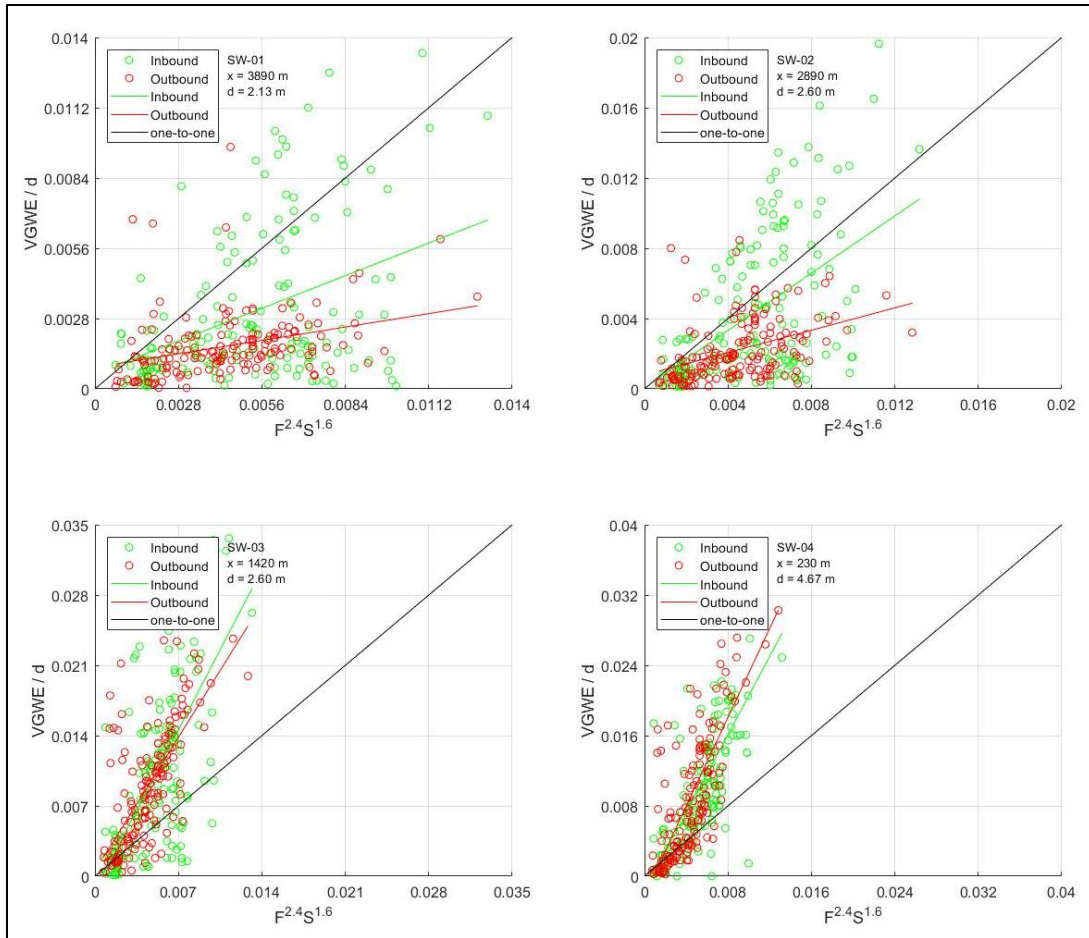


Figure 28: One-to-One correlation plot of measured vessel generated wave energy (VGWE) and the equation from Schoellhamer (1996) for stations SW01 through SW04 categorized by direction of vessel transit. The regression line is color coded to match the respective transit direction.

From Figure 28, SW01 and SW02 appear to show a relationship with transit direction. SW03 and SW04 do not show this same variance nor any other distinguishable characteristics between the transit directions. From the field data collection chapter wave breaking was observed to a higher degree on outbound transits. Wave breaking is, by definition, a loss of energy where by the outbound transits should be measured lower than computed using Equation 15. As a result it can be assumed wave breaking is likely contributing to the scatter observed at SW01 and SW02. Since wave breaking is not a function within Equation 14 these values should not be considered when evaluating the applicability within the correlation plots. However, without further evaluation and better spatial resolution the wave breaking relationship could be a coincidence and not realized in the data.

## South Bay Validation

Following the initial study and upon external and internal peer review it was suggested the lower bay may not be in agreement with results from the field study and regression analysis completed in the northern bay. In response, this study initiated additional field data collection efforts in southern Mobile Bay at the sites shown in Figure 29. Instrumentation was deployed over a period between December 21, 2018 and February 5, 2019. The sampling plan followed the same methodology and processing as the original northern bay deployment described in Chapter 3.

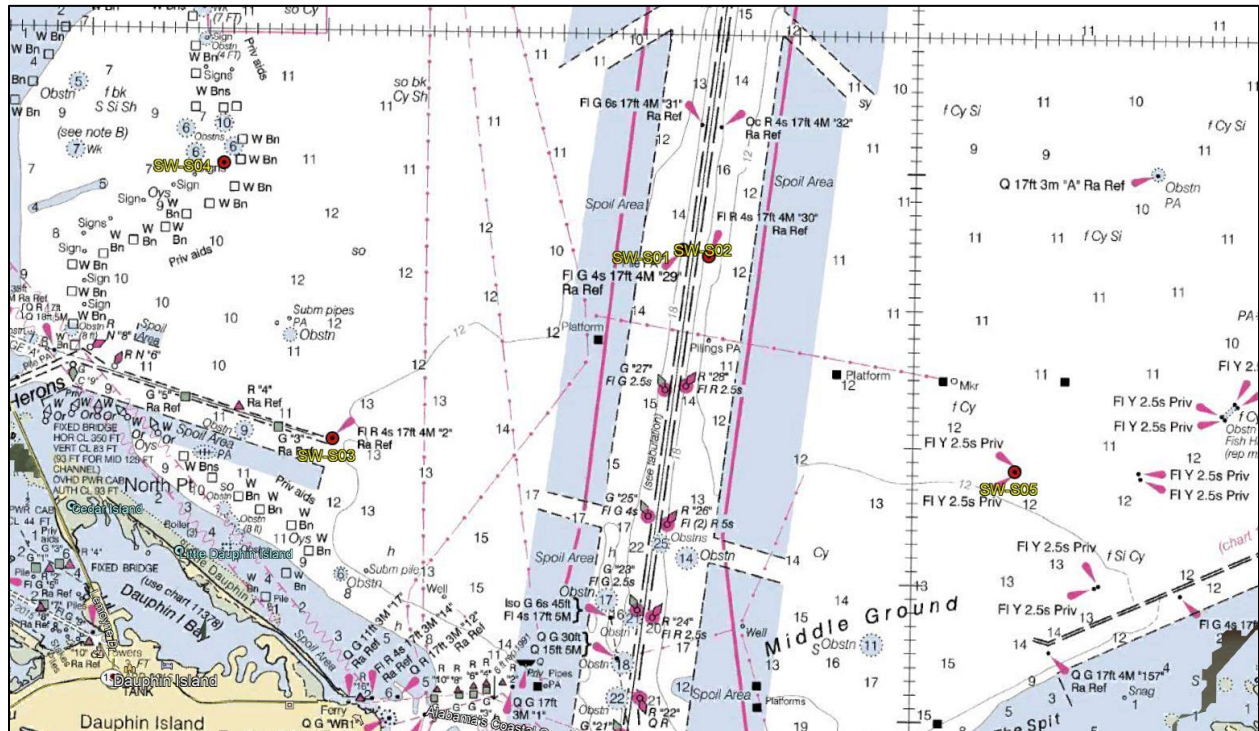


Figure 29: Southern Bay Station Locations

Over the period of deployment 214 vessel transits were obtained from the AIS data for vessel greater than 122 meters. These transits were made up of a similar distribution of vessel dimensions and classes. Meteorological conditions during this period were similar but not identical such that precipitation over the watershed was greater resulting in higher river flows. This difference is insignificant based on the lack of dependence proven during the original deployment. An obvious and relevant difference between the deployments is the distance of sites to the channel. The relationship of site location to channel is noted but accounted for in the processing and does not bias the validation findings. Validation of the Schoellhamer (1996) model based on one-to-one plots is shown in the follow figures.

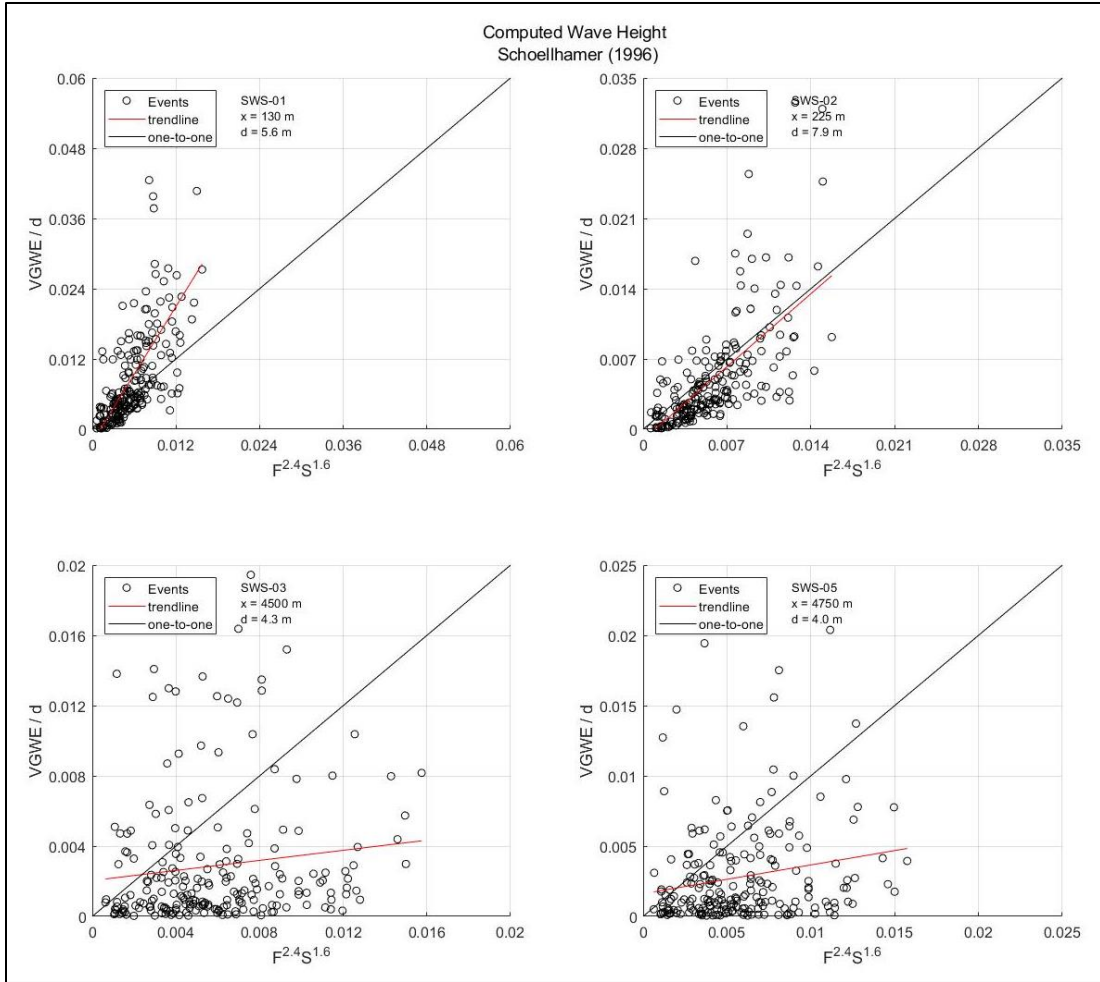


Figure 30: One-to-One correlation plot of measured vessel generated wave energy (VGWE) at the south bay validation sites and the equation from Schoellhamer (1996) for stations SWS01 through SWS03 and SW05.

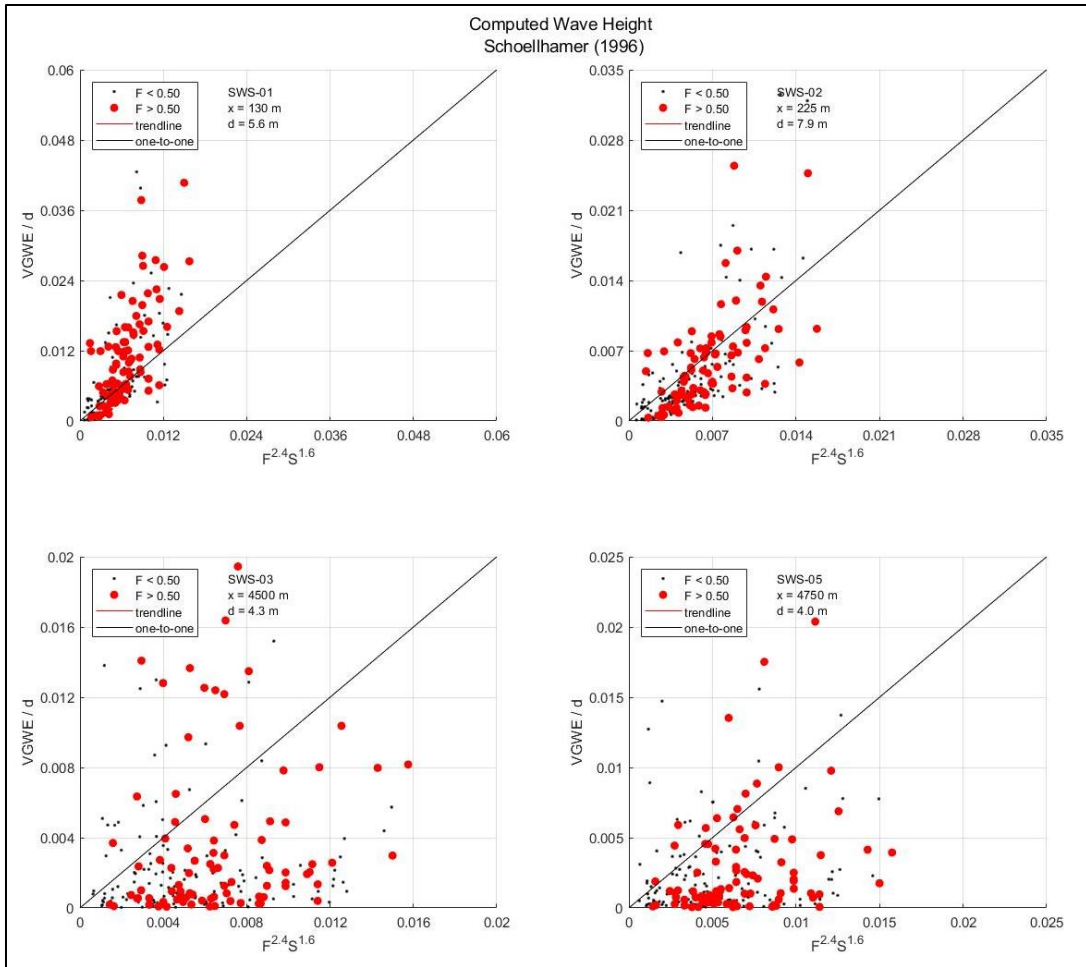


Figure 31: One-to-One correlation plot of measured vessel generated wave energy (VGWE) at the south bay validation sites categorized by Froude number and the equation from Schoellhamer (1996) for stations SWS01 through SWS03 and SW05. The regression line follows Froude numbers greater than 0.5.

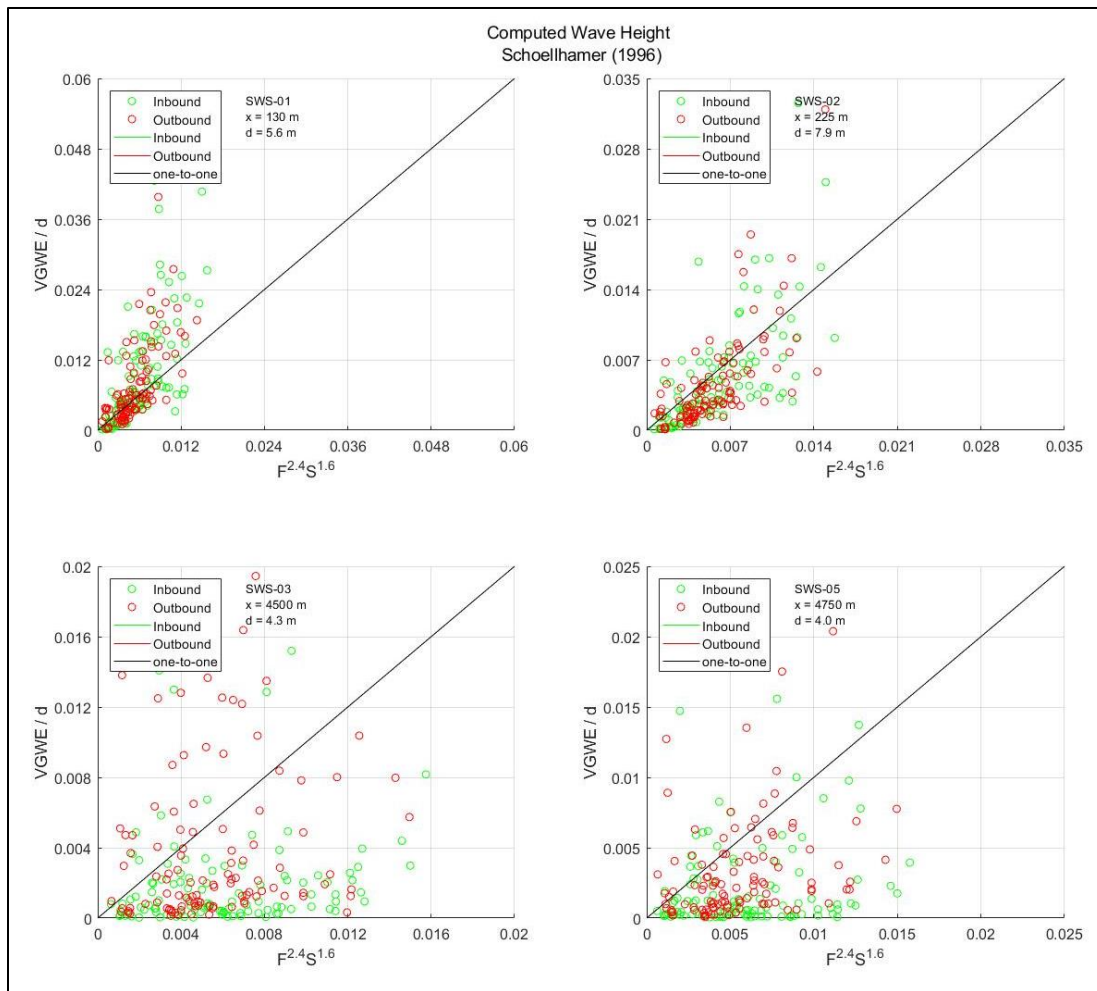


Figure 32: One-to-One correlation plot of measured vessel generated wave energy (VGWE) at the south bay validation sites and the equation from Schoellhamer (1996) for stations SWS01 through SWS03 and SW05 categorized by direction of vessel transit. The regression line is color coded to match the respective

The south bay validation set appears to follow the Schoellhamer (1996) model for SWS01 and SWS02 then largely scattered at the far field sites. Notable there does not appear to be a discernable trend or differentiation for the Froude number or transit direction as was the case at the northern deployment leading to the conclusion that vessel transiting this reach of the channel are not changing in speed as a function of direction. Lack of dependence on the Froude number could indicate VGWE may follow more of a linear wave theory relationship. However, application of the Schoellhamer (1996) model to the south bay is within the range of predictive accuracy.

## Summary

VGWE in Mobile Bay, Alabama was estimated using the model described by Schoellhamer (1996) in Equation 14 and found to underestimate at all measured stations for Froude numbers greater

than 0.5. For Froude numbers less than 0.5 the model tends to overestimate at the far field stations (SW01 and SW02) and underestimate for near measurement stations (SW03 and SW04). The model shows a trend for near field stations implying the model's relationship to VGWE for these stations could be improved to provide a more accurate computation. The increasing spread of data at stations SW01 and SW02 are likely a result of additional dependencies such as wave breaking and dispersion. Absence of vessel length and distance from the sailing line in the model could contribute to the under prediction at the near field stations (vessel length) and lack of precision at the far field stations (distance from sailing line). Validation of the initial study results using data collected in a similar manner between December 21, 2018 and February 5, 2019 is shown to agree with the Schoellhamer (1996) model but with less accuracy. As a result of this analysis, it is recommend the Schoellhamer (1996) should only be applied to Mobile Bay for low precision prediction of far field VGWE at Froude numbers greater than 0.5 with the understanding values could be slightly underestimated.

## 4 Impact Assessment

---

Describing potential impacts of VGWE as a result of the Mobile Harbor Federal Navigation channel proposed deepening project, for this study, is defined as a relative difference between with and without project channel geometry and forecasted vessel class distribution and frequency. This impact analysis relies on finding from Chapters 2 and 3 for prediction of VGWE in Mobile Bay using the model published by Schoellhamer (1996), defined in Equation 14. Fortunately, the proposed changes will not alter the alignment such that the model's lack of dependence on distance from the sailing line,  $x$ , will not vary and therefore the relative difference is zero and negligible. Two locations of interest along the length of the channel, shown in Figure 33, are considered which represent distinctly different geometries along the federal channel reach. Depth,  $h$ , at these locations is extracted from available bathymetric data obtained on February 2018 by the USACE Operations Hydrographic Survey Team at the inflection point of the channel side slope and the native bay elevation. This depth is chosen as it is within the range of applicability of the predictive model validation provided in Chapter 3 and outside the area of influence of channel dredging activities. Dependent variables with respect to these locations are provided in Table 8.

Table 8: Dependent variables used to evaluate Vessel Generated Wave Energy (VGWE) with respect to locations of interest.

Site ID	w/o Project		w/ Project		Adjacent Water Depth, $h$ (m)
	Channel Depth, $d_c$ (m)	Channel Width, $b$ (m)	Channel Depth, $d_c$ (m)	Channel Width, $b$ (m)	
Upper Bay	14.9	234.9	16.2	247.9	3.6
Lower Bay	14.9	219.9	16.2	263.4	5.1

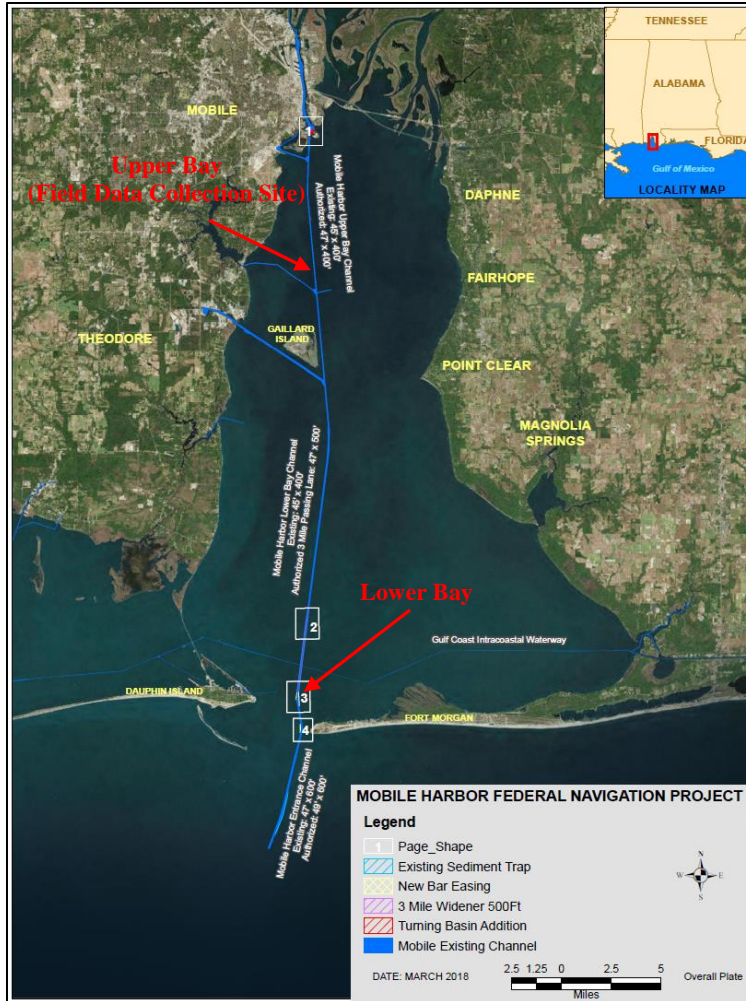


Figure 33: Location of sites used for spatial representation of Vessel Generated Wave Energy (VGWE) impact analysis within Mobile Bay, Alabama

## Vessel Traffic Frequency

Size and frequency of vessels calling the Mobile Harbor was determined through an economic analysis using the base year of 2025 and a future condition year of 2035. Frequency analysis, summarized in Table 9 for 2025 and Table 10 for 2035, categorized vessels by class with associated max vessel dimensions, number of calls, and percent of the total calls for with and without project. This forecasting was completed as part of the Mobile Harbor General Re-evaluation study and details of methods used can be found in documentation associated with that study. The forecasted fleet detailed with respect to distribution of vessel draft within each class and used for the impact analysis, is provided in Appendix B.

Table 9: Forecast summary for the base year 2025 vessel calls delineated by vessel classes for with and without project conditions.

Vessel Class	Max Length (m)	Max Beam (m)	w/o Project	% Fleet	With Project	% Fleet
Bulk Carrier 2	194	32	7	0%		0%
Bulk Carrier 3	228	32	398	13%	386	13%
Bulk Carrier 4	238	32	449	15%	450	15%
Bulk Carrier 5	247	42	77	3%	74	3%
Bulk Carrier 6	258	44	2	0%	2	0%
Bulk Carrier 7	274	44	12	0%	12	0%
Chemical Tanker	182	40	156	5%	156	5%
SubPX	206	30	20	1%	20	1%
Panamax	292	32	461	15%	415	14%
PPXGn1	302	40	236	8%	236	8%
PPXGn2	325	43	188	6%	186	6%
PPXGn3						
Cruise	261	36	182	6%	182	6%
General Cargo 1	183	32	399	13%	399	14%
General Cargo 2	258	36	293	10%	293	10%
Tanker Panamax	241	32	61	2%	101	3%
Aframax Tanker	271	49	72	2%	32	1%
<b>Total</b>			<b>3013</b>		<b>2944</b>	

Table 10: Forecast summary for year 2035 vessel calls delineated by vessel classes for with and without project conditions.

Vessel Class	Max Length (m)	Max Beam (m)	w/o Project	% Fleet	With Project	% Fleet
Bulk Carrier 2	194	32	5	0%		0%
Bulk Carrier 3	228	32	333	10%	403	12%
Bulk Carrier 4	238	32	418	12%	434	13%
Bulk Carrier 5	247	42	82	2%	77	2%
Bulk Carrier 6	258	44	2	0%	2	0%
Bulk Carrier 7	274	44	14	0%	14	0%
Chemical Tanker	182	40	238	7%	238	7%
SubPX	206	30	31	1%	29	1%
Panamax	292	32	260	8%	131	4%
PPXGn1	302	40	295	9%	269	8%
PPXGn2	325	43	187	6%	173	5%
PPXGn3	325	48	268	8%	248	8%
Cruise	261	36	172	5%	172	5%
General Cargo 1	183	32	453	14%	453	14%
General Cargo 2	258	36	347	10%	347	11%
Tanker Panamax	241	32	131	4%	131	4%
Aframax Tanker	271	49	111	3%	111	3%
<b>Total</b>			<b>3347</b>		<b>3232</b>	

Each class of vessels represent a range of vessel lengths and beams. VGWE computed using Equation 14 is proportional to the vessel beam such that the max beam within each vessel class will produce the largest value of VGWE vis-a-vis the largest potential impact. The vessel length is not a variable in Equation 14 but is presented here for awareness and clarity.

The total number and distribution of forecasted vessel calls to the Port of Mobile are generally equal. This is largely due to the methods used for predicting vessel calls and the nature of the proposed project. Northern extents of the proposed deepening project terminate at the Interstate 10 tunnel crossing. The majority of port facilities are north of the tunnel and hence are unchanged as a result of the project. The noticeable difference in number and distribution of calls relates to the containership vessel types between the 2025 and 2035 forecasted fleet. This is a result of the anticipated addition of Post Panamax Generation 3 (PPXGn3) vessels being introduced to the fleet. However, the PPXGn3 vessels will not result in a large net increase in vessel calls but a redistribution of all containership classes where tonnage once carried by several smaller vessel classes will now be transported on fewer larger vessels. Furthermore, the without project distribution also realizes the addition of the PPXGn3 vessel class where the relative difference in with and without project remain similar.

### **Vessel Speed**

VGWE is known to be highly dependent on vessel speed. Equation 14 shows vessel speed is raised to a power of 2.4 where a small change in speed will equate to a large change in VGWE. The forecasted fleet described in the previous section does not provided vessel speed. As a result, vessel speed used in this study is determined based on the current AIS data calling to Mobile Harbor. An annualized summary of vessel speed was extracted from the 2016 calendar year AIS database and delineated by vessel length. Figure 34 is the distribution of vessel speeds with respect to vessel length categories.

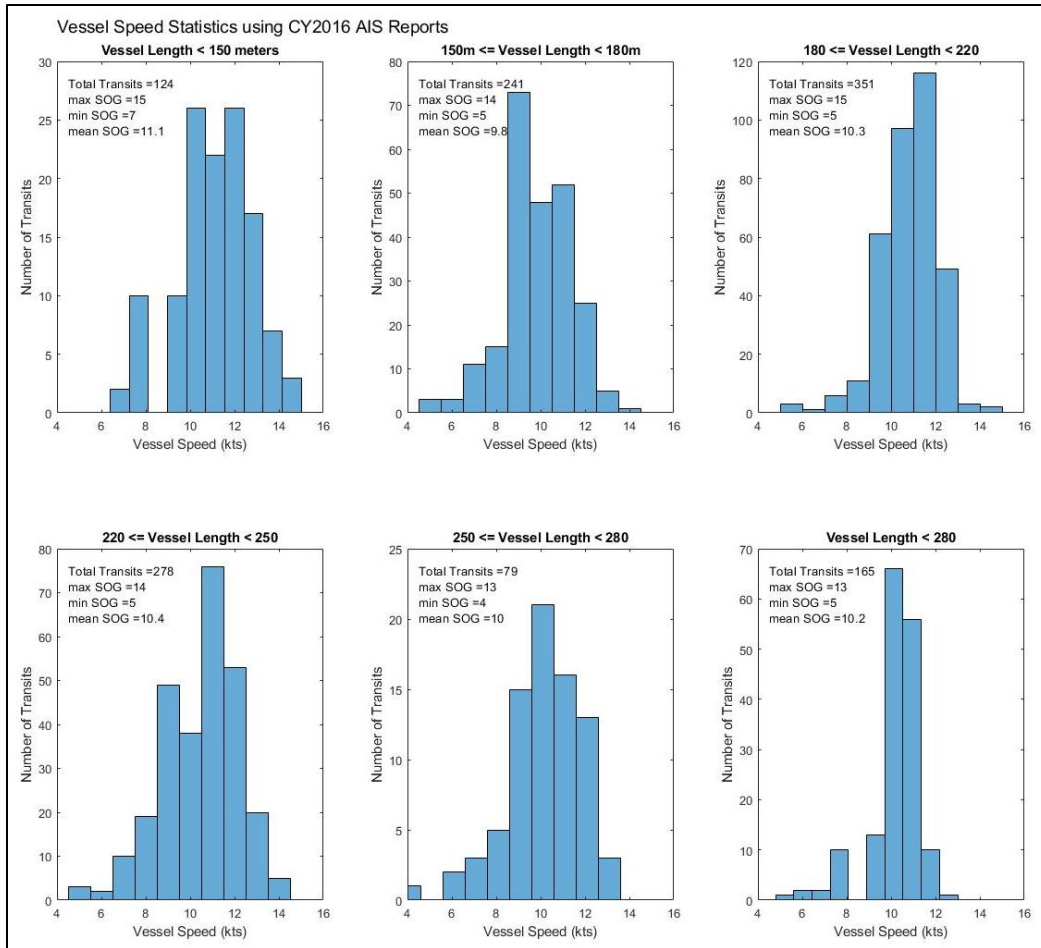


Figure 34: Summary statistics of vessel speed using Shipborne Automated Identification System (AIS) data obtain for the 2016 calendar year for Mobile Bay, Alabama deep draft channel delineated by vessel length.

The majority of vessels transiting Mobile Bay have a speed of around 10 knots, as shown in Figure 34, which is consistent with the vessel speeds recorded during the field investigation. Intuitively, smaller vessels are traveling faster than larger vessels and discussions with the Mobile Harbor Pilots Association confirmed this finding. However, Figure 34 shows maximum vessel speeds up to 15 knots for small vessels and 13 knots for the largest vessels.

Evaluation of vessel speed with respect to two locations along the bay channel sections shown in Figure 35 describes vessel speed variation between these points. To account for this variance and in lieu of a quantified assessment, vessel speed provided in the 2016 AIS summary statistics will be varied as a percentage such that the upper bay is 10% greater and the lower bay is 20% greater than the mean value provided in Figure 34. These values are believed to be conservative and within practical limits but a sensitivity analysis presented later in this study will test these assumptions and maximum values within practical limits.

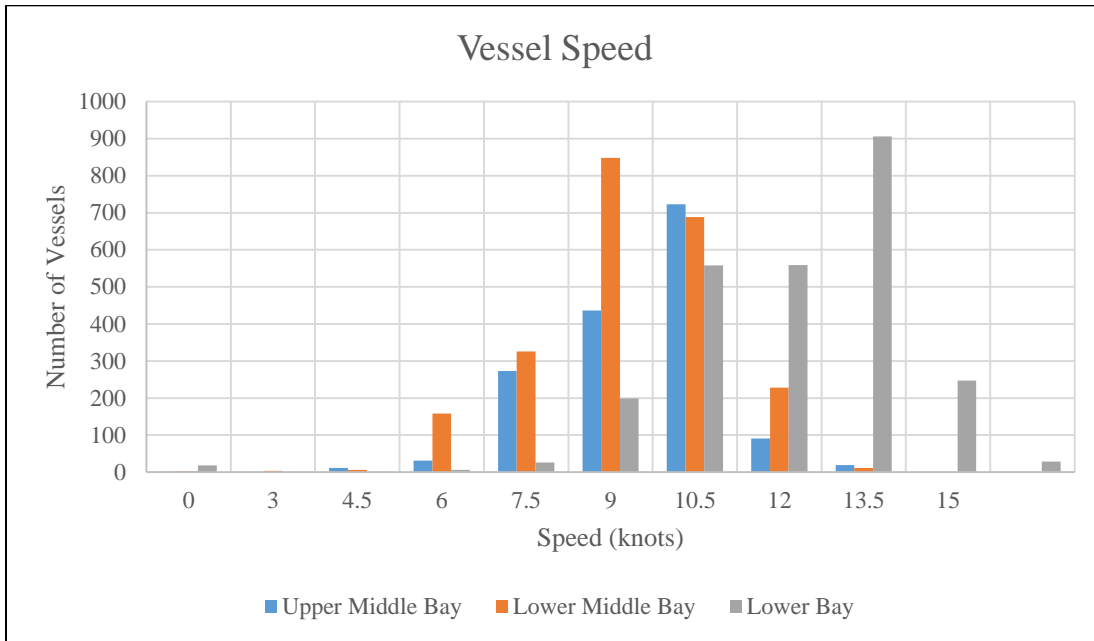


Figure 35: Variation of vessel speed for all classes and categories in Mobile Bay, Alabama with respect to three locations of interest.

This study has shown VGWE is highly dependent on vessel speed and this section has described the magnitude and variation of vessel speed at three discrete points. It is important to note limits and restrictions on vessel speed as it relates to theoretical maximums for confined and semi-confined channels such as Mobile Harbor. Several considerations for theoretical maximums are discussed in literature and relate to the Froude number and ratio of channel cross-section to vessel cross-section. PIANC (1987) found in constricted channels vessel speed cannot exceed  $F_d > 1$  and usually limited by  $0.9F$  due to the method of propulsion creating a critical velocity at the midsection of the vessel. Therefore vessel speed is limited since the propeller cannot move more water than allowed to flow past the vessel. EM 1110-2-1613, *Hydraulic Design of Deep-Draft Navigation Projects*, provides further restrictions to vessel speed for practical applications in terms of the depth based Froude number,  $F_d$ , such that in restricted channels  $F_d$  will not exceed 0.6. Schijf and Jansen (1953) investigated limits of vessel speed as a function of the depth based Froude number and the ratio of the channel and vessel cross-section, for constricted channels, and found a relationship known as Schijf's equation shown below (derivation as provided in EM 1110-2-1613) which is based on Bernoulli's Equation for conservation of energy.

$$F_{hL} = \frac{v_L}{\sqrt{gh}} = \sqrt{8 \cos^3 \left( \frac{\pi}{3} + \frac{\arccos \left( 1 - \frac{1}{B_R} \right)}{3} \right)} \quad (15)$$

Where  $B_R$  is equal to  $S_c$  and  $v_L$  is the limiting velocity. Channel width for the purposes of this analysis is considered to be the width at the inflection of the overbank area graphically shown in

Figure 36 for trench type channels. Schijf's equation has been verified by many researchers with good results but found to only be valid for ships transiting the centerline of a channel and if not the eccentricity should be substituted for the value of  $A_c$  according to PIANC (1985). The eccentricity relationship is noted but for this study all vessels are assumed to be transiting the channel centerline.

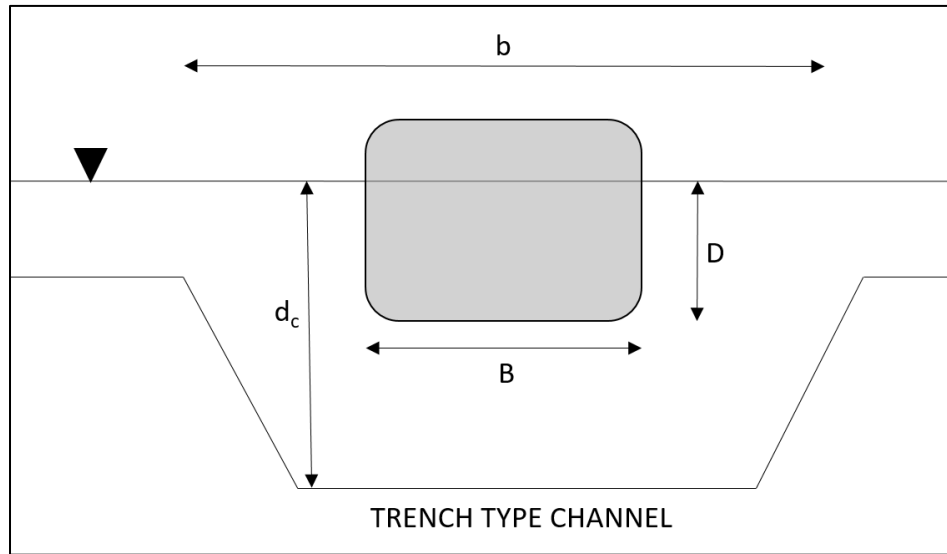


Figure 36: Graphical sketch defining cross-sectional variables used in VGWE and vessel speed computations.

Schijf's equation is used as provided in Equation 15 to valid the practical limits of vessel speed in Mobile Bay for all impact and sensitivity analyses. A comparison of vessel speeds measured using AIS and results using Equation 15 applied to the detailed forecasted fleet as provided in Appendix B show measured vessel speeds are much less than the theoretical maximum. However, this method does not consider squat, bank effects, currents, and other operational factors which are likely more limiting.

### Spatial Representation

Interpolating VGWE over the domain of Mobile Bay requires gross assumptions and presents several challenges. The first and foremost challenge is spatial extrapolation of the recommended model for predicting VGWE validated using data obtained from north of Gaillard Island and west of the federal navigation channel. Depths in this region are slightly less than other regions and features a shallow draft navigation channel (Dog River) which could influence VGWE and applicability to other regions. Furthermore, the northern reach, where model validation was completed, is shown to have a dependence on transit direction.

Influence of the Dog River channel is assumed to be negligible due to the small difference between channel depths and surrounding bathymetry in addition to a relatively narrow channel width. The field data collection chapter noted the influence of transit direction and it was present in the model validation. Examination of vessel speeds (known dependent of VGWE) shows inbound and outbound vessels differ. The combination of vessel speed variance and the observed wave breaking patterns in the field data chapter suggests other regions would not realize a similar dependence on transit direction where inbound and outbound vessels are assumed to exhibit similar magnitudes of VGWE outside of this region as long as consideration for speed and bathymetric features are observed.

For this study two locations of interest, inclusive of the field data collection site, are identified in Figure 33. Site selection was based on the known locations where variables in Equation 14 may change spatially and relative to with and without project. The recommended model provided in Equation 14 computes VGWE as a function of Vessel speed,  $V$ , Beam,  $B$ , and draft,  $D$ , channel depth,  $d_c$ , and width,  $b$ , as well as depth at the point of interest,  $h$ . Channel geometry is the only variable meeting the site selection criteria. The lower bay site is representative of a change in channel width and depth from existing conditions and different than the change defined at the field data collection site. Site specific values for with and without project as well as other dependent variables are provided in Table 8.

### **Computed Impacts**

The objective of this study is to evaluate the relative difference in VGWE for the current fleet and forecasted fleet as a result of deepening the channel. The methods to compute VGWE were presented in Chapter 3 and the dependent variables for each scenario were described previously in this chapter. Results using these values are provided in the following tables.

Table 11: Computed Vessel Generated Wave Energy (VGWE) of with and without project scenarios using the forecasted base year 2025 at the upper bay site.

Vessel Class	2025 Arrival				2025 Departure			
	# of Vessels		VGWE		# of Vessels		VGWE	
	w/o Project	w/ Project	w/o Project	w/ Project	w/o Project	w/ Project	w/o Project	w/ Project
Bulk Carrier 1								
Bulk Carrier 2	4		0.025		3		0.055	
Bulk Carrier 3	229	223	1.702	1.208	169	163	2.551	1.768
Bulk Carrier 4	250	250	1.747	1.268	199	200	2.516	1.924
Bulk Carrier 5	38	36	1.057	0.738	39	38	1.320	1.014
Bulk Carrier 6	1	1	0.010	0.007	1	1	0.033	0.024
Bulk Carrier 7	6	6	0.057	0.042	6	6	0.210	0.171
Chemical Tanker	78	78	0.427	0.310	78	78	0.659	0.479
SubPX	10	10	0.113	0.082	10	10	0.102	0.074
Panamax	232	208	3.260	2.120	229	207	3.308	2.148
PPXGn1	117	118	2.688	2.211	119	118	2.765	2.347
PPXGn2	94	94	2.430	1.979	94	92	2.531	2.031
PPXGn3								
Cruise	91	91	0.931	0.676	91	91	0.901	0.654
General Cargo 1	199	199	1.037	0.752	200	200	1.103	0.801
General Cargo 2	146	146	0.837	0.607	147	147	1.080	0.784
Tanker Panamax	32	72	0.359	0.685	29	29	0.202	0.147
Aframax Tanker	72	32	1.698	0.468				
	<b>1599</b>	<b>1564</b>	<b>18.376</b>	<b>13.153</b>	<b>1414</b>	<b>1380</b>	<b>19.337</b>	<b>14.366</b>

Table 12: Computed Vessel Generated Wave Energy (VGWE) of with and without project scenarios using the forecasted base year 2025 at the lower bay site.

Vessel Class	2025 Arrival				2025 Departure			
	# of Vessels		VGWE		# of Vessels		VGWE	
	w/o Project	w/ Project	w/o Project	w/ Project	w/o Project	w/ Project	w/o Project	w/ Project
Bulk Carrier 1								
Bulk Carrier 2	4		0.048		3		0.106	
Bulk Carrier 3	229	223	3.303	1.914	169	163	4.949	2.800
Bulk Carrier 4	250	250	3.389	2.009	199	200	4.882	3.048
Bulk Carrier 5	38	36	2.051	1.168	39	38	2.562	1.607
Bulk Carrier 6	1	1	0.019	0.011	1	1	0.063	0.039
Bulk Carrier 7	6	6	0.111	0.066	6	6	0.407	0.270
Chemical Tanker	78	78	0.829	0.491	78	78	1.279	0.758
SubPX	10	10	0.220	0.130	10	10	0.199	0.118
Panamax	232	208	6.324	3.358	229	207	6.417	3.403
PPXGn1	117	118	5.214	3.503	119	118	5.363	3.718
PPXGn2	94	94	4.714	3.135	94	92	4.910	3.217
PPXGn3								
Cruise	91	91	1.806	1.071	91	91	1.748	1.036
General Cargo 1	199	199	2.011	1.192	200	200	2.141	1.269
General Cargo 2	146	146	1.623	0.962	147	147	2.096	1.242
Tanker Panamax	32	72	0.696	1.085	29	29	0.392	0.233
Aframax Tanker	72	32	3.294	0.742				
	<b>1599</b>	<b>1564</b>	<b>35.650</b>	<b>20.838</b>	<b>1414</b>	<b>1380</b>	<b>37.514</b>	<b>22.759</b>

Table 13: Computed Vessel Generated Wave Energy (VGWE) of with and without project scenarios using the forecasted year 2035 at the upper bay site.

Vessel Class	2035 Arrival				2035 Departure			
	# of Vessels		VGWE		# of Vessels		VGWE	
	w/o Project	w/ Project	w/o Project	w/ Project	w/o Project	w/ Project	w/o Project	w/ Project
Bulk Carrier 1								
Bulk Carrier 2	3		0.018		2		0.037	
Bulk Carrier 3	199	199	1.689	1.226	134	204	2.105	1.890
Bulk Carrier 4	199	218	1.371	1.082	219	216	2.616	1.921
Bulk Carrier 5	40	38	1.035	0.725	42	39	1.437	1.058
Bulk Carrier 6	1	1	0.010	0.007	1	1	0.033	0.024
Bulk Carrier 7	7	7	0.067	0.049	7	7	0.245	0.201
Chemical Tanker	120	120	0.671	0.487	118	118	1.003	0.728
SubPX	16	15	0.178	0.122	15	14	0.151	0.103
Panamax	130	66	1.822	0.672	130	65	1.897	0.704
PPXGn1	147	134	3.366	2.508	148	135	3.568	2.629
PPXGn2	93	86	2.377	1.777	94	87	2.513	1.891
PPXGn3	135	124	4.150	3.107	133	124	4.250	3.244
Cruise	86	86	0.880	0.639	86	86	0.852	0.618
General Cargo 1	226	226	1.190	0.864	227	227	1.217	0.884
General Cargo 2	173	173	0.993	0.721	174	174	1.276	0.926
Tanker Panamax	65	65	0.688	0.499	66	66	0.435	0.316
Aframax Tanker	55	55	1.295	0.940	56	56	1.216	0.882
	<b>1695</b>	<b>1613</b>	<b>21.799</b>	<b>15.425</b>	<b>1652</b>	<b>1619</b>	<b>24.850</b>	<b>18.019</b>

Table 14: Computed Vessel Generated Wave Energy (VGWE) of with and without project scenarios using the forecasted year 2035 at the lower bay site.

Vessel Class	2035 Arrival				2035 Departure			
	# of Vessels		VGWE		# of Vessels		VGWE	
	w/o Project	w/ Project	w/o Project	w/ Project	w/o Project	w/ Project	w/o Project	w/ Project
Bulk Carrier 1								
Bulk Carrier 2	3		0.036		2		0.059	
Bulk Carrier 3	199	199	3.276	1.942	134	204	3.314	2.430
Bulk Carrier 4	199	218	2.659	1.714	219	216	4.118	2.470
Bulk Carrier 5	40	38	2.007	1.148	42	39	2.263	1.360
Bulk Carrier 6	1	1	0.019	0.011	1	1	0.051	0.031
Bulk Carrier 7	7	7	0.130	0.077	7	7	0.385	0.258
Chemical Tanker	120	120	1.302	0.772	118	118	1.579	0.936
SubPX	16	15	0.346	0.193	15	14	0.238	0.132
Panamax	130	66	3.535	1.065	130	65	2.986	0.905
PPXGn1	147	134	6.530	3.974	148	135	5.618	3.380
PPXGn2	93	86	4.612	2.815	94	87	3.957	2.432
PPXGn3	135	124	8.051	4.923	133	124	6.691	4.171
Cruise	86	86	1.707	1.012	86	86	1.341	0.795
General Cargo 1	226	226	2.309	1.368	227	227	1.917	1.136
General Cargo 2	173	173	1.927	1.142	174	174	2.009	1.191
Tanker Panamax	65	65	1.335	0.791	66	66	0.685	0.406
Aframax Tanker	55	55	2.513	1.490	56	56	1.914	1.134
	<b>1695</b>	<b>1613</b>	<b>42.292</b>	<b>24.436</b>	<b>1652</b>	<b>1619</b>	<b>39.124</b>	<b>23.167</b>

Computed VGWE in the tables above is representative of the deep water statistically significant wave height,  $H_{mo}$ . The equivalent deep water wave height,  $H_{mo}$ , is not generally used to describe VGWE in this manner but this study chose not to compute the wave power (energy/unit length) to give the reader a direct comparison and relationship to VGWE measured and provided in Chapter 3 without bias or needed conversions. Forgoing the conversion to wave power does not induce bias in the comparison as dependent variables in the conversion are indifference between with and without project scenarios.

Comparison of with and without project for any case or combination thereof shows no increase in VGWE as a result of the proposed project. The comparison proves further within all vessel classes the without project condition VGWE is less than with project and can be contributed to the decrease in vessel transits as a result of project construction. Comparing Table 11 and Table 12 or Table 13 and Figure 14 shows a diverging relationship between the lower bay site and upper bay site proving a larger channel cross-section will result in less VGWE. These findings are not unexpected and make clear the impact/relationship of channel geometry in confined channels. In Chapter 1, the theoretical background of VGWE suggested vessels transiting confined channels tend to create a larger disturbance in the water surface elevation and is proportional to the VGWE. The results of this study agree with this theoretical relationships and strengthens the finding of no increase in VGWE for the proposed project.

### **Sensitivity Analysis**

Methods used in this study to compute VGWE relied on assumptions of vessel speed being invariable between with and without project conditions. Other degrees of freedom for channel geometry and vessel dimensions were incorporated in the computed VGWE from previous sections of this chapter and found to be insignificant. Vessel speed is discussed numerous times in this chapter and previous chapters as being a significant and proportional function of VGWE. For this study vessel speed was assumed equivalent to the mean speed derived from AIS data obtained for the 2016 calendar year, categorized by vessel length, and associated with vessel types. However, Figure 34 showed maximum vessel speed may far exceed the mean values, and further, speed could be related to the channel depth to vessel draft ratio or more explicitly the Froude number,  $F_d$ , such that vessel speed increases as the under keel clearance increases. This sensitivity is tested in the most simplistic manner using the results of Table 11 (2025, upper bay) for departures since the computed VGWE difference between with and without project is smallest (4.971). Three test conditions, described below, are used evaluate vessel speed sensitivity.

- Constant multiplier of 1.25 (+25%) applied to all vessel types for with and without project conditions.
- Constant multiplier of 1.25 (+25%) applied only to with project condition.

- Froude number,  $F_d$ , held constant for computed VGWE, with respect to each vessel class and respective draft, for with and without project conditions.

Table 15: Results of three unique vessel speed sensitivity tests for the 2025 forecasted arrivals at the upper bay site.

Sensitivity Test Case	VGWE w/o Project	VGWE w/ Project	Difference
2025 Forecasted (Table 11)	19.337	14.366	4.971
Equivalent 1.25 Speed Multiplier	26.28	19.524	6.756
1.25 Multiplier for w/Project	19.337	19.524	-0.187
2025 Forecasted Equivalent Froude Number	19.337	15.883	3.454

Sensitivity test results in Table 15 show variation in vessel speed for with and without project conditions create a case where impacts may be realized as a result of the proposed project. However, the case of vessel speed arbitrarily increased for the with project condition and no change to vessel speed for the without project is likely impractical. Previously in this chapter, maximum vessel speed of large vessels transiting the semi-confined channel in Mobile Bay was shown to be limited by channel geometry, vessel squat, and most importantly safety and as a matter of economic efficiency it is reasonable to assume vessels are transiting the channel at the maximum speed possible within these constraints. Ignoring safety as a limiting factor and only considering the quantifiable constraints as a relationship between vessel dimensions and channel geometry, the last sensitivity case where the Froude number is considered equivalent between with and without project conditions is the most probable case to evaluate the highest likelihood of potential impacts from VGWE. In this practical case, it is shown total VGWE for with project condition does not exceed the without project total VGWE, whereby it is proven for practical variances in vessel speed between with and without project conditions there will be no impact as a result of the proposed project.

## Summary

Potential impacts of VGWE were evaluated by comparing the relative difference of with and without project conditions using forecasted vessel calls for years 2025 and 2035. Vessel speed was obtained from a statistical summary of 2016 AIS data categorized by vessel length. VGWE was computed using the model published by Schoellhamer (1996), defined in Equation 14. No increase in VGWE was determined as a result of the proposed project. The confidence of this finding was tested with respect to the assumption of vessel speed which determined for practical potential increases in vessel speed as a result of the project the relative difference in VGWE does not become negative.

## 5 Cumulative Impacts Assessment

---

Cumulative impacts related to the Mobile Harbor Federal Navigation Channel is investigated using the rate of shoreline change along the western shore of Mobile Bay as a proxy for determining cumulative impacts, associated with vessel generated wave energy, with respect to modification of the federal navigation channel as a function of vessel callings to the port of Mobile. It is hypothesized the number of vessels transiting the federal navigation channel is inversely related to the rate of shoreline change represented as length per year. This hypothesis relies on a firm understanding of all forces acting on the shoreline. However, this is generally not fully understood and instead will be inferred and qualitatively assessed by way of documented channel modifications and shoreline characterization.

Potential for error is high due to the uncertainties and will be minimized to the greatest extent possible. Possible sources of error are shoreline delineation, vessel counts, and density of temporal shoreline data points. The absence of temporal data for shoreline change over the period examined is one of the largest uncertainties. An assumption of linear rate of change between points will be used.

### Vessel Callings

Number of vessel callings is obtained from the Waterborne Commerce of the United States (WCUS). The WCUS compiles an annual report of vessel traffic and associated commodities for all U.S. navigable waterways. Publication of these reports was authorized by the River and Harbor Act of September 22, 1922. The methodology used to obtain the data can be found in these reports and will not be detailed here. The resulting data available and used in this report for vessel calling is delineated by vessel class, draft, inbound/outbound, and origin (foreign/domestic). The cumulative impacts analysis in this report obtained reports for all calendar years between 1956 and 2017. These data were filtered for vessel classes 1 and 2 for all directions and origins then aggregated by 1 foot increments of draft greater than or equal to 19 feet. A summary plot of all vessel calls as a function of vessel draft and year is shown in Figure 37 and aggregated by year in Figure 38.

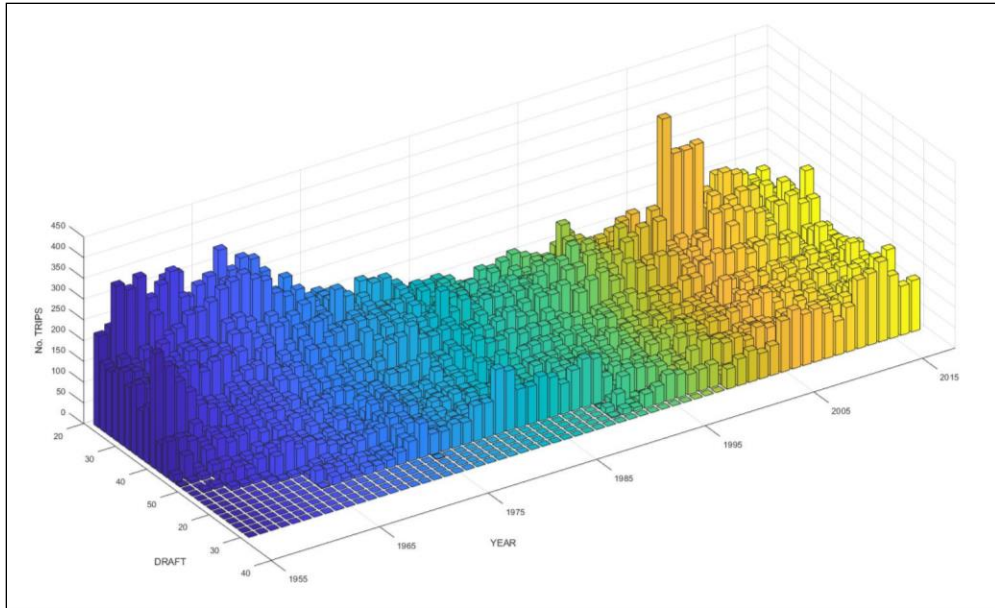


Figure 37: Summary of class 1 and 2 vessel calls obtained from WCUS annual reports (1956-2017) aggregated by draft plotted as a function of year.

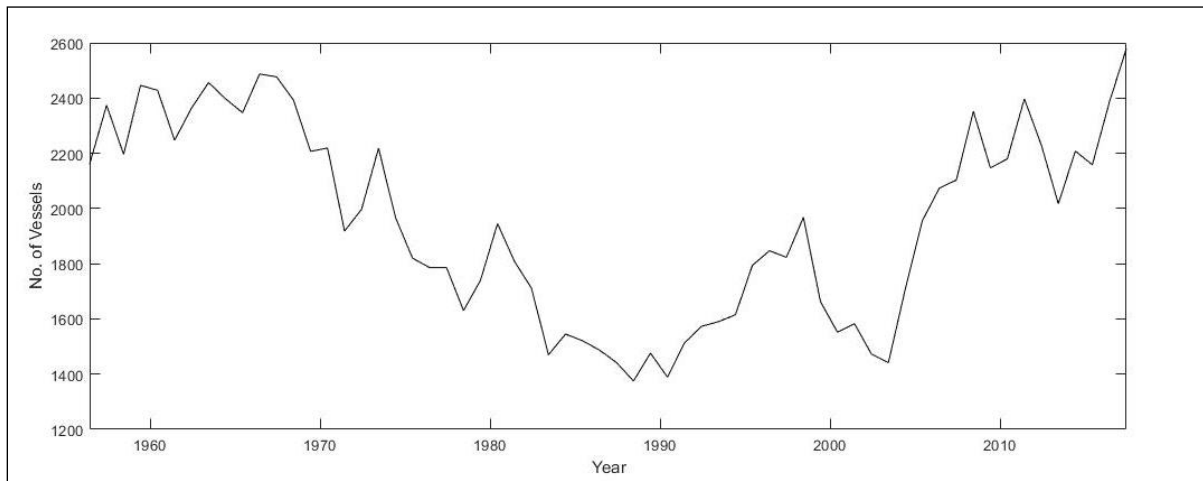


Figure 38: All class 1 and 2 vessel calls obtained from WCUS annual reports (1956-2017) by year for all drafts greater than or equal to 19 feet.

## Shoreline Inventory

Shoreline position data were compiled at 7 selected locations along the western shoreline of Mobile Bay from Brookley Aeroplex (approx. latitude 30.6060°) to Alabama Port (approx. latitude 30.3400°) defined by tributaries, orientation, recognized unincorporated communities and qualitative visual observation of shoreline classification, see Figure 39. These sites were screened for locations having greater than 10 points of shoreline position data between 1840 and 2011. Three locations (SL1, SL3, and SL6) met the screening criteria and carried forward in the analysis.

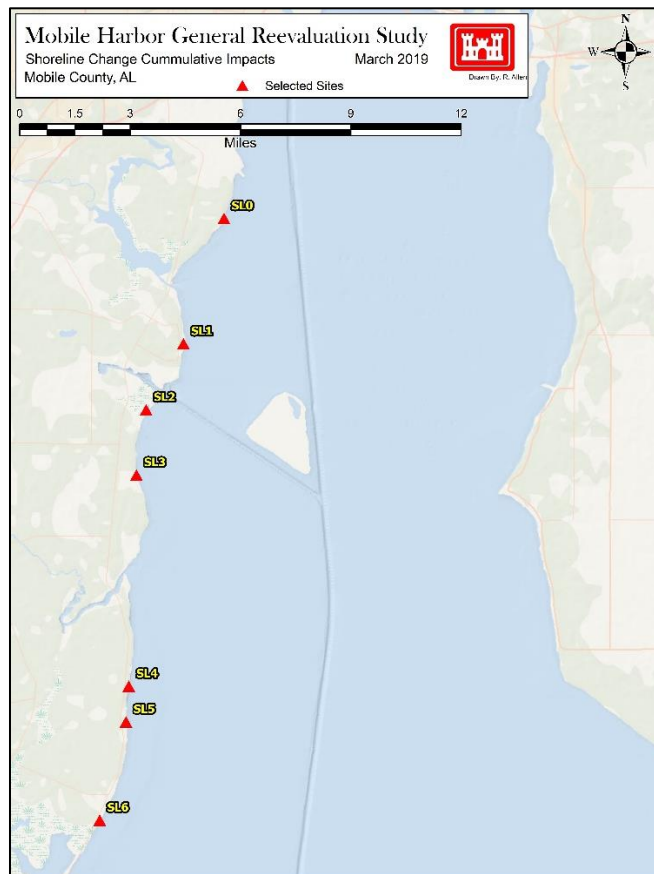


Figure 39: Selected sites used to evaluate shoreline change.

Shoreline position data were extracted from the National Oceanic and Atmospheric Administration (NOAA) Shoreline Database (NOAA, 2019) and augmented using historical aerial imagery obtained from the University of Alabama (University of Alabama, 2019). Aerial imagery obtained from the University of Alabama was processed using manual shoreline delineation methods (Li et al., 2001; Morton et al., 2004; Boak and Turner, 2005; Zarillo et al., 2008; Byrnes et al., 2013; Eulie et al., 2013). The methodology consisted of geo-rectifying the imagery using a minimum of 6 consistent control points at each site which were identifiable through the temporal range of analysis. The rectified image must have less than 1 meter of error in the rectification process. The high water line was used to delineate the shoreline based on a hierarchy of visual criteria developed by Byrnes et al., (2008) and consistent with other methods used for developing NOS T-sheet shorelines (Shalowitz, 1964). A list of applicable shorelines with, source, estimated error, and site applicability is provided in Table 16. The estimated random error related to these shorelines is based on the uncertainty described by Byrnes et al., 2008. While the error generally exceeds the computed changes, this study assumes it to be negligible but acknowledges this will likely result in a large distribution of values. The distribution will be minimized to the greatest extent through finer sampling resolution within each site and averaging of the error along with professional

judgment used for omission of sample transects indicating extreme error in the delineation technique.

Table 16: Inventory of shoreline position data, applicable locations, source, and selected data quality parameters.

Date	Source	Type	Scale	Estimated Error (ft)	SL1	SL3	SL6
1849-06-01	Applied Coastal	T-Sheet, Surveyed	1:20,000	+/- 36 ft		1	1
1850-06-01	Applied Coastal	T-Sheet, Surveyed	1:20,000	+/- 36 ft	1		
1918-04-01	Applied Coastal	T-Sheet, Surveyed	1:40,000	+/- 36 ft	1	1	1
1934-07-16	NOAA	T-Sheet from interpreted Imagery	1:20,000	+/- 33 ft	1	1	1
1940-06-01	UA Maps	Rectified Aerial Imagery	1:3,500	+/- 60 ft		1	1
1950-06-01	UA Maps	Rectified Aerial Imagery	1:3,500	+/- 60 ft			1
1952-06-01	UA Maps	Rectified Aerial Imagery	1:3,500	+/- 60 ft	1		
1957-11-01	NOAA	T-Sheet from interpreted Imagery	1:10,000	+/- 20 ft	1	1	
1957-11-19	NOAA	T-Sheet from interpreted Imagery	1:10,000	+/- 20 ft			1
1960-06-01	UA Maps	Rectified Aerial Imagery	1:2,500	+/- 12 ft	1		1
1974-06-01	UA Maps	Rectified Aerial Imagery	1:2,500	+/- 12 ft	1	1	1
1982-03-01	NOAA	T-Sheet from interpreted Imagery	1:20,000	+/- 13 ft	1	1	1
1992-06-01	UA Maps	Rectified Aerial Imagery	1:2,500	+/- 12 ft			1
1993-06-01	UA Maps	Rectified Aerial Imagery	1:2,500	+/- 12 ft	1	1	
1997-06-01	UA Maps	Rectified Aerial Imagery	1:2,500	+/- 12 ft	1	1	1
2009-06-01	UA Maps	Rectified Aerial Imagery	1:2,500	+/- 8 ft	1	1	1
2010-10-09	Applied Coastal	Orthorectified Imagery	1:2,000	+/- 6 ft	1	1	
2011-05-07	Applied Coastal	Orthorectified Imagery	1:2,000	+/- 6 ft			1
		<b>Total:</b>			<b>12</b>	<b>11</b>	<b>13</b>

Shoreline positions for all time periods were imported to a desktop mapping program at the three locations aforementioned. Shore perpendicular transects were generated at 20 meter (65.6 feet) intervals connected to an onshore baseline. The USGS program Digital Shoreline Analysis System (DSAS) the distance from baseline was computed for the shorelines along each transect. The incremental linear distance between temporal shoreline positions was computed along with the respective rate of change (feet/year), where negative values represent erosion. A linear regression fit rate of change between the 1849/1850 and 2010/2011 shoreline positions was also computed to evaluate the overall trend spanning the dataset. Figure 40, Figure 41, and Figure 42 are the results of the linear regression, where the transect lines are colored by rate of shoreline change. The linear regression rate of change is clearly net erosion for all locations with the exception of a few outlying transects for the temporal range of 1849/50 to 2010/11. The result is largely due to the shoreline position between 1849/50 and 1917/18. Detailed shoreline change analysis is shown later in the report.

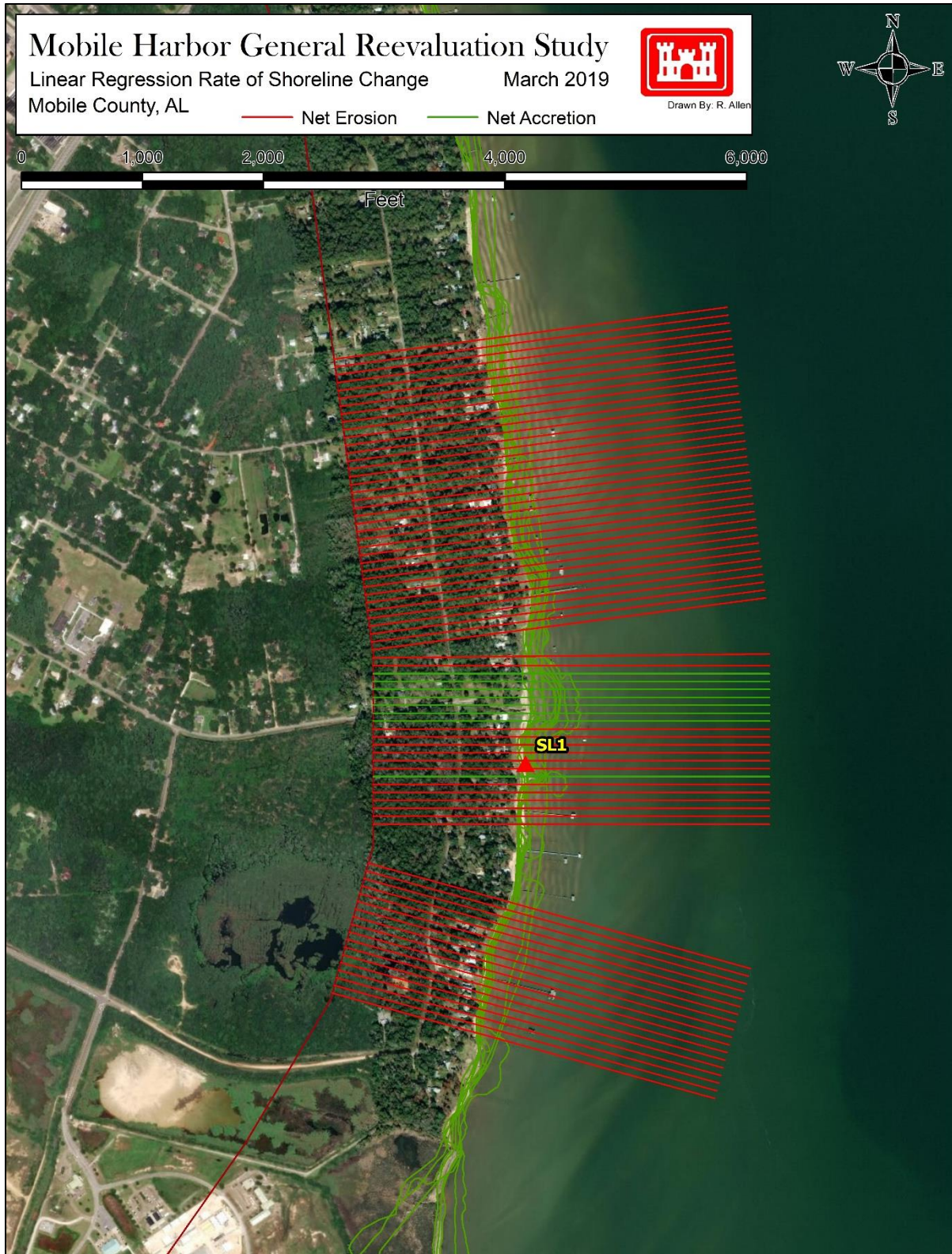


Figure 40: Linear regression rate of shoreline change for SL1 for 1849/1850 through 2010/2011.

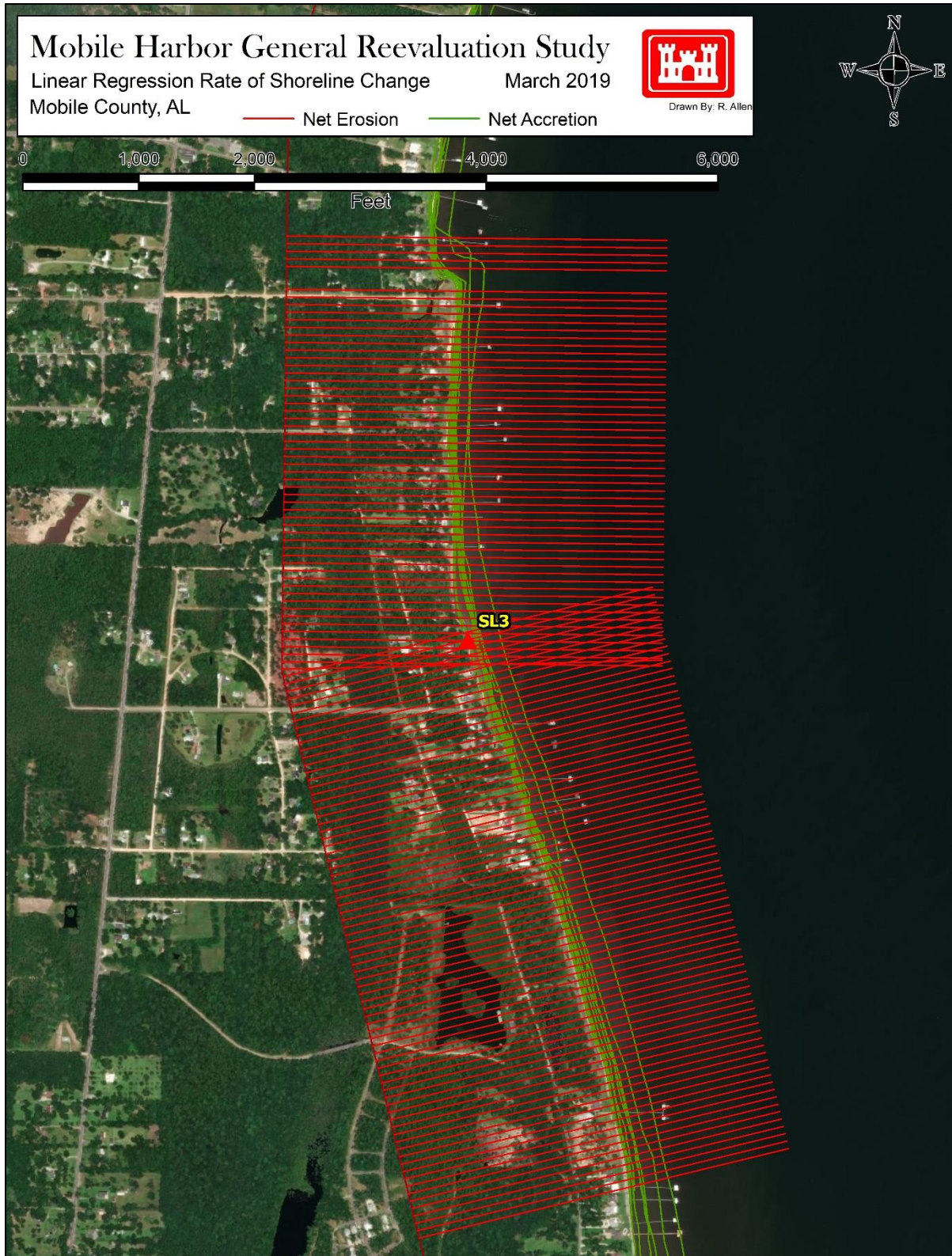


Figure 41: Linear regression rate of shoreline change for SL3 for 1849/1850 through 2010/2011.

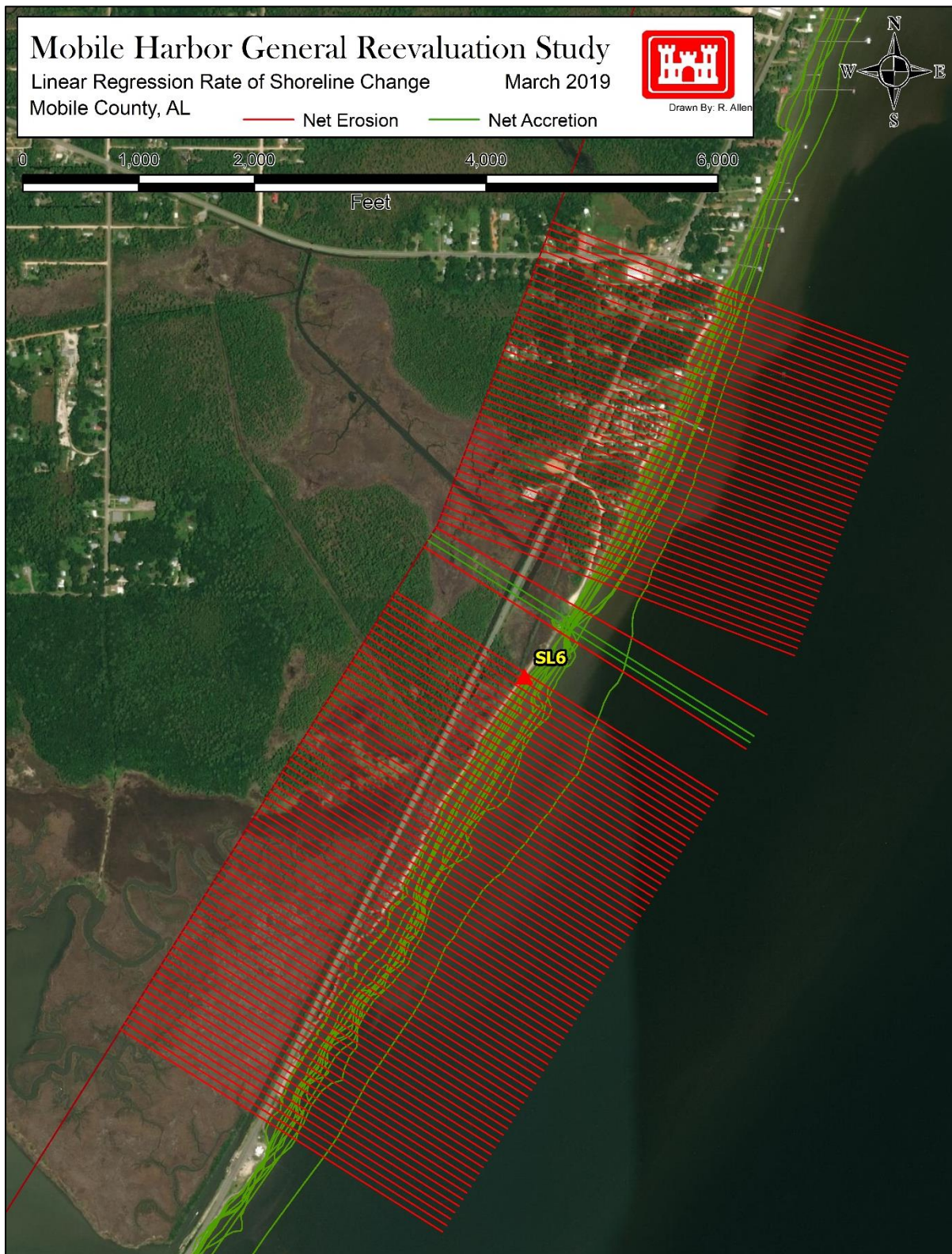


Figure 42: Linear regression rate of shoreline change for SL6 for 1849/1850 through 2010/2011.

## Mobile Bay Ship Channel Dimensions

The Mobile Bay Federal Navigation Channel has undergone multiple improvement through the years. The first recorded authorization for the channel occurred in the early 1800's with dredging at various sections along the present alignment. It was not until the River and Harbor Act of June 25, 1910 authorized a continuous channel 27 feet deep by 200 feet wide channel, completed in 1913, from Dauphin Island to the Mobile River along the present day alignment. Following this the channel was deepened and widened four additional times between 1913 and 1989 to the current maintained dimensions of 45 ft x 400 ft. The dates and dimensions for these channel modifications are provided in Table 17 plotted as total cross-sectional area of the navigable portion of the channel (i.e. depth x bottom width) in Figure 43.

Table 17: Summary of Channel Modifications between 1913 and 1989.

Date Completed	Channel Dimensions (ft)
August 15, 1913	27 x 200
July 25, 1926	30 x 300
July 19, 1933	32 x 300
November 10, 1964	40 x 400
July 3, 1989	45 x 400

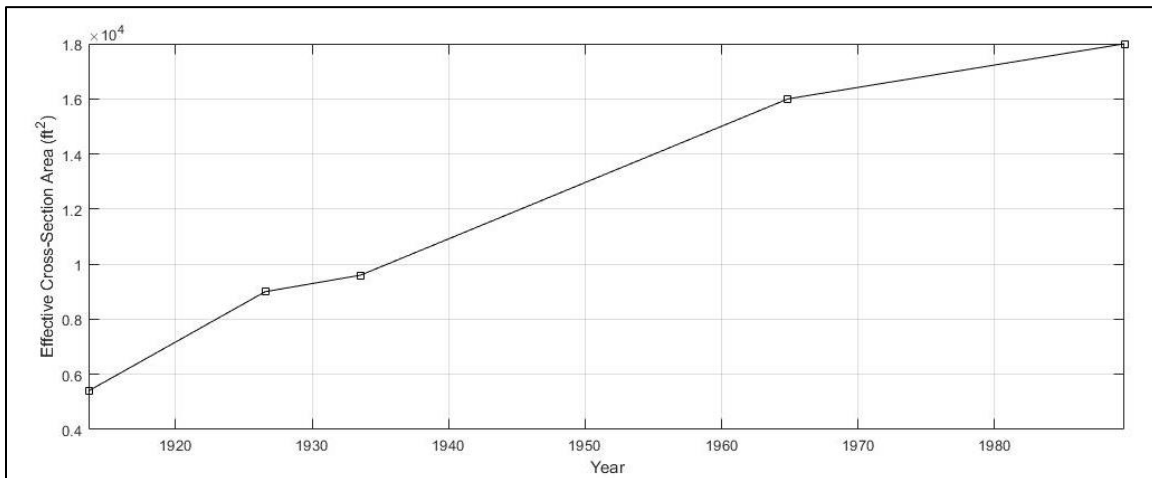


Figure 43: Temporal plot of channel modifications between 1913 and 1989. Channel dimensions are represented as a cross-sectional area in square feet of the navigable portion

## Shoreline Characterization and Change Analysis

Shoreline composition along the western shore of Mobile Bay is generally classified as, sloped sandy beach, vegetated marsh, or structured. Byrnes et al., (2013) completed a comprehensive spatial and temporal dependent classification of shorelines delineated by zones for Mobile Bay.

Byrnes et al., (2013) found a mostly erosive environment for the western shore over the analysis period and between points. The general shoreline classifications from Byrnes et al., (2013) will be used in this analysis for describing shoreline type to the extent applicable.

Douglass and Pickel (1999) investigated shoreline development/armoring along the shorelines of Mobile Bay between 1955 and 1997 using aerial photography and determined the rate of armoring to be increasing and generally follows the population growth for Mobile and Baldwin Counties during the study period. Spatial and temporal distribution of shoreline armoring concluded by Douglass and Pickel (1999) is shown in Figure 44 and an annual rate of change between 0.3 and 1.1 percent armored per year.

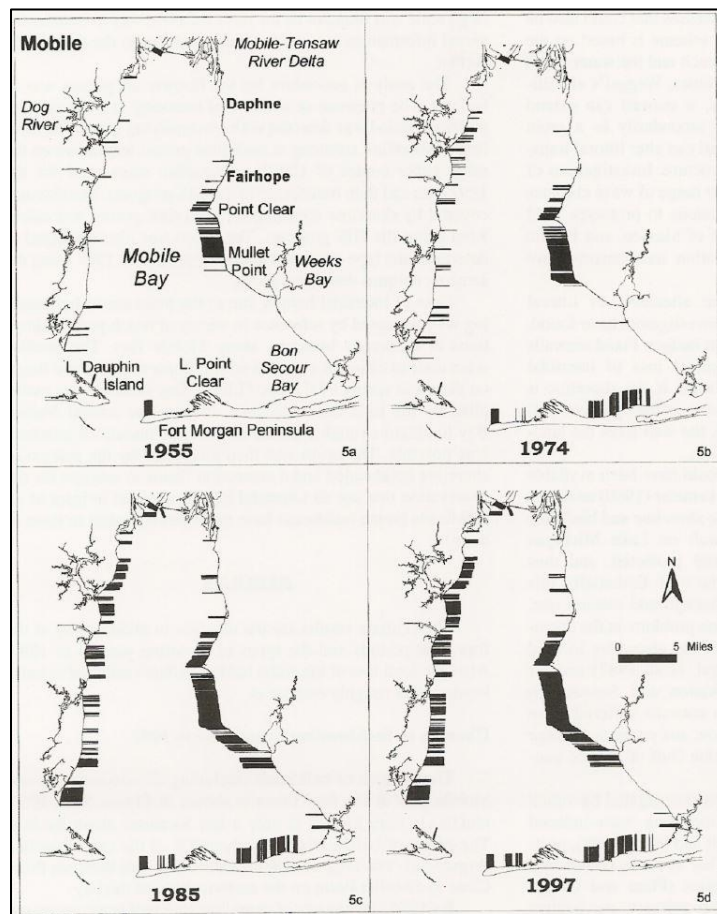


Figure 44: Spatial and Temporal Distribution of shoreline armoring between 1955 and 1997 extracted from Douglass and Pickel (1999).

### *SL1 Site Characterization and Shoreline Change Results*

SL1 includes approximately 1800 meters (5906 feet) of linear shoreline located south of Dog River and north of the Theodore Ship Channel along a shoreline generally known as Hollinger’s Island.

The shore normal incident angles range between 82° and 105°. The offshore bathymetry is gently sloping. In 1943 discrete placements of dredge material related to excavation of Hollinger’s Channel occurred along the shoreline and dominate the SL1 reach. These sites are distinguish by un-natural undulations in the shoreline. The Theodore Ship Channel and Gaillard Island, constructed between 1979 and 1981, are located to the southeast and could influence the temporal trend of change. Examination of aerial imagery from 1952 to 2011 indicates a high rate of development and armoring beginning in 1993.

Shoreline change computations found the average linear regression rate of change from 1917/18 to 2010/11 for all transects was -0.28 m/yr (0.9 ft/yr). The temporal trend of shoreline change rates computed at each available shoreline position are shown graphically below.

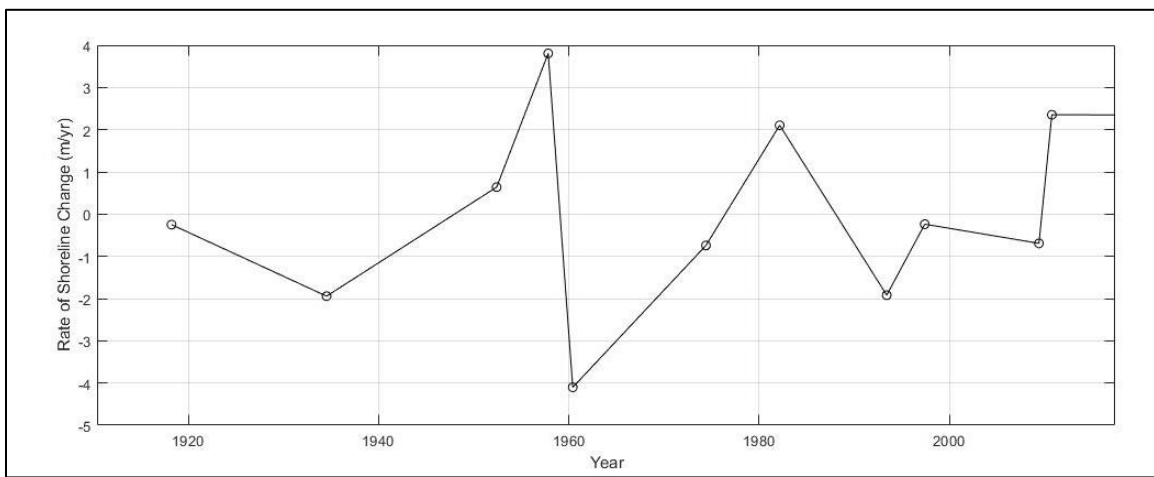


Figure 45: Temporal distribution of shoreline change rates at SL1 between 1917/18 and 2010/11 with linearly interpolated rate of rate of change.

Shoreline change rate magnitude changes over time are consistent with the results of Byrnes et al., (2013) and indicative of the evolutionary changes to the shoreline characteristics. The highest rate of change of erosion rate between 1957 and 1960 shoreline position is a result of the termination of dredge material placement with a reducing trend of erosion rates between 1960 and 1982 as the constructed marsh areas equilibrated. From 1982 and 1993 the erosion rates increased and could be attributed to extensive shoreline development, observed in aerial photography, related to Theodore Ship Channel operations. A second decreasing trend between 1993 and present is likely related to shoreline armoring and perhaps a “shadowing” effect of Gaillard Island from dominate southeast winds.

### *SL3 Site Characterization and Shoreline Change Results*

SL3 includes approximately 2500 meters (8203 feet) of linear shoreline located South of Theodore Ship Channel and North of Fowl River. The shore normal incident angles range between 76° and

91° with a gently sloping, unobstructed, offshore bathymetry. Theodore Ship Channel and Gaillard Island, constructed between 1979 and 1981, are located to the northeast and could influence the temporal trend of change. Aerial photography in 1940 indicates most of the shoreline is undeveloped with a sandy shoreline backed by forested areas with no clear visually identified armoring until 1997. In 2009 the conversion of sandy beach to armored shorelines is more prevalent; however, sandy shorelines are still the majority. Adjacent shorelines are similar in characteristics and trends and should pose little differing influence.

Shoreline change computations found the average linear regression rate of change from 1917/18 to 2010/11 for all transects was -0.47 m/yr (1.5 ft/yr). The temporal trend of shoreline change rates computed at each available shoreline position are shown graphically below.

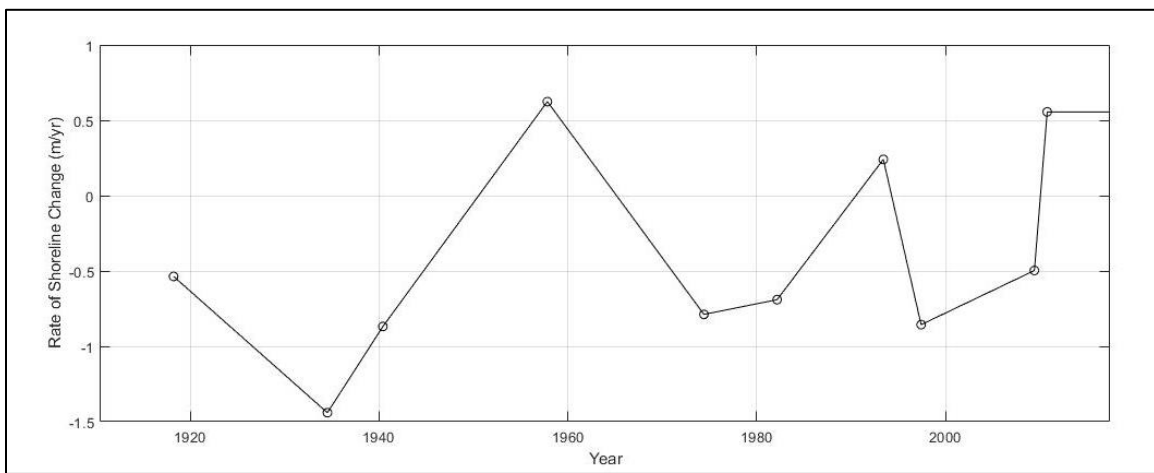


Figure 46: Temporal distribution of shoreline change rates at SL3 between 1917/18 and 2010/11 with linearly interpolated rate of rate of change.

Shoreline change rate magnitude changes over time are consistent with the results of Byrnes et al., (2013) and indicative of the evolutionary changes to the shoreline characteristics. The transition of erosional to accretion between 1934 and 1957 Byrnes et al., (2013) related this to construction of Hollinger's Ship Channel; however, this site is situated south of the channel where sediment transport and dominant wave directions would not be influenced and unrelated. The accretional trend dictated by the 1957 point then returning to erosional in 1974 is more than likely a product of error in the shoreline interpretation method and likely should be omitted. Comparison of aerial imagery from 1940 and 1974 shows minor development but no clear indications of shoreline armoring further supporting the erroneous shoreline position in 1957. Reviewing the trend shown in Figure 46, ignoring the 1957 point, closely follows an undeveloped shoreline with a possible influence of sea level rise and minimal development influence. The rate of shoreline change rate has a slight positive slope until visible vertical armoring is seen around 1997 and continued to increase (decreasing erosional rate) in subsequent years.

## SL6 Site Characterization and Shoreline Change Results

SL6 includes approximately 2500 meters (8203 feet) of linear shoreline located south of Fowl River, just north of Cedar Point, and generally referred to as Alabama Port. The shore normal incident angles range between  $111^{\circ}$  and  $122^{\circ}$  with a gently sloping unobstructed offshore bathymetry. SL6 is within close proximity to Cedar Point which is a known focal point with high rates of erosion prior to construction of U. S. Highway 193 bridge abutment, effectively fixing the point and altering astronomical tide exchange between Heron and Mobile Bay. This modification appears to have also influenced regional sediment transport pathways based on the large morphological change of the ebb and flood shoals associated with Pass aux Herons, determined using a visual comparison of aerial photography in 1940 and 1974.

Shoreline change computations found the average linear regression rate of change from 1917/18 to 2010/11 for all transects was  $-0.82$  m/yr ( $2.7$  ft/yr). The temporal trend of shoreline change rates computed at each available shoreline position are shown graphically below.

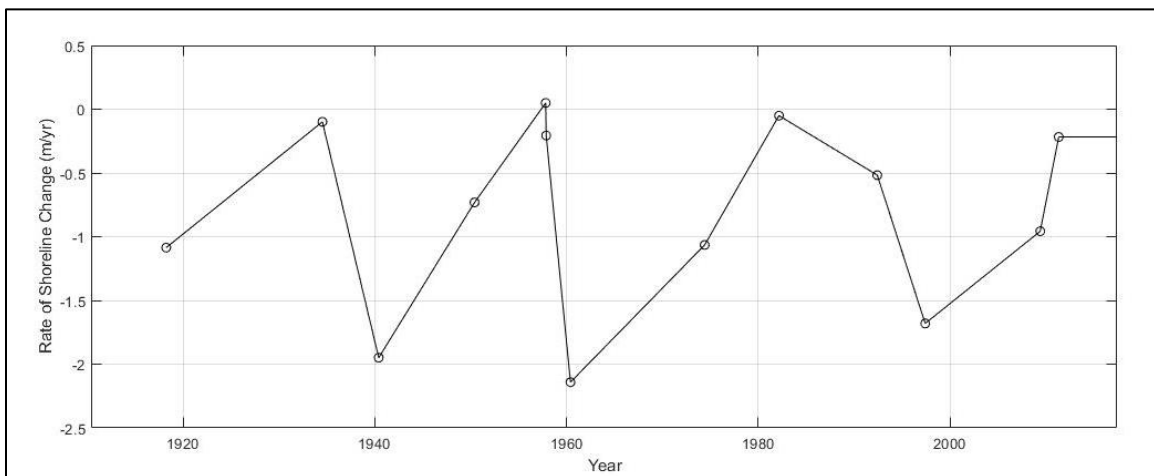


Figure 47: Temporal distribution of shoreline change rates at SL3 between 1917/18 and 2010/11 with linearly interpolated rate of rate of change.

Temporal trends of shoreline change rates at SL6 in Figure 47 do not show an immediate discernable pattern. The fluctuation could be associated with error or some function of extreme events as suggested by Byrnes et al., (2013). Overall, there does not appear to be a positive or negative net change in shoreline change rates.

## Comparison of Shoreline Change and Vessel Calls

The previous section described shoreline change rates and the trend thereof without consideration of influence by the Mobile Ship Channel. This section will attempt to make correlations of trends

in shoreline change rates to annual vessel call counts. As stated the hypothesis of this analysis is the number of vessels transiting the federal navigation channel is inversely related to the rate of shoreline change represented as length per year. The analysis will first look holistically at the vessel counts and the combined trend of shoreline change from all three sites (Figure 48) followed by subsets and samples of vessel counts and shoreline lengths.

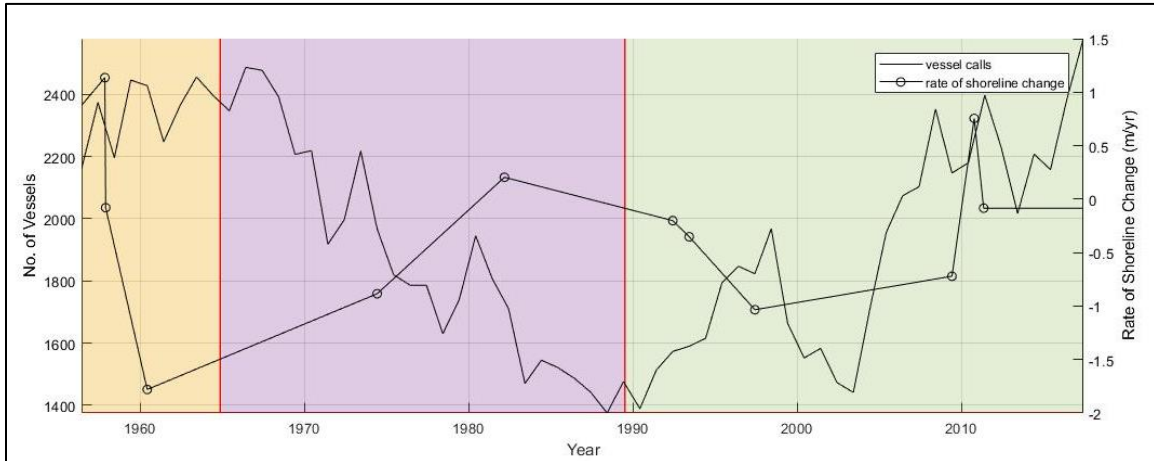


Figure 48: Plot of vessel count for Mobile Harbor between 1956 and 2017 of all vessels having a draft greater than 19 feet compared to combined average shoreline change rates for sites SL1, SL3, and SL6. Channel dimension changes are identified using the plot background.

Figure 48 appears to show an inverse correlation between shoreline change and vessel calls between 1957 and around 2000 indicating the more vessels calling to port results in an increase in shoreline erosion rates. The lack of correlation after 2000 is expected as shoreline armoring becomes much more prevalent after this time (Douglass and Pickel, 1999)

While the holistic approach does indicate an inverse correlation of temporal shoreline change rates as a function of vessel callings, a detailed assessment, on a site-by-site basis, is warranted to confirm it is not a coincidence or explained by other means such as locality, extreme events, and wave climate. The first step, site dependency, is plotted in Figure 49 followed by discussion of other forcings relationships and trends at each site.

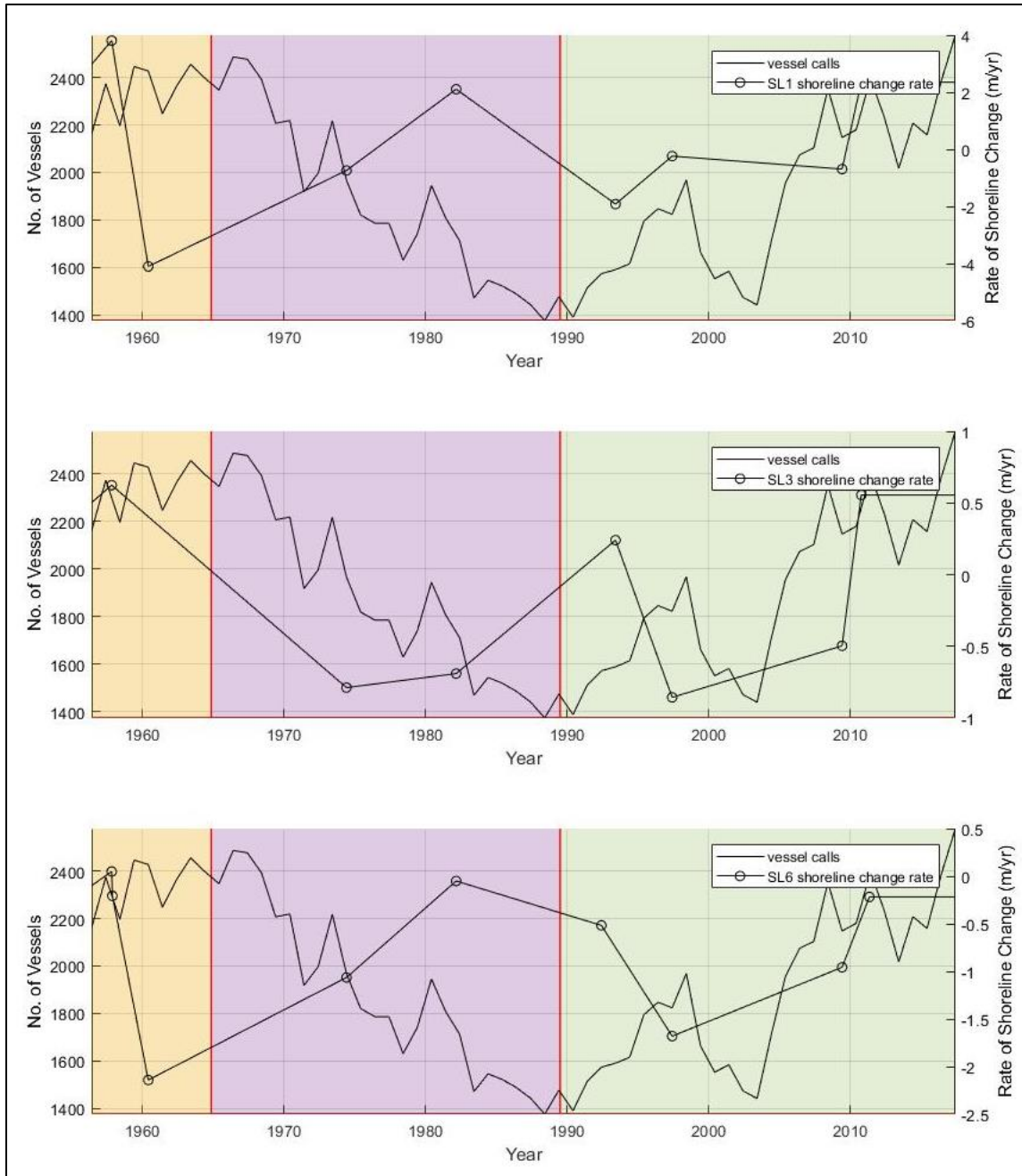


Figure 49: Plot of vessel count for Mobile Harbor between 1956 and 2017 of all vessels having a draft greater than 19 feet compared to average shoreline change rates computed for each site. Channel dimension changes are identified using the plot background color.

Correlations of vessel calls to temporal trends in the shoreline rate of change for each site generally agree (varying magnitude) from 1997 to present with a positive trend (less erosion) which is, again, expected based on the increased percentage of shoreline armoring. However, the trend between 1960 and 1993 for SL3 appears to be starkly different than SL1 and SL6 and does not follow the inverse correlation with vessel calls. Reasons for this dissimilarity are unknown. Of the two sites

that follow the inverse relationship with vessel calls, SL1 represents a much larger magnitude than SL6. The range of shoreline change rates for SL1 is between -4.1 and 3.8 meters/year while SL6 ranges between -2.1 and 0.05 meters/year. While the range is greater for SL1 it is generally centered about the zero axis whereas SL6 is more consistently erosional. The higher range at SL1 is most likely correlated to the placement of dredge material during construction of Hollinger's Island Ship Channel, construction of Gaillard Island, and in bay dredge material placement practices north of Gaillard Island and along the Mobile Ship Channel. The drastic fluctuations between erosional and accretional appear to be more similarly related to placement (accretion) and equilibration (erosion) as a result of these activities. Influence of other activities in the vicinity of SL1 does question the correlation of vessel calls to the visual trends shown in Figure 49 and where the trend of shoreline change rates and the influence of the Mobile Ship Channel is not able to be quantifiably correlated using the available data. SL6 is much further than SL1 from other anthropogenic changes and does appear to have an inversely correlated trend to vessel calls. However, the range of shoreline change rates is small and error associated with delineation of shoreline positions is inherently large (Byrnes et al., 2013) such that additional work would not lead to a more precise result. Furthermore, the unavailability of additional shoreline data points induces large interpolated ranges masking additional temporal trends.

## **Summary**

An investigation of cumulative impacts resulting from construction and proposed deepening of the Mobile Harbor Federal navigation channel was completed. The assessment sought to correlate temporal trends in shoreline change rates at three representative locations along the western shore of Mobile Bay to annualized vessel transits. Shoreline position data at 10 points between 1917/18 and 2010/11 was obtained or generated as part of the study. Vessels calling to the Port of Mobile for 1956 to 2017 were obtained from the Water Borne Commerce of the United States (WCUS) annual summary reports. These data were plotted along a temporal scale and indicate a possible inverse correlation where an increase in vessel calls results in increased erosion. In detail only one site (SL6) cannot be explained otherwise but to have a weak correlation; however, the range of shoreline change rates falls within the error band and likely a product of random error in the shoreline position delineation. As for long term effect arising from constructing the recommended plan, it is clear the vast majority of shoreline is armored and all sites agree that from 1997 to present there is no relationship between the number of vessel calls and shoreline change rates. Therefore, present and foreseeable cumulative impacts of VGWE on Mobile Bay shorelines are considered not significant.

## 6 References

---

- Bhowmik, N. G. (1975). Boat-Generated Waves in Lakes. Technical Note, Journal of the Hydraulics Division. American Society of Civil Engineers. pp. 1465-1468.
- Blaauw, H.G., de Groot, M.T., Knaap, F. C. M., Pilarczyk, K.W. (1985). Design of Bank Protection of Inland Navigation Fairways. Proceedings of the Conference on Flexible Armoured Revetments Incorporating Geotextiles, Thomas Telford, London, England, pp. 39-66.
- Capilier, C., Rousseaux, G., Calluau, D., David. L. (2015). An Experimental Study of the Effects of Finite Water Depth and Lateral Confinement of Ship Wake and Drag. Congress SHF: Hydrodynamics and Simulation Applied to Inland Waterway and Port Approaches. Meudon.
- Chen, Q., Zhao, H., Hu, K., Douglass, S. L. (2005). Prediction of Wind Waves in a Shallow Estuary. Journal of Waterway, Port, Coastal, and Ocean Engineering. American Society of Civil Engineers. 131(4), pp. 137-148.
- Chuang, L. Z., Wu, L., Wang, J. (2013). Continuous Wavelet Transform Analysis of Acceleration Signals Measured from a Buoy. Sensors 2013(13). MDPI, Basel, Switzerland. pp. 10909-10930.
- David, C. G., Roeber, V., Goseberg, N., Schlurmann, T. (2017). Generation and Propagation of Ship-Borne Waves – Solutions from a Boussinesq-Type Model. Journal of Coastal Engineering, 127(2017), pp. 170-187.
- de John, M. P. C., Roelvink, D., Reijmerink, S.P., Breederveld, C. (2013). Numerical Modelling of Passing-Ship Effects in Complex Geometries and on Shallow Water. Smart Rivers 2013, PIANC, Maastricht, The Netherlands.
- Didenkulova, I., Sheremet, A. Torsvik, T., Soomere, T. (2013). Characteristic Properties of Different Vessel Wake Signals. Proceedings 12<sup>th</sup> International Coastal Symposium (Plymouth, England), Journal of Coastal Research, Special Issue No. 65, pp. 213-218.
- Gates, E. T. and Herbich, J. B. (1977). Mathematical Model to Predict the Behavior of Deep-Draft Vessels in Restricted Waterways. Report TAMU-SG-77-206. Texas A&M University, College Station, Texas.

- Gibbons, D. T., Jones, G., Siegel, E., Hay, A., Johnson, F. (2015). Performance of a New Submersible Tide-Wave Recorder. RBR Limited. Ottawa, Ontario, Canada.
- Havelock, T.H. (1908). The Propagation of Groups of Waves in Dispersive Media, with Application to Waves on Water Produced by a Travelling Disturbance. Proceedings of the Royal Society of London. 81(549), pp. 398-430.
- International Maritime Organization (IMO) (2015). Revised Guidelines for the Onboard Operational Use of Shipborne Automatic Identification Systems (AIS). 29<sup>th</sup> Session, Agenda Item 10. Resolution A.1106(29). International Maritime Organization, London, England.
- Javanmardi, M., Binns, J., Renilson, M., Thomas, G. (2017). Influence of Channel Shape on Wave-Generated Parameters by a Pressure Source in Shallow Water. Journal of Waterway, Port, Coastal, Ocean Engineering. American Society of Civil Engineers. 143(5), pgs. 9.
- Jiang, T., Henn, R., Sharma, S. D. (2002). Wash Waves Generated by Ships Moving on Fairways of Varying Topography. 24<sup>th</sup> Symposium on Naval Hydrodynamics, Fukuoka, Japan, pgs. 15.
- Kriebel, D.L. and Seelig, W. N. (2005). An Empirical Model for Ship-Generated Waves. 7<sup>th</sup> International Conference on Mathematical and Numerical Aspects of Waves (Waves 05), Madrid, Spain.
- Mallet, S. (2009). A Wavelet Tour of Signal Processing – The Sparse Way. Academic Press as an Imprint of Elsevier. Burlington, Massachusetts.
- Maynard, S. (2007). Ship Forces on the Shoreline of the Savannah Harbor Project. Technical Report ERDC/CHL TR-06-19, U.S. Army Corps of Engineers, Engineering Research and Development Center, Vicksburg, Mississippi.
- Maynard, S. (2011). Reanalysis of Ship Forces at the Shoreline using Updated Draft Information, Savannah Harbor, Savannah, Georgia. Draft Report, U.S. Army Corps of Engineers, Engineering Research and Development Center, Vicksburg, Mississippi.
- National Oceanic and Atmospheric Administration (NOAA) (2018). Coast Guard Sector Mobile, Alabama – Station ID: 8736897. Center for Operational Oceanographic Products and Services (CO-OPS), Silver Spring, Maryland.

- Parnell, K. E., Soomere, T., Zaggia, L., Rodin, A., Lorenzetti, G., Rapaglia, J., Scarpa, G. M. (2015). Ship-Induced Solitary Riemann Waves of Depression in Venice Lagoon. *Physical Letters A*(2015), <http://dx.doi.org/10.1016/j.physleta.2014.12.004>.
- Pelinovsky, E., Talipova, T., Kurkin, A., Kharif, C. (2001). Nonlinear Mechanism of Tsunami Wave Generation by Atmospheric Disturbances. *Natural Hazards and Earth System Sciences*, European Geophysical Society, pp. 243-250.
- Pendygraft, S. L. and Gelfenbaum, G. R (1994) Wave Data in Mobile Bay, Alabama from March 1991 to May 1992. OF 94-0017, U.S. Geological Survey, St. Petersburg, Florida.
- Permanent International Association of Navigation Congresses (PIANC) (1987). Guidelines for the Design and Construction of Flexible Revetments Incorporating Geotextiles for Inland Waterways. Working Group 4 of the Permanent Technical Committee, Brussels.
- Permanent International Association of Navigation Congresses (PIANC) (1985). Underkeel Clearance for Large Ships in Maritime Fairways with Hard Bottom. Supplement to Bulletin No. 51, Brussels, Belgium.
- Rapaglia, J., Zaggia, L., Ricklefs, K., Gelinis, M., Bokuniewicz, H., (2011). Characteristics of Ships' Depression Waves and Associated Sediment Resuspension in Venice Lagoon, Italy. *Journal of Marine Systems*. 85(2011), pp. 45-56.
- RBR Limited (2012). RBRsolo User Guide. Document RBR0000215, RBR Ltd, Ottawa, Ontario, Canada.
- Rodin, A., Soomere, T., Parnell, K. E., Zaggia, L. (2015). Numerical Simulation of the Propagation of Ship-Induced Riemann Waves of Depression into the Venice Lagoon. *Proceedings of the Estonian Academy of Sciences*. 64(1), pp. 22-35.
- Schijf, J.B. and Jansen, P.P. (1953). Eighteenth International Navigation Conference, Section I, Communications 1, Rome, Italy.
- Schoellhamer, D. H. (1996). Anthropogenic Sediment Resuspension Mechanisms in a Shallow Microtidal Estuary. *Estuarine, Coastal, and Shelf Science*. Academic Press Limited. 43:533-548.
- Sheremet, A., Gravois, U., Tian, M. (2013). Boat-Wake Statistics at Jensen Beach, Florida. *Journal of Waterway, Port, Coastal, and Ocean Engineering*. American Society of Civil Engineers. 139, pp. 286-294.

- Soomere, T. (2006). Nonlinear Ship Wake Waves as a Model of Rouge Waves and a Source of Danger to the Coastal Environment: A Review. *Oceanologia*, Institute of Oceanology, 48(S), pp. 185-202.
- Sorensen, R. (1966). Ship Waves. Technical Report HEL-12-2. University of California, Berkeley, California.
- Sorensen, R. M. (1973). Ship-Generated Waves. *Advances in Hydrosience*, Academic Press, New York, Illinois. pp. 49-83.
- Sorensen, R. M. and Weggel, J. R. (1984). Development of Ship Wave Design Information. Proceedings of the 19<sup>th</sup> Conference on Coastal Engineering, Houston, Texas. American Society of Civil Engineers. New York, Illinois. pp. 3227-3243.
- Sorensen, R. M. (1997), Prediction of Vessel-Generated Waves with Reference to Vessels Common to the Upper Mississippi River System. ENV Report 4. Lehigh University, Bethlehem, Pennsylvania.
- Thompson, W. (Lord Kelvin) (1887). On Ship Waves. Proceedings of the Institute of Mechanical Engineering, London, England. 38(1), pp. 409-433.
- U.S. Army Corps of Engineers, (2006), Coastal Engineering Manual (CEM), U.S. Army Corps of Engineers, Washington, D.C. (6 volumes). EM 1110-2-1100.
- U. S. Army Corps of Engineers. (2006). Hydraulic Design of Deep Draft Navigation Projects. U.S. Army Corps of Engineers, Washington, D.C. EM 1110-2-1613.
- U. S. Army Corps of Engineers (2010). Wave Information Studies (WIS), Station 73154. U.S. Army Corps of Engineers, Engineering Research and Development Center, Vicksburg, Mississippi.
- U.S. Army Corps of Engineers, Huntington District. (1980). Gallipolis Locks and Dam Replacement, Ohio River, Phase I – Advanced Engineering and Design Study. General Design Memorandum, Huntington, West Virginia.
- Weggel J. and Sorensen, R. (1986). Ship Wave Prediction for Port and Channel Design. Proceedings of the Ports '86 Conference, Oakland, California. American Society of Civil Engineers, New York. pp 797-814.

## **Appendix A**

### **Vessel Generated Wave Energy Data by Transit**

ID	MMSI	Class	Length (m)	Width (m)	Draft (m)	SOG	Direction	SW01_Hmo	SW02_Hmo	SW03_Hmo	SW04_Hmo	SW05_Hmo
1	636017004	2	134	16	7.2	12	'outbound'	0.0007	0.0013	0.0028	0.0038	0.0003
2	249944000	3	229	37	13.8	7	'outbound'	0.0008	0.0016	0.0034	0.0084	0.0004
3	477178300	3	292	32	12.9	11	'outbound'	0.0098	0.0167	0.0757	0.1268	0.0061
4	353486000	4	260	32	8.2	13	'inbound'	0.0206	0.0350	0.0447	0.0661	0.0054
5	249550000	1	244	42	8.2	10	'outbound'	0.0042	0.0018	0.0215	0.0339	0.0026
6	538003413	2	190	32	6.7	10	'outbound'	0.0042	0.0018	0.0215	0.0339	0.0026
7	305367000	2	132	16	5.4	12	'inbound'	0.0047	0.0044	0.0047	0.0037	0.0081
8	563635000	2	176	35	5.8	8	'outbound'	0.0028	0.0030	0.0042	0.0032	0.0070
9	353486000	4	260	32	8.2	11	'outbound'	0.0068	0.0104	0.0246	0.0180	0.0096
10	538006092	1	239	42	11.9	9	'inbound'	0.0007	0.0021	0.0139	0.0449	0.0170
11	309587000	2	190	31	9	11	'outbound'	0.0028	0.0071	0.0287	0.0484	0.0409
12	248092000	2	169	27	7.8	11	'outbound'	0.0043	0.0059	0.0194	0.0694	0.0533
13	370261000	2	178	29	6.3	11	'outbound'	0.0019	0.0081	0.0117	0.0223	0.0202
14	309689000	2	131	20	7	11	'inbound'	0.0010	0.0027	0.0047	0.0065	0.0164
15	305057000	2	138	21	6	13	'inbound'	0.0050	0.0074	0.0074	0.0090	0.0216
16	305057000	3	138	21	6	13	'inbound'	0.0050	0.0074	0.0074	0.0090	0.0216
17	636091328	3	275	40	11.6	12	'inbound'	0.0232	0.0354	0.0682	0.1162	0.0174
18	311053600	3	229	32	13.7	10	'inbound'	0.0039	0.0068	0.0208	0.0657	0.0094
19	305367000	2	132	16	5	12	'outbound'	0.0017	0.0042	0.0067	0.0110	0.0080
20	338302000	1	182	36	11.3	10	'inbound'	0.0030	0.0042	0.0245	0.0400	0.0011
21	311923000	1	186	32	8.2	12	'inbound'	0.0109	0.0183	0.0318	0.0356	0.0032
22	305057000	2	138	21	5.6	13	'outbound'	0.0010	0.0043	0.0049	0.0084	0.0010
23	538006092	1	239	42	8.1	10	'outbound'	0.0028	0.0048	0.0267	0.0298	0.0022
24	352179000	1	228	42	12.2	9	'inbound'	0.0007	0.0014	0.0039	0.0255	0.0014
25	477077800	3	261	32	10.9	12	'inbound'	0.0189	0.0342	0.0784	0.0994	0.0021
26	636091328	3	275	40	13	11	'outbound'	0.0078	0.0083	0.0518	0.1414	0.0088
27	235070707	2	198	33	10.4	11	'inbound'	0.0072	0.0137	0.0349	0.0335	0.0016
28	338302000	1	182	36	8.1	10	'outbound'	0.0027	0.0024	0.0083	0.0085	0.0011
29	210516000	3	226	30	9.8	11	'inbound'	0.0031	0.0049	0.0144	0.0131	0.0005
30	538004997	2	200	32	12.2	10	'inbound'	0.0026	0.0040	0.0079	0.0381	0.0005
31	477077800	3	261	32	11.4	10	'outbound'	0.0016	0.0020	0.0610	0.0374	0.0018
32	371208000	3	293	32	11.6	10	'inbound'	0.0026	0.0043	0.0282	0.0416	0.0028
33	210516000	3	226	30	9.6	10	'outbound'	0.0026	0.0044	0.0287	0.0419	0.0027
34	564939000	1	237	42	11.5	9	'inbound'	0.0041	0.0067	0.0221	0.0859	0.0184
35	255805596	3	318	42	10.2	11	'inbound'	0.0093	0.0229	0.0868	0.1421	0.0142
36	371208000	3	293	32	11.7	11	'outbound'	0.0045	0.0071	0.0487	0.1018	0.0121
37	235070707	2	198	33	9.8	11	'outbound'	0.0043	0.0029	0.0175	0.0206	0.0067
38	352179000	1	228	42	8.5	10	'outbound'	0.0027	0.0016	0.0309	0.0344	0.0076
39	563936000	1	247	42	11.6	10	'inbound'	0.0024	0.0063	0.0247	0.0752	0.0152
40	563775000	1	175	36	5.6	9	'inbound'	0.0011	0.0025	0.0063	0.0110	0.0153
41	353486000	4	260	32	8	13	'inbound'	0.0144	0.0258	0.0372	0.0484	0.0166
42	311923000	1	186	32	9.4	10	'outbound'	0.0026	0.0050	0.0211	0.0359	0.0089
43	353486000	4	260	32	8.2	12	'outbound'	0.0040	0.0146	0.0287	0.0727	0.0089
44	255805596	3	318	42	10	8	'outbound'	0.0046	0.0053	0.0167	0.0338	0.0056
45	257881000	2	199	32	7.1	11	'inbound'	0.0045	0.0053	0.0156	0.0341	0.0056
46	538004997	2	200	32	9.2	10	'outbound'	0.0024	0.0054	0.0203	0.0336	0.0052
47	219219000	3	292	32	12.1	11	'inbound'	0.0005	0.0213	0.0743	0.0935	0.0059
48	305859000	2	155	23	8.9	12	'inbound'	0.0080	0.0131	0.0155	0.0181	0.0017
49	563775000	1	175	36	5.9	9	'outbound'	0.0023	0.0006	0.0038	0.0026	0.0006
50	563936000	1	247	42	8.8	9	'outbound'	0.0024	0.0033	0.0159	0.0270	0.0016
51	311053600	3	229	32	7.6	12	'outbound'	0.0057	0.0120	0.0215	0.0400	0.0042
52	219219000	3	292	32	12.4	11	'outbound'	0.0037	0.0105	0.0577	0.0955	0.0032
53	538006564	3	293	40	11.8	11	'inbound'	0.0285	0.0429	0.0843	0.1771	0.0039
54	564939000	1	237	42	8.8	10	'outbound'	0.0030	0.0069	0.0355	0.0431	0.0039
55	305859000	2	155	23	8.4	12	'outbound'	0.0044	0.0034	0.0106	0.0133	0.0013
56	311071300	2	143	22	5.8	12	'inbound'	0.0009	0.0017	0.0033	0.0034	0.0004

ID	MMSI	Class	Length (m)	Width (m)	Draft (m)	SOG	Direction	SW01_Hmo	SW02_Hmo	SW03_Hmo	SW04_Hmo	SW05_Hmo
57	477464400	3	261	32	10.5	11	'inbound'	0.0118	0.0238	0.0378	0.0119	0.0013
58	305598000	2	146	18	5.4	11	'inbound'	0.0047	0.0021	0.0385	0.0812	0.0021
59	538006564	3	293	40	9.2	10	'outbound'	0.0045	0.0019	0.0362	0.0700	0.0022
60	305598000	2	146	18	5.4	11	'outbound'	0.0006	0.0004	0.0011	0.0012	0.0008
61	477464400	3	261	32	10.4	11	'outbound'	0.0054	0.0035	0.0390	0.0632	0.0044
62	636016708	2	199	32	8.4	11	'inbound'	0.0046	0.0132	0.0298	0.0262	0.0021
63	353486000	4	260	32	7.9	13	'inbound'	0.0219	0.0310	0.0390	0.0685	0.0013
64	353486000	4	260	32	8.1	12	'outbound'	0.0042	0.0112	0.0256	0.0481	0.0032
65	311071300	2	143	22	7.8	12	'outbound'	0.0033	0.0034	0.0095	0.0091	0.0014
66	636016708	2	199	32	8.1	11	'outbound'	0.0023	0.0028	0.0150	0.0145	0.0005
67	311000236	2	200	32	9.4	11	'inbound'	0.0035	0.0009	0.0197	0.0262	0.0005
68	257314000	2	198	30	8.8	11	'inbound'	0.0030	0.0049	0.0170	0.0267	0.0004
69	248092000	2	169	27	5.5	11	'inbound'	0.0006	0.0016	0.0040	0.0044	0.0004
70	563635000	2	176	35	5.6	9	'inbound'	0.0004	0.0004	0.0010	0.0032	0.0005
71	636091916	3	225	28	8.6	12	'inbound'	0.0078	0.0209	0.0293	0.0314	0.0044
72	353445000	3	226	32	13.7	9	'inbound'	0.0011	0.0006	0.0047	0.0371	0.0003
73	636091916	3	225	28	8.8	13	'outbound'	0.0041	0.0118	0.0293	0.0685	0.0028
74	563635000	2	176	35	6.1	9	'outbound'	0.0005	0.0009	0.0035	0.0029	0.0003
75	354891000	3	295	32	11.1	11	'inbound'	0.0038	0.0035	0.0343	0.0487	0.0007
76	374459000	3	293	45	9	8	'inbound'	0.0015	0.0017	0.0050	0.0111	0.0008
77	367416750	NaN	166	22	5.4	10	'inbound'	0.0005	0.0004	0.0006	0.0011	0.0004
78	257314000	2	198	30	7.8	11	'outbound'	0.0026	0.0044	0.0128	0.0149	0.0014
79	248092000	2	169	27	7.8	10	'outbound'	0.0013	0.0006	0.0028	0.0094	0.0002
80	354891000	3	295	32	10.9	9	'outbound'	0.0013	0.0019	0.0168	0.0200	0.0000
81	257532000	2	198	31	7.9	11	'inbound'	0.0021	0.0046	0.0370	0.1412	0.0061
82	636017642	3	318	43	10.3	11	'inbound'	0.0024	0.0047	0.0870	0.1417	0.0019
83	367416750	NaN	166	22	4.6	10	'outbound'	0.0007	0.0010	0.0049	0.0032	0.0026
84	309689000	2	131	20	8.9	13	'outbound'	0.0015	0.0015	0.0082	0.0085	0.0010
85	353486000	4	260	32	8	12	'inbound'	0.0107	0.0207	0.0379	0.0589	0.0065
86	636017642	3	318	43	9.8	10	'outbound'	0.0032	0.0026	0.0418	0.0798	0.0039
87	311000236	2	200	32	7.4	9	'outbound'	0.0034	0.0019	0.0420	0.0801	0.0022
88	305463000	2	140	26	6.1	13	'inbound'	0.0033	0.0021	0.0425	0.0802	0.0022
89	636017006	3	294	32	10.3	11	'inbound'	0.0088	0.0187	0.0587	0.0710	0.0009
90	338302000	1	182	36	11	11	'inbound'	0.0051	0.0199	0.0607	0.0793	0.0012
91	308045000	4	273	42	8.3	11	'inbound'	0.0011	0.0018	0.0166	0.0479	0.0011
92	353486000	4	260	32	8.1	13	'outbound'	0.0068	0.0130	0.0403	0.0569	0.0043
93	353445000	3	226	32	7.4	12	'outbound'	0.0066	0.0021	0.0247	0.0282	0.0037
94	636092722	3	260	43	8.1	10	'inbound'	0.0012	0.0068	0.0381	0.0490	0.0008
95	563775000	1	175	36	5.6	9	'inbound'	0.0002	0.0003	0.0003	0.0014	0.0002
96	305463000	2	140	26	6.1	13	'outbound'	0.0012	0.0032	0.0047	0.0078	0.0011
97	308045000	4	273	42	8.5	12	'outbound'	0.0093	0.0156	0.0536	0.0930	0.0058
98	636017006	3	294	32	11	11	'outbound'	0.0061	0.0149	0.0608	0.0998	0.0020
99	636014410	3	293	40	11.2	11	'inbound'	0.0002	0.0148	0.0843	0.1263	0.0015
100	338302000	1	182	36	9.5	11	'outbound'	0.0073	0.0068	0.0153	0.0199	0.0019
101	538004241	3	229	32	7	12	'inbound'	0.0134	0.0188	0.0371	0.0479	0.0043
102	563775000	1	175	36	6	9	'outbound'	0.0140	0.0191	0.0378	0.0492	0.0044
103	477004700	3	261	32	10.3	11	'inbound'	0.0127	0.0241	0.0636	0.0651	0.0016
104	374459000	3	293	45	13.5	7	'outbound'	0.0029	0.0011	0.0058	0.0337	0.0010
105	636014410	3	293	40	12.4	9	'outbound'	0.0012	0.0008	0.0143	0.0405	0.0001
106	311071300	2	143	22	5.5	12	'inbound'	0.0014	0.0017	0.0028	0.0037	0.0002
107	477004700	3	261	32	10.1	10	'outbound'	0.0038	0.0068	0.0085	0.0236	0.0020
108	304968000	2	143	23	9	12	'inbound'	0.0059	0.0078	0.0166	0.0153	0.0008
109	257532000	2	198	31	7.9	10	'outbound'	0.0061	0.0078	0.0186	0.0153	0.0016
110	636091685	1	244	42	12.1	10	'inbound'	0.0015	0.0024	0.0137	0.0656	0.0007
111	636016824	2	190	32	12.3	9	'inbound'	0.0055	0.0052	0.0125	0.0295	0.0122
112	371245000	3	324	43	9	11	'inbound'	0.0065	0.0173	0.0562	0.0722	0.0168

ID	MMSI	Class	Length (m)	Width (m)	Draft (m)	SOG	Direction	SW01_Hmo	SW02_Hmo	SW03_Hmo	SW04_Hmo	SW05_Hmo
113	257457000	2	208	32	8.2	10	'inbound'	0.0046	0.0179	0.0573	0.0731	0.0169
114	353486000	4	260	32	8.1	13	'inbound'	0.0212	0.0321	0.0457	0.0692	0.0198
115	636091685	1	244	42	8.1	11	'outbound'	0.0052	0.0078	0.0334	0.0541	0.0049
116	538004241	3	229	32	10.5	10	'outbound'	0.0067	0.0078	0.0269	0.0967	0.0249
117	311000508	2	220	30	8.5	11	'inbound'	0.0070	0.0189	0.0372	0.0997	0.0286
118	353486000	4	260	32	8.2	12	'outbound'	0.0068	0.0136	0.0396	0.0666	0.0174
119	371245000	3	324	43	8.6	11	'outbound'	0.0073	0.0075	0.0512	0.1471	0.0234
120	311071300	2	143	22	7.8	11	'outbound'	0.0074	0.0085	0.0551	0.1473	0.0201
121	352652000	3	255	43	13.7	8	'inbound'	0.0028	0.0046	0.0125	0.0583	0.0301
122	477177100	3	260	32	10.8	11	'inbound'	0.0069	0.0195	0.0360	0.0502	0.0301
123	357405000	3	294	31	11.2	11	'inbound'	0.0135	0.0250	0.0527	0.0852	0.0247
124	563635000	2	176	35	5.8	9	'inbound'	0.0016	0.0033	0.0099	0.0244	0.0403
125	477177100	3	260	32	10.7	11	'outbound'	0.0034	0.0063	0.0308	0.0823	0.0213
126	563635000	2	176	35	5.9	9	'outbound'	0.0006	0.0006	0.0042	0.0046	0.0105
127	305560000	2	144	18	6.4	12	'inbound'	0.0007	0.0018	0.0027	0.0043	0.0096
128	246580000	1	136	23	6.7	12	'inbound'	0.0016	0.0028	0.0047	0.0151	0.0041
129	636092722	3	260	43	13.3	7	'outbound'	0.0016	0.0028	0.0047	0.0151	0.0041
130	357405000	3	294	31	12.3	10	'outbound'	0.0028	0.0056	0.0368	0.0815	0.0064
131	477001700	3	261	32	10.6	11	'inbound'	0.0089	0.0120	0.0225	0.0283	0.0033
132	636016080	1	247	42	12	10	'inbound'	0.0063	0.0130	0.0295	0.0750	0.0032
133	248092000	2	169	27	5.4	12	'inbound'	0.0018	0.0023	0.0047	0.0041	0.0027
134	304968000	2	143	23	8.8	11	'outbound'	0.0010	0.0021	0.0090	0.0158	0.0043
135	311000508	2	220	30	11	9	'outbound'	0.0016	0.0022	0.0299	0.0543	0.0040
136	636016824	2	190	32	5.9	12	'outbound'	0.0012	0.0044	0.0107	0.0180	0.0051
137	374900000	2	199	33	13.2	8	'inbound'	0.0009	0.0017	0.0025	0.0169	0.0007
138	477001700	3	261	32	11.5	10	'outbound'	0.0019	0.0030	0.0280	0.0428	0.0002
139	563722000	3	277	40	11.9	10	'inbound'	0.0063	0.0177	0.0577	0.0746	0.0040
140	257457000	2	208	32	9	11	'outbound'	0.0029	0.0090	0.0216	0.0506	0.0022
141	305560000	2	144	18	6.2	12	'outbound'	0.0006	0.0018	0.0035	0.0047	0.0005
142	353486000	4	260	32	8.2	13	'inbound'	0.0165	0.0289	0.0384	0.0600	0.0057
143	311000221	1	243	42	9.2	10	'inbound'	0.0087	0.0021	0.0364	0.0666	0.0006
144	636016080	1	247	42	8.6	10	'outbound'	0.0032	0.0080	0.0259	0.0472	0.0056
145	246580000	1	136	23	8.4	8	'outbound'	0.0041	0.0026	0.0382	0.0656	0.0036
146	563722000	3	277	40	12.3	8	'outbound'	0.0046	0.0028	0.0311	0.0383	0.0088
147	353486000	4	260	32	8.1	13	'outbound'	0.0035	0.0140	0.0331	0.0733	0.0041
148	248092000	2	169	27	7.3	11	'outbound'	0.0021	0.0024	0.0062	0.0080	0.0028
149	370235000	3	229	32	13.6	6	'outbound'	0.0006	0.0004	0.0011	0.0058	0.0024
150	210516000	3	226	30	9.1	12	'inbound'	0.0131	0.0235	0.0335	0.0429	0.0138
151	311000221	1	243	42	8.5	10	'outbound'	0.0027	0.0054	0.0268	0.0683	0.0125
152	215724000	3	294	32	11.3	11	'inbound'	0.0053	0.0096	0.0597	0.0559	0.0050
153	239746000	3	225	33	7.3	11	'inbound'	0.0023	0.0098	0.0595	0.0560	0.0050
154	210516000	3	226	30	9.5	12	'outbound'	0.0032	0.0092	0.0313	0.0666	0.0042
155	477620700	2	199	32	9.9	11	'inbound'	0.0042	0.0121	0.0290	0.0408	0.0098
156	215724000	3	294	32	11.4	11	'outbound'	0.0035	0.0050	0.0459	0.1128	0.0135
157	218582000	3	325	43	10.3	11	'inbound'	0.0095	0.0088	0.0650	0.0959	0.0007
158	352652000	3	255	43	6.8	10	'outbound'	0.0021	0.0045	0.0220	0.0290	0.0009
159	370273000	3	275	32	11.5	11	'inbound'	0.0145	0.0273	0.0650	0.1034	0.0028
160	218582000	3	325	43	10.2	10	'outbound'	0.0035	0.0081	0.0431	0.1085	0.0034
161	374900000	2	199	33	6.8	11	'outbound'	0.0035	0.0049	0.0070	0.0130	0.0021
162	565671000	2	186	28	11.3	11	'inbound'	0.0004	0.0055	0.0224	0.0268	0.0000
163	636015526	1	228	42	12.2	10	'inbound'	0.0007	0.0047	0.0248	0.0068	0.0005
164	305614000	2	123	18	5.5	12	'inbound'	0.0007	0.0009	0.0014	0.0019	0.0003
165	477620700	2	199	32	9	11	'outbound'	0.0021	0.0042	0.0185	0.0225	0.0019
166	370273000	3	275	32	12	11	'outbound'	0.0015	0.0041	0.0497	0.0977	0.0000
167	311000222	1	243	42	11.2	10	'inbound'	0.0018	0.0051	0.0392	0.0963	0.0000
168	255805674	3	278	40	11.6	10	'inbound'	0.0033	0.0108	0.0530	0.0749	0.0000

ID	MMSI	Class	Length (m)	Width (m)	Draft (m)	SOG	Direction	SW01_Hmo	SW02_Hmo	SW03_Hmo	SW04_Hmo	SW05_Hmo
169	311071300	2	143	22	5.6	12	'inbound'	0.0024	0.0034	0.0057	0.0069	0.0000
170	305614000	2	123	18	5.4	12	'outbound'	0.0008	0.0016	0.0037	0.0032	0.0000
171	308268000	2	188	29	11.8	9	'inbound'	0.0009	0.0018	0.0025	0.0114	0.0000
172	239746000	3	225	33	12.5	9	'outbound'	0.0025	0.0048	0.0280	0.0293	0.0000
173	636015526	1	228	42	8.6	11	'outbound'	0.0054	0.0054	0.0240	0.0548	0.0000
174	563775000	1	175	36	5.8	9	'inbound'	0.0024	0.0014	0.0012	0.0063	0.0000
175	353486000	4	260	32	8	8	'inbound'	0.0034	0.0019	0.0020	0.0064	0.0000
176	477752400	3	261	32	10.8	11	'inbound'	0.0151	0.0208	0.0463	0.0783	0.0000
177	366235000	2	207	23	7.2	9	'outbound'	0.0144	0.0208	0.0468	0.0780	0.0000
178	255805674	3	278	40	12.6	10	'outbound'	0.0032	0.0087	0.0500	0.1030	0.0000
179	353486000	4	260	32	8.2	12	'outbound'	0.0034	0.0106	0.0344	0.0641	0.0000
180	477752400	3	261	32	11.2	12	'outbound'	0.0056	0.0070	0.0561	0.1517	0.0000
181	311000222	1	243	42	8.3	11	'outbound'	0.0044	0.0083	0.0413	0.0482	0.0000
182	311071300	2	143	22	7.9	12	'outbound'	0.0014	0.0031	0.0102	0.0104	0.0000
183	565671000	2	186	28	6.3	12	'outbound'	0.0036	0.0048	0.0097	0.0163	0.0000
184	563775000	1	175	36	5.8	8	'outbound'	0.0027	0.0014	0.0040	0.0035	0.0000
185	538003248	2	190	32	6.7	11	'inbound'	0.0014	0.0026	0.0072	0.0000	0.0000
186	308976000	3	230	32	12.2	10	'inbound'	0.0018	0.0023	0.0047	0.0000	0.0000
187	367006560	NaN	175	24	7.9	8	'inbound'	0.0019	0.0017	0.0047	0.0000	0.0019
188	636091916	3	225	28	8.4	12	'inbound'	0.0108	0.0150	0.0385	0.0348	0.0072
189	563635000	2	176	35	5.6	9	'inbound'	0.0025	0.0017	0.0041	0.0036	0.0093
190	248092000	2	169	27	5.5	12	'inbound'	0.0023	0.0032	0.0052	0.0184	0.0064
191	352468000	3	229	32	13	10	'inbound'	0.0021	0.0048	0.0129	0.0372	0.0053
192	235103314	2	177	28	7.4	11	'inbound'	0.0017	0.0024	0.0083	0.0101	0.0026
193	636012630	1	228	32	11.7	10	'inbound'	0.0018	0.0041	0.0090	0.0527	0.0028
194	367006560	NaN	175	24	6.1	10	'outbound'	0.0006	0.0005	0.0028	0.0022	0.0014
195	308976000	3	230	32	9.5	10	'outbound'	0.0028	0.0051	0.0305	0.0419	0.0011
196	538003248	2	190	32	6.4	10	'outbound'	0.0026	0.0047	0.0301	0.0305	0.0012
197	563635000	2	176	35	5.6	9	'outbound'	0.0020	0.0019	0.0040	0.0016	0.0006
198	636091916	3	225	28	8.5	12	'outbound'	0.0054	0.0069	0.0199	0.0292	0.0026
199	353486000	4	260	32	8.4	13	'inbound'	0.0162	0.0241	0.0366	0.0494	0.0016
200	353486000	4	260	32	8.2	12	'outbound'	0.0036	0.0095	0.0273	0.0595	0.0030
201	367115000	NaN	162	24	7.9	10	'inbound'	0.0005	0.0008	0.0005	0.0026	0.0008
202	235103314	2	177	28	7	10	'outbound'	0.0001	0.0012	0.0089	0.0054	0.0000
203	636012630	1	228	32	8.1	11	'outbound'	0.0036	0.0052	0.0198	0.0173	0.0022
204	636018018	3	299	42	9.5	11	'inbound'	0.0176	0.0419	0.0863	0.0913	0.0069
205	308268000	2	188	29	7.5	9	'outbound'	0.0063	0.0041	0.0094	0.0068	0.0024
206	248092000	2	169	27	7.9	9	'outbound'	0.0051	0.0033	0.0178	0.0223	0.0033
207	636018018	3	299	42	9.8	11	'outbound'	0.0045	0.0101	0.0450	0.1164	0.0111
208	305394000	2	140	16	4.6	12	'inbound'	0.0020	0.0006	0.0012	0.0018	0.0069
209	219217000	3	293	32	11.8	9	'inbound'	0.0032	0.0107	0.0284	0.0249	0.0028
210	368589000	1	183	32	11.5	8	'inbound'	0.0026	0.0028	0.0158	0.0288	0.0021
211	477832300	3	261	32	11	12	'inbound'	0.0150	0.0278	0.0566	0.0862	0.0027
212	305394000	2	140	16	4.6	12	'outbound'	0.0002	0.0009	0.0010	0.0017	0.0003
213	219217000	3	293	32	12.5	10	'outbound'	0.0049	0.0020	0.0380	0.0662	0.0044
214	367115000	NaN	162	24	7.9	9	'outbound'	0.0050	0.0020	0.0384	0.0667	0.0046
215	477832300	3	261	32	11.6	11	'outbound'	0.0056	0.0046	0.0418	0.0581	0.0086
216	368589000	1	183	32	7.7	10	'outbound'	0.0033	0.0016	0.0167	0.0146	0.0109
217	636014069	1	250	40	12.2	8	'inbound'	0.0047	0.0066	0.0189	0.0697	0.0407
218	477334100	2	170	27	9.6	10	'inbound'	0.0030	0.0056	0.0125	0.0169	0.0117
219	538007510	2	200	32	10.7	10	'inbound'	0.0054	0.0079	0.0283	0.0443	0.0025
220	338302000	1	182	36	11	10	'inbound'	0.0038	0.0051	0.0228	0.0366	0.0012
221	538007655	2	199	33	10.7	9	'inbound'	0.0027	0.0029	0.0058	0.0169	0.0018
222	563775000	1	175	36	5.8	9	'inbound'	0.0016	0.0021	0.0032	0.0251	0.0053
223	353486000	4	260	32	8	10	'inbound'	0.0038	0.0045	0.0046	0.0162	0.0109
224	311071300	2	143	22	5.7	12	'inbound'	0.0016	0.0022	0.0038	0.0043	0.0003

ID	MMSI	Class	Length (m)	Width (m)	Draft (m)	SOG	Direction	SW01_Hmo	SW02_Hmo	SW03_Hmo	SW04_Hmo	SW05_Hmo
225	636014069	1	250	40	8.2	11	'outbound'	0.0046	0.0039	0.0258	0.0552	0.0030
226	372197000	1	144	23	5.6	12	'inbound'	0.0017	0.0073	0.0107	0.0112	0.0006
227	305663000	2	153	22	6.7	12	'inbound'	0.0017	0.0073	0.0107	0.0112	0.0006
228	636092187	2	144	23	8.6	12	'inbound'	0.0032	0.0045	0.0088	0.0065	0.0002
229	353486000	4	260	32	8.2	12	'outbound'	0.0047	0.0120	0.0313	0.0687	0.0024
230	563775000	1	175	36	6	8	'outbound'	0.0006	0.0013	0.0064	0.0023	0.0019
231	247275300	1	249	44	10.7	9	'inbound'	0.0041	0.0042	0.0196	0.0926	0.0033
232	352652000	3	255	43	13.7	8	'inbound'	0.0036	0.0013	0.0037	0.0483	0.0018
233	338302000	1	182	36	9.2	10	'outbound'	0.0042	0.0072	0.0144	0.0180	0.0110
234	352468000	3	229	32	8.3	11	'outbound'	0.0058	0.0123	0.0388	0.0997	0.0075
235	311968000	3	225	32	7.4	10	'inbound'	0.0172	0.0142	0.0208	0.0234	0.0170
236	249249000	1	147	24	6.5	12	'inbound'	0.0061	0.0077	0.0097	0.0127	0.0069
237	247275300	1	249	44	8.5	10	'outbound'	0.0048	0.0083	0.0341	0.0557	0.0100
238	311000222	1	243	42	11.6	9	'inbound'	0.0036	0.0039	0.0324	0.0932	0.0076
239	477334100	2	170	27	5.3	12	'outbound'	0.0024	0.0019	0.0053	0.0078	0.0024
240	255805597	3	318	43	10.5	10	'inbound'	0.0031	0.0153	0.0710	0.0933	0.0011
241	311968000	3	225	32	13.7	8	'outbound'	0.0016	0.0020	0.0075	0.0163	0.0021
242	311071300	2	143	22	8	11	'outbound'	0.0018	0.0022	0.0074	0.0107	0.0041
243	305663000	2	153	22	7.3	12	'outbound'	0.0018	0.0024	0.0075	0.0106	0.0031
244	255805597	3	318	43	11.3	10	'outbound'	0.0022	0.0108	0.0386	0.1728	0.0068
245	210516000	3	226	30	9.2	11	'outbound'	0.0036	0.0096	0.0241	0.0588	0.0090
246	538005562	2	204	32	7.5	13	'inbound'	0.0066	0.0277	0.0319	0.0446	0.0046
247	255805595	3	318	42	10.1	11	'inbound'	0.0186	0.0325	0.0684	0.1541	0.0109
248	215209000	2	190	32	9.1	10	'inbound'	0.0022	0.0043	0.0187	0.0200	0.0108
249	314277000	2	138	21	6.7	12	'inbound'	0.0015	0.0021	0.0029	0.0032	0.0079
250	255805595	3	318	42	10.1	10	'outbound'	0.0011	0.0145	0.0442	0.1236	0.0098
251	351160000	2	190	33	6.8	11	'outbound'	0.0026	0.0039	0.0172	0.0239	0.0128
252	353486000	4	260	32	8.2	12	'inbound'	0.0054	0.0127	0.0236	0.0334	0.0147
253	353486000	4	260	32	8.2	11	'outbound'	0.0031	0.0114	0.0257	0.0538	0.0134
254	563775000	1	175	36	5.7	9	'inbound'	0.0004	0.0003	0.0008	0.0025	0.0068
255	370633000	2	190	32	12.2	10	'inbound'	0.0018	0.0052	0.0132	0.0301	0.0066
256	257424000	2	198	31	8	11	'outbound'	0.0032	0.0043	0.0235	0.0365	0.0057
257	636017757	3	229	32	7.1	12	'inbound'	0.0121	0.0201	0.0267	0.0403	0.0030
258	538005562	2	204	32	7.3	12	'outbound'	0.0137	0.0203	0.0227	0.0467	0.0027
259	353594000	3	229	32	13.7	9	'inbound'	0.0011	0.0012	0.0158	0.0533	0.0005
260	477195100	3	291	32	10.8	11	'inbound'	0.0134	0.0248	0.0535	0.1014	0.0038
261	563775000	3	175	36	5.7	9	'outbound'	0.0006	0.0006	0.0038	0.0022	0.0003
262	314277000	2	138	21	6.8	12	'outbound'	0.0008	0.0032	0.0046	0.0115	0.0006
263	477464500	3	261	32	9.9	12	'inbound'	0.0239	0.0335	0.0529	0.0805	0.0061
264	477195100	3	291	32	11.7	10	'outbound'	0.0043	0.0033	0.0299	0.0551	0.0054
265	431501000	3	292	46	12.7	8	'outbound'	0.0019	0.0017	0.0341	0.0695	0.0002
266	477464500	3	261	32	9.8	11	'outbound'	0.0038	0.0111	0.0212	0.0382	0.0055
267	215209000	2	190	32	6.2	12	'outbound'	0.0028	0.0033	0.0113	0.0131	0.0020
268	308371000	1	214	32	7.6	11	'inbound'	0.0044	0.0067	0.0198	0.0266	0.0007
269	311071300	2	143	22	5.5	12	'inbound'	0.0094	0.0069	0.0120	0.0112	0.0027
270	636014357	3	304	40	11.4	10	'inbound'	0.0195	0.0258	0.0661	0.0948	0.0039
271	353884000	2	199	36	11.6	10	'inbound'	0.0026	0.0042	0.0078	0.0378	0.0016
272	353486000	4	260	32	8.3	12	'inbound'	0.0194	0.0212	0.0450	0.0559	0.0039
273	308371000	1	214	32	8.5	11	'outbound'	0.0205	0.0220	0.0456	0.0560	0.0037
274	636014357	3	304	40	12.2	11	'outbound'	0.0127	0.0138	0.0615	0.1232	0.0118
275	538006041	2	200	32	8	10	'inbound'	0.0253	0.0370	0.0564	0.1354	0.0155
276	353486000	4	260	32	8.2	12	'outbound'	0.0066	0.0103	0.0283	0.0413	0.0032
277	353594000	3	229	32	7.3	12	'outbound'	0.0063	0.0021	0.0227	0.0181	0.0038
278	636017757	3	229	32	13.7	9	'outbound'	0.0034	0.0020	0.0112	0.0337	0.0033
279	636091916	3	225	28	8.7	13	'inbound'	0.0182	0.0263	0.0277	0.0485	0.0054
280	370633000	2	190	32	6.5	12	'outbound'	0.0031	0.0050	0.0131	0.0173	0.0021

ID	MMSI	Class	Length (m)	Width (m)	Draft (m)	SOG	Direction	SW01_Hmo	SW02_Hmo	SW03_Hmo	SW04_Hmo	SW05_Hmo
281	311044500	2	200	30	11.9	9	'inbound'	0.0003	0.0009	0.0027	0.0188	0.0005
282	308976000	3	230	32	8	11	'inbound'	0.0054	0.0103	0.0207	0.0280	0.0006
283	311071300	2	143	22	8.5	11	'outbound'	0.0026	0.0135	0.0321	0.0070	0.0006
284	636091916	3	225	28	8.9	10	'outbound'	0.0045	0.0062	0.0271	0.0185	0.0031
285	538003048	2	189	32	11.6	9	'inbound'	0.0045	0.0062	0.0271	0.0185	0.0031
286	257496000	3	228	32	9	12	'inbound'	0.0199	0.0275	0.0336	0.0588	0.0054
287	215679000	3	229	32	7.6	12	'inbound'	0.0116	0.0166	0.0177	0.0302	0.0031
288	538006041	2	200	32	7.1	12	'outbound'	0.0036	0.0046	0.0152	0.0165	0.0019
289	563635000	2	176	35	5.3	9	'inbound'	0.0003	0.0003	0.0003	0.0024	0.0000
290	255805596	3	318	42	10	12	'inbound'	0.0221	0.0511	0.0875	0.1743	0.0040
291	248092000	2	169	27	5.5	11	'inbound'	0.0015	0.0024	0.0076	0.0045	0.0008
292	311044500	2	200	30	9.8	10	'outbound'	0.0024	0.0015	0.0104	0.0127	0.0008
293	257496000	3	228	32	9	10	'outbound'	0.0031	0.0044	0.0150	0.0206	0.0016
294	636091452	3	293	32	10.5	12	'inbound'	0.0268	0.0358	0.0788	0.0874	0.0070
295	255805596	3	318	42	9.5	10	'outbound'	0.0049	0.0059	0.0426	0.0266	0.0027
296	308976000	3	230	32	12.8	9	'outbound'	0.0018	0.0044	0.0253	0.0353	0.0026
297	563635000	2	176	35	4.8	9	'outbound'	0.0006	0.0018	0.0293	0.0356	0.0029
298	636016080	1	247	42	12.2	9	'inbound'	0.0020	0.0038	0.0202	0.0669	0.0344
299	538006145	2	199	32	6.4	12	'inbound'	0.0040	0.0074	0.0149	0.0340	0.0495
300	338302000	1	182	36	11	10	'inbound'	0.0033	0.0095	0.0281	0.0408	0.0343
301	353486000	4	260	32	8.1	12	'inbound'	0.0052	0.0068	0.0206	0.0382	0.0490
302	636012630	1	228	32	11.5	10	'inbound'	0.0030	0.0122	0.0335	0.0671	0.0782
303	636091452	3	293	32	9.9	10	'outbound'	0.0034	0.0106	0.0239	0.0780	0.0539
304	353884000	2	199	36	8.4	8	'outbound'	0.0034	0.0047	0.0144	0.0310	0.0381
305	248092000	2	169	27	8.6	8	'outbound'	0.0023	0.0046	0.0090	0.0187	0.0395
306	353486000	4	260	32	8.2	12	'outbound'	0.0036	0.0147	0.0344	0.0864	0.0319
307	215679000	3	229	32	12.9	7	'outbound'	0.0026	0.0039	0.0140	0.0310	0.0220
308	353594000	3	229	32	7.5	12	'inbound'	0.0130	0.0212	0.0278	0.0388	0.0239
309	636016080	1	247	42	8.6	11	'outbound'	0.0028	0.0080	0.0212	0.0480	0.0165
310	563775000	1	175	36	5.6	9	'inbound'	0.0050	0.0037	0.0075	0.0232	0.0357
311	636017004	2	134	16	5.3	12	'inbound'	0.0038	0.0072	0.0115	0.0200	0.0163
312	338302000	1	182	36	9.4	10	'outbound'	0.0021	0.0031	0.0134	0.0297	0.0117
313	538003048	2	189	32	6	9	'outbound'	0.0024	0.0015	0.0063	0.0083	0.0125
314	636012630	1	228	32	8.1	11	'outbound'	0.0024	0.0046	0.0171	0.0350	0.0089
315	477765800	3	261	32	10.7	13	'inbound'	0.0169	0.0330	0.0424	0.0657	0.0081
316	352652000	3	255	43	13.7	8	'inbound'	0.0007	0.0015	0.0046	0.0522	0.0003
317	563775000	1	175	36	6.1	9	'outbound'	0.0004	0.0004	0.0039	0.0011	0.0003
318	477765800	3	261	32	10.6	11	'outbound'	0.0046	0.0103	0.0371	0.0785	0.0041
319	311681000	2	199	30	11.7	10	'inbound'	0.0050	0.0125	0.0431	0.0890	0.0024
320	538006145	2	199	32	13.1	7	'outbound'	0.0001	0.0004	0.0015	0.0100	0.0001
321	368589000	1	183	32	11.8	9	'inbound'	0.0024	0.0049	0.0131	0.0263	0.0263
322	538004242	3	229	32	7.5	11	'inbound'	0.0087	0.0163	0.0267	0.0430	0.0282
323	353486000	4	260	32	8	12	'inbound'	0.0146	0.0183	0.0303	0.0555	0.0102
324	538002319	2	189	30	7.2	10	'inbound'	0.0033	0.0020	0.0053	0.0094	0.0027
325	353486000	4	260	32	8.2	12	'outbound'	0.0041	0.0100	0.0206	0.0679	0.0045
326	311071300	2	143	22	5.5	13	'inbound'	0.0035	0.0040	0.0054	0.0069	0.0027
327	636013275	1	249	44	10.8	9	'inbound'	0.0017	0.0028	0.0069	0.0438	0.0004



## **Appendix B**

### **Detailed Forecasted Vessel Frequency**

Table B-1: Detailed forecast of **arriving** vessel calls for 2025 **without** Project

Draft (m)	Bulk Carrier 2	Bulk Carrier 3	Bulk Carrier 4	Bulk Carrier 5	Bulk Carrier 6	Bulk Carrier 7	Chemical Tanker	SubPX	Panamax	PPXGn1	PPXGn2	PPXGn3	Cruise	General Cargo 1	General Cargo 2	Tanker Panamax	Aframax Tanker
2.1																	
2.4							2										
2.7							5										
3.0							5										
3.4							6								1		
3.7							6								3		
4.0			3				8								10		
4.3		1	5				10								20		
4.6			12				9							12	22		
4.9			10				7							48	17		
5.2			6				4							38	10		
5.5			5				3							12	10		
5.8			5				4							17	8	1	
6.1	4	156	141	8	1	6	3							72	9	1	
6.4		2	4				2								11	3	
6.7		3	4				2								6	3	
7.0		4	3												7	2	
7.3		4	6												7	3	
7.6		11	5				1						44		2	1	
7.9		13	6										47		3	2	
8.2		12	7				1									1	
8.5		8	7														2
8.8		6	6													1	4
9.1		5	3					6	8							1	11
9.4		2	3						1								18
9.8		1	2					1	86	10	6					2	17
10.1		1	3					2	25	5	8					2	13
10.4			1					1	21	10	7					2	5
10.7			2						31	9	9					2	2
11.0			1						28	17	11					1	
11.3				1					13	17	11					2	
11.6				2					11	13	12					1	
11.9				2					5	15	10					1	
12.2				3					1	10	11						
12.5				2					1	5	3						
12.8				3					1	6	6						
13.1				3													
13.4				2													
13.7				12													
14.0																	
14.3																	
14.6																	
14.9																	
<b>Total</b>	4	229	250	38	1	6	78	10	232	117	94	0	91	199	146	32	72

Table B-2: Detailed forecast of **departing** vessel calls for 2025 **without** Project

Draft (m)	Bulk Carrier 2	Bulk Carrier 3	Bulk Carrier 4	Bulk Carrier 5	Bulk Carrier 6	Bulk Carrier 7	Chemical Tanker	SubPX	Panamax	PPXGn1	PPXGn2	PPXGn3	Cruise	General Cargo 1	General Cargo 2	Tanker Panamax	Aframax Tanker
2.1																	
2.4																	
2.7																	
3.0																	
3.4																	
3.7																	
4.0																	
4.3																	
4.6																	
4.9														33			
5.2														41			
5.5														18			
5.8							69							23		15	
6.1		33	94				2							72	111	4	
6.4			4				2								7		
6.7		1	2				1							6	10	3	
7.0		2	3											4	7	3	
7.3		3	3				1							3	6		
7.6		5	5										91		3	1	
7.9		7	4				2								2	1	
8.2		6	1				1								1	1	
8.5		7						5									
8.8		5						1									
9.1		3	1					1	1								
9.4		2						2	29								
9.8			1					1	10	10							
10.1			2						58	4	8						
10.4		1	2						34	9	8						
10.7		2	2						22	10	6					1	
11.0		5	1						23	12	8						
11.3		1	1						22	18	10						
11.6	1	5	3	2					11	14	11						
11.9	1	5	1	1					11	14	12						
12.2		5	7	1					4	10	9						
12.5	1	5	5	2					2	18	11						
12.8		9	5	3					2		11						
13.1		57	7	5	1												
13.4			5	5													
13.7			40	20		6											
14.0																	
14.3																	
14.6																	
14.9																	
<b>Total</b>	<b>3</b>	<b>169</b>	<b>199</b>	<b>39</b>	<b>1</b>	<b>6</b>	<b>78</b>	<b>10</b>	<b>229</b>	<b>119</b>	<b>94</b>	<b>0</b>	<b>91</b>	<b>200</b>	<b>147</b>	<b>29</b>	<b>0</b>

Table B-3: Detailed forecast of **arriving** vessel calls for 2025 **with** Project

Draft (m)	Bulk Carrier 2	Bulk Carrier 3	Bulk Carrier 4	Bulk Carrier 5	Bulk Carrier 6	Bulk Carrier 7	Chemical Tanker	SubPX	Panamax	PPXGn1	PPXGn2	PPXGn3	Cruise	General Cargo 1	General Cargo 2	Tanker Panamax	Aframax Tanker
2.1																	
2.4							2										
2.7							5										
3.0							5										
3.4							6								1		
3.7							6								3		
4.0			3				8								10		
4.3		1	5				10								20		
4.6			12				9							12	22		
4.9			10				7							48	17		
5.2			6				4							38	10		
5.5			5				3							12	10		
5.8			5				4							17	8		1
6.1		150	141	10	1	6	3							72	9		1
6.4		2	4				2								11		3
6.7		3	4				2								6		3
7.0		4	3												7		2
7.3		4	6												7		3
7.6		11	5				1						44		2		1
7.9		13	6										47		3		2
8.2		12	7				1										1
8.5		8	7														2
8.8		6	6														4
9.1		5	3					6	8								11
9.4		2	3						1								18
9.8		1	2					1	77	1	1						17
10.1		1	3					2	22	1							13
10.4			1					1	18	3	1						5
10.7			2						28	6	5						2
11.0			1						26	4	8						1
11.3				1					12	11	7						2
11.6				1					10	10	10						1
11.9				1					4	18	10						1
12.2				1						18	14						
12.5				2						13	10						
12.8				1					1	15	12						
13.1				3					1	8	7						
13.4				3						4	5						
13.7				1						5	4						
14.0				1						1							
14.3				3													
14.6				2													
14.9				6													
<b>Total</b>	0	223	250	36	1	6	78	10	208	118	94	0	91	199	146	72	32

Table B-4: Detailed forecast of **departing** vessel calls for 2025 **with** Project

Draft (m)	Bulk Carrier 2	Bulk Carrier 3	Bulk Carrier 4	Bulk Carrier 5	Bulk Carrier 6	Bulk Carrier 7	Chemical Tanker	SubPX	Panamax	PPXGn1	PPXGn2	PPXGn3	Cruise	General Cargo 1	General Cargo 2	Tanker Panamax	Aframax Tanker
2.1																	
2.4																	
2.7																	
3.0																	
3.4																	
3.7																	
4.0																	
4.3																	
4.6																	
4.9														33			
5.2														41			
5.5														18			
5.8							69							23		15	
6.1		33	94				2							72	111	4	
6.4			4				2								7		
6.7		1	2				1							6	10	3	
7.0		2	3											4	7	3	
7.3		3	3				1							3	6		
7.6		5	5										91		3	1	
7.9		7	4				2								2	1	
8.2		6	1				1								1	1	
8.5		7						5									
8.8		5						1									
9.1		3	1					1	1								
9.4		2						2	37								
9.8			1					1	13								
10.1			2						41	1	1						
10.4			1						31		1						
10.7		1	1						22	3	1					1	
11.0		6	1						22	5	5						
11.3		1	1						17	3	7						
11.6		4	4	1					7	9	6						
11.9		6	1	1					9	10	8						
12.2		4	4	1					2	14	10						
12.5		4	8	1					3	18	12						
12.8		8	3	1						14	11						
13.1		55	8	2					1	14	9						
13.4			4	4	1				1	10	11						
13.7			4	4						9	3						
14.0			2	5		1				8	7						
14.3			3	4													
14.6			35	5		1											
14.9				9		4											
<b>Total</b>	0	163	200	38	1	6	78	10	207	118	92	0	91	200	147	29	0

Table B-5: Detailed forecast of **arriving** vessel calls for 2035 **without** Project

Draft (m)	Bulk Carrier 2	Bulk Carrier 3	Bulk Carrier 4	Bulk Carrier 5	Bulk Carrier 6	Bulk Carrier 7	Chemical Tanker	SubPX	Panamax	PPXGn1	PPXGn2	PPXGn3	Cruise	General Cargo 1	General Cargo 2	Tanker Panamax	Aframax Tanker
2.1							1										
2.4							3										
2.7							7										
3.0							7										
3.4							11										
3.7							10								5		
4.0			3				12								13		
4.3			9				19							1	20		
4.6			15				14							15	26		
4.9			15				6							39	22		
5.2		1	5				6							46	14		
5.5			7				3							19	10	1	
5.8			8				3							21	9	3	
6.1	3	76	72	12	1	7	4							85	12	3	
6.4		2	5				6								12	3	
6.7		3	8				1								9	5	
7.0		7	6												7	5	
7.3		11	4				2								6	5	
7.6		19	7				1						42		5	4	
7.9		22	7				1						44		3	5	
8.2		20	5				1										3
8.5		14	7				1										3
8.8		14	4														2
9.1		6	3					11	7								3
9.4		3	2						2								2
9.8		1	1				1	2	42	10	8	10					2
10.1			2					2	14	11	5	9					3
10.4			1					1	14	10	10	11					3
10.7			2						21	18	7	12					3
11.0			1						15	20	11	15					3
11.3				1					5	15	13	21					3
11.6				2					5	19	14	14					1
11.9				2					3	17	10	18					
12.2				2						13	10	13					
12.5				2					1	8	2	6					
12.8				2					1	6	3	6					
13.1				3													
13.4				2													
13.7				12													
14.0																	
14.3																	
14.6																	
14.9																	
<b>Total</b>	3	199	199	40	1	7	120	16	130	147	93	135	86	226	173	65	55

Table B-6: Detailed forecast of **departing** vessel calls for 2035 **without** Project

Draft (m)	Bulk Carrier 2	Bulk Carrier 3	Bulk Carrier 4	Bulk Carrier 5	Bulk Carrier 6	Bulk Carrier 7	Chemical Tanker	SubPX	Panamax	PPXGn1	PPXGn2	PPXGn3	Cruise	General Cargo 1	General Cargo 2	Tanker Panamax	Aframax Tanker
2.1																	
2.4																	
2.7																	
3.0																	
3.4																	
3.7																	
4.0																	
4.3																	
4.6																	
4.9														44			
5.2														51			
5.5														21			
5.8							105							25		51	
6.1		46	105				4							83	131	2	
6.4		0	6												11	2	
6.7		0	7				1							1	11	4	
7.0		0	6				1							1	7	2	
7.3		0	4				1							1	6		
7.6		0	5				1						86		6	1	
7.9		0	2				3								1		
8.2		0	2				1								1	1	
8.5		0						10									
8.8		0					1		1								
9.1		0						1	1								56
9.4		0	2					3	14								
9.8		0	4					1	9			1					
10.1		1	5						28	10	9	11					
10.4		0	1						16	10	5	8					
10.7		1	1						11	10	9	11				1	
11.0		2	1						14	16	7	10				1	
11.3		2	1						14	18	11	17				1	
11.6		4	2	1					10	16	12	19					
11.9	1	3	2	1					6	17	14	15					
12.2		3	4	1					3	14	9	14					
12.5	1	3	2	2					2	18	11	15					
12.8		5	4	3					1	19	7	12					
13.1		64	4	5	1												
13.4			5	4													
13.7			44	25		7											
14.0																	
14.3																	
14.6																	
14.9																	
<b>Total</b>	2	134	219	42	1	7	118	15	130	148	94	133	86	227	174	66	56

Table B-7: Detailed forecast of **arriving** vessel calls for 2035 **with** Project

Draft (m)	Bulk Carrier 2	Bulk Carrier 3	Bulk Carrier 4	Bulk Carrier 5	Bulk Carrier 6	Bulk Carrier 7	Chemical Tanker	SubPX	Panamax	PPXGn1	PPXGn2	PPXGn3	Cruise	General Cargo 1	General Cargo 2	Tanker Panamax	Aframax Tanker
2.1																	
2.4																	
2.7																	
3.0																	
3.4																	
3.7																	
4.0																	
4.3																	
4.6																	
4.9														44			
5.2														51			
5.5														21			
5.8							105							25		51	
6.1		74	105				4							83	131	2	
6.4		1	6												11	2	
6.7		2	7				1							1	11	4	
7.0		2	6				1							1	7	2	
7.3		4	4				1							1	6		
7.6		8	5				1						86		6	1	
7.9		8	2				3								1		
8.2		9	2				1								1	1	
8.5		7						9									
8.8		4					1		2								
9.1		2						1									56
9.4		3	2					3	3								
9.8		1	4					1	7	1							
10.1			5						10	1	1	2					
10.4			1						8	2	1						
10.7		2	1						6	3	2	3				1	
11.0		2	1						6	7	6	7				1	
11.3		2	1						7	10	4	7				1	
11.6		4	3						8	10	9	10					
11.9		2	1	1					4	11	6	10					
12.2		2	2	1					1	19	11	16					
12.5		3	4	1					1	14	11	17					
12.8		4	3	2					1	15	14	13					
13.1		58	3	2					1	15	7	15					
13.4			3	4	1					13	10	13					
13.7			4	3						6	2	5					
14.0			4	2						8	3	6					
14.3			3	5		1											
14.6			34	5		1											
14.9				13		5											
<b>Total</b>	0	204	216	39	1	7	118	14	65	135	87	124	86	227	174	66	56

Table B-8: Detailed forecast of **departing** vessel calls for 2035 **with** Project

Draft (m)	Bulk Carrier 2	Bulk Carrier 3	Bulk Carrier 4	Bulk Carrier 5	Bulk Carrier 6	Bulk Carrier 7	Chemical Tanker	SubPX	Panamax	PPXGn1	PPXGn2	PPXGn3	Cruise	General Cargo 1	General Cargo 2	Tanker Panamax	Aframax Tanker
2.1																	
2.4																	
2.7																	
3.0																	
3.4																	
3.7																	
4.0																	
4.3																	
4.6																	
4.9														44			
5.2														51			
5.5														21			
5.8							105							25		51	
6.1		74	105				4							83	131	2	
6.4		1	6												11	2	
6.7		2	7				1							1	11	4	
7.0		2	6				1							1	7	2	
7.3		4	4				1							1	6		
7.6		8	5				1						86		6	1	
7.9		8	2				3								1		
8.2		9	2				1								1	1	
8.5		7						9									
8.8		4					1		2								
9.1		2						1									56
9.4		3	2					3	3								
9.8		1	4					1	7	1							
10.1			5						10	1	1	2					
10.4			2						8	2	1						
10.7		2	3						6	3	2	3				1	
11.0		2	1						6	7	6	7				1	
11.3		2	1						7	10	4	7				1	
11.6		4	3						8	10	9	10					
11.9		2	1	1					4	11	6	10					
12.2		2	2	1					1	19	11	16					
12.5		3	4	1					1	14	11	17					
12.8		4	3	2					1	15	14	13					
13.1		54	3	2					1	15	7	15					
13.4			3	4	1					13	10	13					
13.7			4	3						6	2	5					
14.0			4	2						8	3	6					
14.3			3	5		1											
14.6			34	5		1											
14.9				13		5											
<b>Total</b>	0	200	219	39	1	7	118	14	65	135	87	124	86	227	174	66	56